HYDRODYNAMICS OF BLADE GAP FORMERS

By

Alireza Roshanzamir

B.Sc. (Mechanical Engineering) Amir Kabir University of Technology

M.A.Sc. (Mechanical Engineering) Concordia University

A THESIS SUBMITTED IN PARTIAL FULFILLMENT OF

THE REQUIREMENTS FOR THE DEGREE OF

DOCTOR OF PHILOSOPHY

in

THE FACULTY OF GRADUATE STUDIES

DEPARTMENT OF MECHANICAL ENGINEERING

We accept this thesis as conforming

to the required standard

THE UNIVERSITY OF BRITISH COLUMBIA

2000

In presenting this thesis in partial fulfilment of the requirements for an advanced degree at the University of British Columbia, I agree that the Library shall make it freely available for reference and study. I further agree that permission for extensive copying of this thesis for scholarly purposes may be granted by the head of my department or by his or her representatives. It is understood that copying or publication of this thesis for financial gain shall not be allowed without my written permission.

Department of Mechanical Engineering
The University of British Columbia
2356 Main Mall
Vancouver, Canada
V6T 1Z4

Date:

Oct. 13, 2000

Abstract

In blade gap forming in papermaking, a headbox discharges a pulp suspension into a gap between two moving permeable fabrics under tension. As these fabrics wrap around fixed blades, sizeable pressure pulses are induced in the gap between the fabrics. These pressure pulses cause drainage through the fabrics during which pulp fibres are deposited by a filtration process to form a mat.

The objective of this study was to improve our understanding of this process. To achieve this, three aspects of the problem were addressed: fluid flow, fabric deflection, and mat resistance. Simplified one-dimensional and numerical viscous two-dimensional models were developed. The effects of key variables on pressure pulses generated by a single blade were first considered, then the effect of applied suction between two adjacent blades was added. In the final step, the effect of pressure in the stagnation zone at the contact point between a moving fabric and stationary blade was included.

It was confirmed that a wide flat blade ($> 2\,cm$) generates two distinguishable pulses, one at the leading edge of the blade and the other at the trailing edge. As blade width decreases to approximately 1 cm, the two pulses converge in a single pressure pulse. The magnitude of the pulses depends on a number of variables, such as fabric tension, fabric velocity, and fibre mat resistance.

It was further confirmed that blade curvature exerts a strong effect on the pulses. As a flat surface assumes a curved shape, the pressure pulses at each edge merge into a single pressure pulse over the blade surface. This convergence occurs at rather small curvatures that are within the range of wear of plastic blades found in commercial paper machines.

This study also examined the effect of suction in one side of fabric between blades. It was found that such suction induced a negative pressure in the gap between fabrics just downstream of the first (upstream) blade. This negative pressure increased to a positive value at the second (downstream) blade. The net increase in pressure from the negative value corresponded to a pressure pulse that was larger in amplitude than one created in

the absence of suction. This was attributed to the larger wrap angle at the leading edge of the second blade induced by the downward deflection of the fabric resulting from suction.

Other aspects of blade forming examined in this study were the effect of inertial force on drainage and viscosity on the flow between fabrics. Inertial effects were found to be small, even for modest levels of mat build-up ($10\ g/m^2$). Inclusion of viscosity in the analysis gave a boundary layer in the flow parallel of the fabric, but this was very thin owing to the drainage perpendicular to the fabric which drew off the boundary layer.

Lastly, the effect of the stagnation zone pressure at the leading edge of a blade in contact with a moving fabric was examined. The size of this zone was found to depend on the radius of curvature of the edge of the blade. Under typical papermachine conditions, the pressure acting on the fabric from the stagnation zone was found to be about 50% of the stagnation point pressure. The size of the zone over which the pressure extended was a few millimeters. This pressure increased the pressure between the fabrics by 30% to 100%, depending on the radius of curvature of the blade edge. The stagnation zone pressure also forced some water back into the gap between the fabrics, but the amount was small only about 10% of the drained water.

Table of Contents

List of Tables

List of Figures

Chapter 1

Introduction

1.1 Background

Papermaking is an ancient art that originated in China two thousand years ago. Around the year 1000 the art of papermaking reached Europe and become well established by the beginning of the 15^{th} century. More than two centuries ago, the ancient art of papermaking was adapted for continuous operation by introduction of the Fourdrinier paper machine in 1800. These machines use a continuous porous fabric or wire, Figure 1.1, on which a pulp suspension at approximately 0.5% weight concentration (consistency) is allowed to impinge more or less horizontally [1]. Drainage on the Fourdrinier paper machine is accomplished by hydraulic pressure gradients. The gradients other than those caused by the weight of stock on the fabric and the inertial impingement of stock from the slice, are induced by the drainage elements (table rolls, foils, suction boxes, etc.) along the fabric. Research work aimed at explaining the drainage process on paper machines started around 1950. The function of table rolls was the main subject of these studies. These rolls cause large-scale motion of the fibres in the pulp suspension. The studies showed that the action of a table while, improving paper formation [1] at low machine speed, could disrupt formation at higher machine speed. Paper manufactured on a Fourdrinier has a relatively coarse structure on the fabric side of the sheet, and is more closed or finer textured on the top side. This two-sidedness is caused by a difference in fibre composition on the two sides. The slow speed of production and the high degree of two-sidedness of Fourdrinier papers were the main reasons for developing a completely new alternative for the manufacturing of paper, called gap forming or twin-wire forming.

Gap formers have become a standard of the industry for tissue and newsprint forming section, and the number of installations is rapidly increasing [2]. Not only are twin-wires

[1]Formation is a measure of the mass uniformity of fibres in the paper.

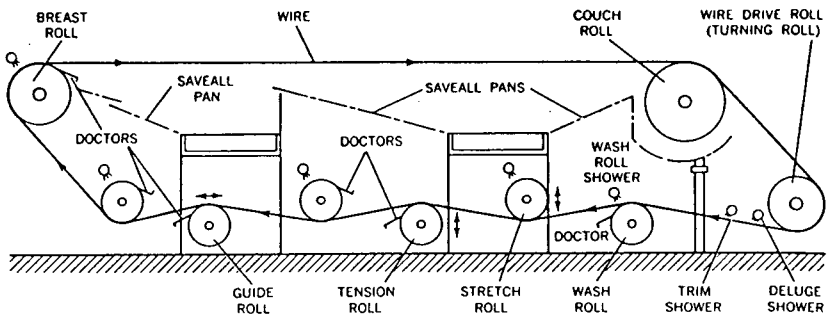

Figure 1.1: Diagram of Fourdrinier wet-end [1].

favored over Fourdrinier forming sections for new paper machines, but there were also an increasing number of top wire rebuilds of existing Fourdrinier machines [3-6]. The initial advantages of gap formers were increased speed and reduction of two-sidedness. In general these promises have been amply fulfilled. In additions, other benefits which are commonly observed include improved formation, improved sheet surface characteristics, more compact installation, improved fabric life, and reduced drive and vacuum requirements. On the negative side, however, there have been frequent complaints of poor retention[2].

The development of modern gap former started in the late forties to meet the demand for ever increasing productivity. David Webster, then superintendent at Consolidated Paper Corp. Ltd., Canada, conducted private experiments in which pulp suspension was introduced between a rotating roll and a wire wrapping this roll, Figure 1.2. His original patent application is the first to describe a roll former in which the wrapping wire is free to move in a direction transverse to the roll periphery and in which two-sided dewatering could be achieved. It was also in the early fifties that Brian Atwood and co-workers at St Anne's Board Mill, England, developed the Inverform, a twin-wire process for making multi-ply product. The development work was carried out by several people, but the early patents were assigned to R. J. Thomas, mill manager at St Anne's Board Mill at the time [7]. In 1958 the Inverform went into industrial production as the first commercial twin-wire machine.

The first gap former to achieve wide acceptance for newsprint manufacturing was the

[2]The fraction of solids from a headbox retained on the forming fabrics is called the first pass retention.

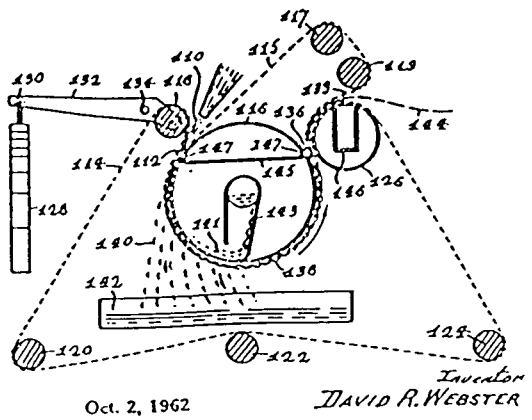

Figure 1.2: Roll former according to Webster's patent [7].

Vertiforma. This former started commercial operation in the late sixties [7]. A review of commercial twin-wire applications is given in [8].

1.2 Gap Formers

Forming a web at higher speeds is more readily controlled with a gap former.

There are two basic types of pure gap formers for paper grades: roll formers and blade formers. These two types of formers produce differing paper properties [9]. In modern papermaking, rolls and blades are used in various combinations to optimize these properties [10-15].

1.2.1 Roll Former

In a roll former, Figure 1.3, the headbox jet is directed between two fabrics wrapping a solid or open forming roll. The roll former has been studied by a number of authors [16-23]. Two-sided dewatering may be obtained if the forming roll is porous. To obtain an even dewatering pressure requires a constant, or slowly changing, fabric curvature. The curvature of the inner fabric is that of the forming roll, and that of the outer fabric is approximately equal to that of the forming roll. The dewatering pressure is:

$$p = \frac{T}{R} \tag{1.1}$$

where T is the tension per unit width on the fabric and R is the local fabric radius of curvature. This pressure can be measured by a pressure sensor mounted in the surface of a solid forming roll. An example of a dewatering pressure curve is shown in Figure 1.4.

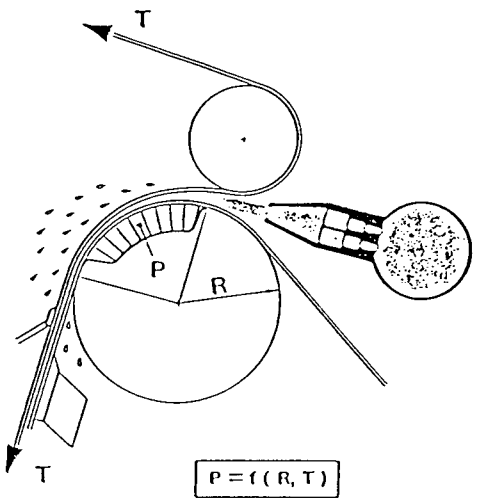

Figure 1.3: The dewatering principle in the roll former [16].

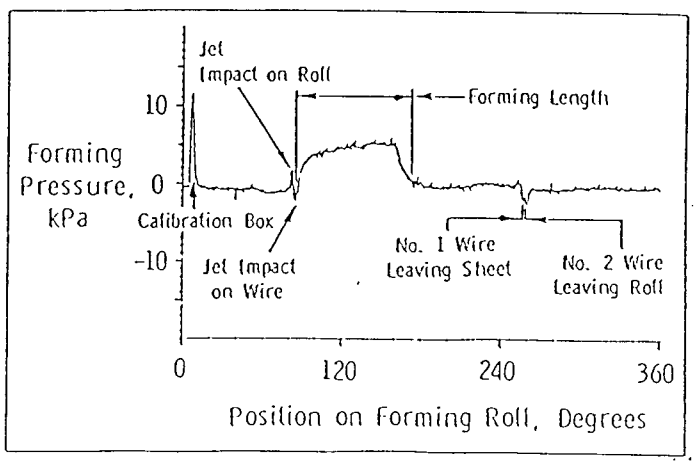

Figure 1.4: Typical roll former pressure profile [17].

1.2.2 Blade Formers

A blade gap former is one in which the headbox jet is injected between two converging fabrics, and the sandwich moves over fixed blades. Pressure pulses are created between the fabrics where passing over blades, causing shear in the forming zone. Compared to roll formers, blade formers tend to have superior formation but lower first pass retention. Figure 1.5 shows a typical blade gap former.

Experimental Studies

There are relatively few experimental studies of the pressure pulses in blade gap formers. Measurements of pressure pulses have been reported by [6], [8], and [24-26]. In those studies, the pressure pulses were measured at accessible blades in the forming zone of paper machine by inserting a thin probe from the headbox slice into the fibre suspension between the two fabrics. Figure 1.6 shows typical measured pressure profiles.

Garner and Pye [27] conducted a photographic analysis of the operation of a single blade, having a 73 *mm* face. They showed that changing the angle of attack had a significant effect on the drainage. At large angles of attack a considerable amount of water was doctored by the leading edge and generally followed the surface of the blade. A small amount of water was also pushed through the fabric above the tip of the blade, only to be reabsorbed over the blade within about one centimeter. At the heel of the blade,

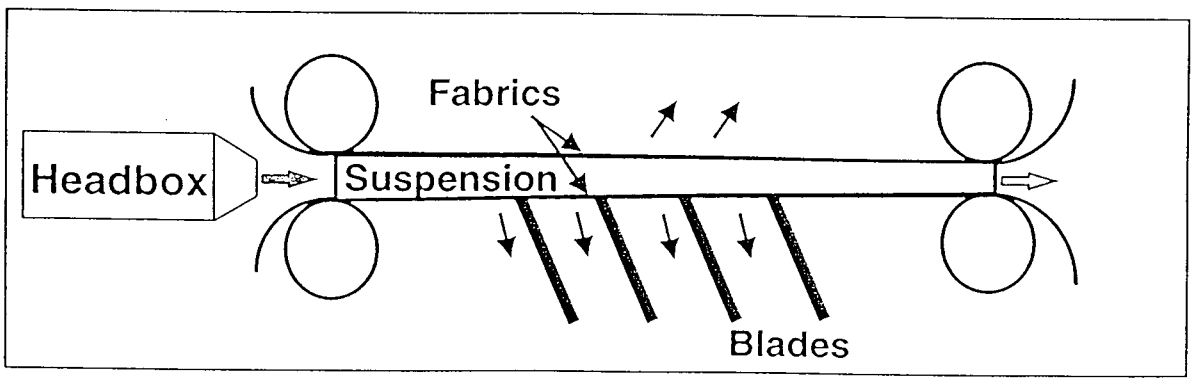

Figure 1.5: Typical blade gap former.

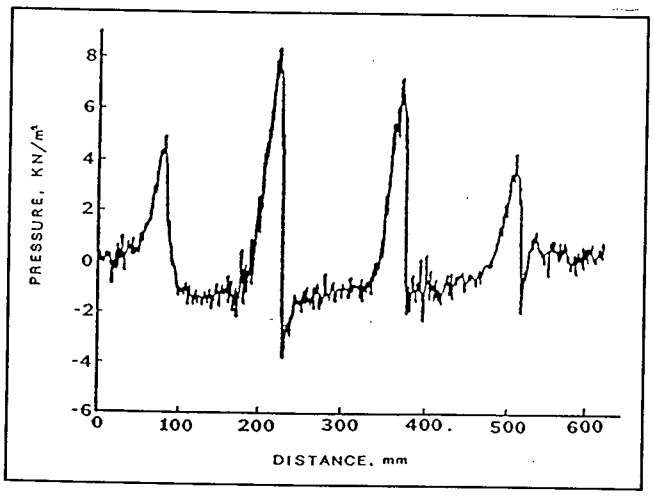

Figure 1.6: Pressure pulses measured on a pilot paper machine [6].

water was pushed through the fabric starting about one centimeter before the leading edge.

Zhao and Kerekes [28] carried out a number of tests on a pilot paper machine at Paprican in which the pressure over the surface of the blade was measured at 10 pressure taps, as shown in Figure 1.7. They simulated an infinitely thin blade by taking all of the fabric wrap over the heel (downstream tip) of a 35 *mm* wide blade. The face of the blade was parallel to the fabric upstream, giving zero fabric incident angle.

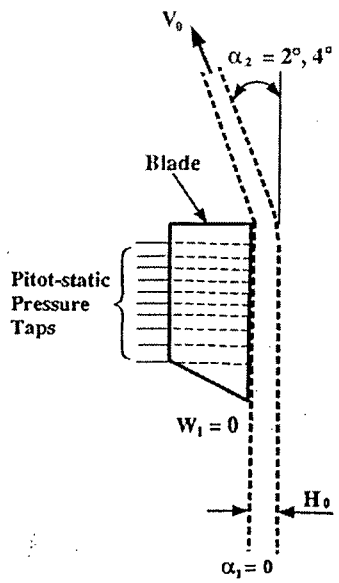

Figure 1.7: Schematic diagram of the blade and location of pressure taps [28].

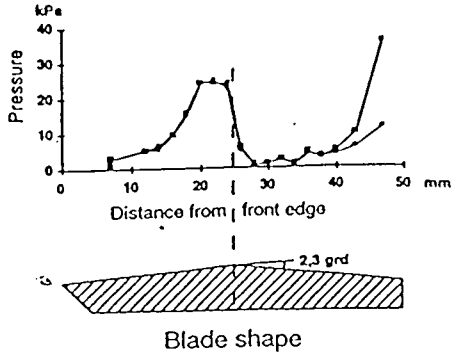

Figure 1.8: Pressure profile along a 50 mm blade [29].

The studies of pressure pulses along a flat 50 *mm* long deflection blade with a 2, 3 degrees angle at the centre has been performed on the FEX machine.[3] [29]. Figure 1.8 shows a typical result obtained in that study.

Theoretical Studies

The basic concepts of gap formers were explained by Norman [7] and [29]. He characterized gap forming and pointed out the pulsating dewatering pressure that occurs in blade gap formers. Since the early study of blade gap formers, several attempts were made [6], [24], and [25] to analyze the pressure pulses. However, the first successful mathematical model to predict the pressure distribution between forming fabrics was made by Zhao and Kerekes [28]. Explicit equations for pressure distributions were obtained for the case of an infinitely thin blade and zero fabric stiffness. In their work, the pulp suspension was modelled as an incompressible inviscid fluid and the variation of flow quantities in the direction normal to the fabric was neglected. The most important result of their study was that a thin blade produces a single pressure pulse, located immediately upstream of the blade. As discussed earlier, they carried out a number of tests on a paper machine at Paprican for comparison with this theory. Figure 1.9 shows good agreement between experiment and theory, which implies that the theory captures most of the relevant physics

[3]FEX is an experimental paper machine at the Swedish Pulp and Paper Research Institute (STFI).

of blade forming.

Zhao and Kerekes [30] employed their newly-developed model to estimate the effect of consistency on pressure pulses in blade gap formers. They showed that an approximate correlation exists between formation improvement and a displacement distance related to stock flow relative to the fabrics caused by the pressure pulses.

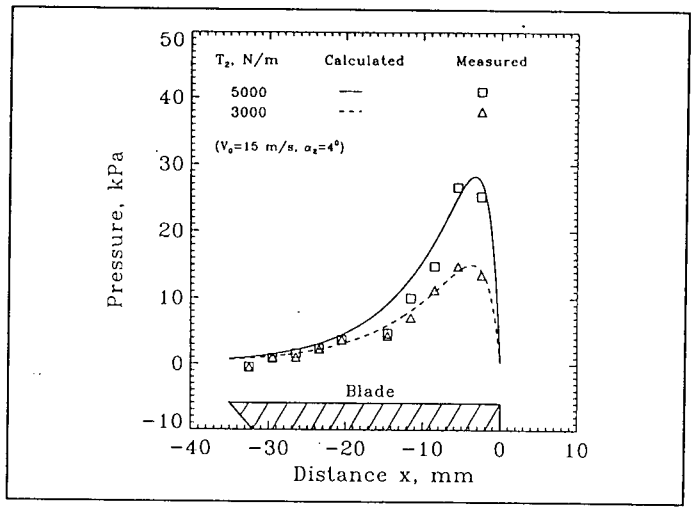

Figure 1.9: Surface pressure measurements [28].

Zahrai and Bark [31] developed a two-dimensional potential flow model for blade forming in which the variation of pressure in the direction normal to the fabrics was considered. Figure 1.10 shows a typical pressure pulse obtained by their model: the pressure varies in the direction normal to the fabrics, and close to the location of the blade the lower fabric experiences a negative pressure peak.

Green [32] has carried out a control volume analysis of blade forming. His key results were: the integrated pressure between forming fabrics developed as the fabric wraps a blade is $T_{top} sin\alpha_{total}$, where T_{top} is the tension on the top fabric and α_{total} is the total fabric wrap angle around the blade; the displacement of pulp relative to the fabric is the integrated pressure pulse divided by the dynamic pressure of the pulp suspension; and the change in gap size is given by the product of the average permeability and integrated pressure pulse, divided by the fabric velocity.

Green, Zhao, and Kerekes [33] and Green and Kerekes [34] followed up that research by developing a one-dimensional computer simulation that computes the behavior of flat,

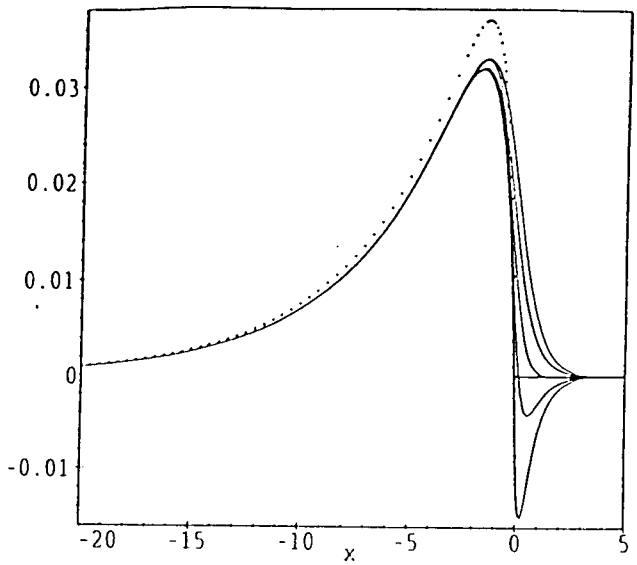

Figure 1.10: Pressure distribution as a function of x at different locations between fabrics, ... ZK model [31].

finite width blades. They showed that wide flat blades generate two pressure pulses, one associated with fabric wrap at the blade heel and one with fabric wrap at the toe of the blade. Those pulses merge into a single pulse as the blade width narrows. Increasing the tension of the top fabric can increase the magnitude of pressure pulses, consistent with the analysis of Green [32]. They also found that variations in mat resistance and the pressure induced by a blade as a result of deflecting water adhering to the lower forming fabric can increase the magnitude of pressure pulses.

Concurrent with some of the above work, Zahrai, Bark, and Norman [35] extended their model to predict the pressure pulses generated by finite width blades. They validated the results of the in model by comparing the numerical results with experiment conducted on the FEX paper machine.

A study of two blades with applied suction between them was done by Green [36] and [37]. He developed a one-dimensional numerical model to study the effect of applied suction, mat resistance, and blade separation on the pressure pulses.

Shands [38] also developed a one-dimensional model for the forming section of a pilot paper machine. He studied the effects of the number and position of blades. The ability to apply vacuum outside of the fabric was included, but the influence of pressure generated as a results of water deflection in the stagnation zone by blades were not simulated.

In addition to the above fundamental studies of pressure pulses in the blade gap, a number of studies have been done on characteristics of forming fabrics and fibre mats [39-48]. The results of these studies can be used to evaluate the influence of fabrics and fibre mat resistance on the drainage behavior of gap formers.

1.3 Overall Objective

Initially, it was planned to build a small test pilot paper machine and perform an extensive experimental study of pressure pulses. A careful consideration of the design of such a machine revealed its substantial complexity and cost. In view of these factors, it was decided to perform extensive numerical modelling to identify the important variables involved in the problem. The findings of the modelling would help future researchers to simplify any new experimental procedure and focus on keys parameters. Experimental validation of the model is indirect; the numerical model described below was compared with a one-dimensional analytical model of blade forming, which itself has been found to agree well with experiments.

The overall objective of this thesis is to develop a comprehensive two-dimensional model of blade formers by including the effects of:

1. Blade surface shape
2. Applied suction between two adjacent blades
3. Size of blade separation
4. Stagnation zone created by doctored water close to the blade leading edge
5. Inertia effect in flow in fabrics

The main body of the thesis consists of three parts:

1. Analysis of a single blade
2. Study of two adjacent blades with applied suction between them

3. Study of the stagnation zone close to the leading edge of a blade

Part I consists of three chapters, 2, 3, and 4. In Chapter 2 a one-dimensional analytical solution of a single blade is presented by modelling first a thin blade, then finite flat blades, and then curved shaped blades. For this solution, it is assumed that the pulp suspension is an inviscid fluid. The results obtained in Chapter 2 will be used as initial guesses for a two-dimensional viscous model presented in the following chapter where the full Navier-Stokes equations are solved for the flow in the gap. Chapter 4 is devoted to study the fluid inertial effect on drainage resistance.

Part II, in almost parallel structure, includes two chapters. In Chapter 5 the one-dimensional analytical model developed in Chapter 2 is extended to include two adjacent thin blades with suction applied between them. In the following chapter the viscous two-dimensional model is extended to include the effect of the applied suction on pressure pulses. In many respects, Part II is simply an extension of the Part I study of a single blade. However, two new terms are introduced, namely, the applied suction and the blade separation.

Part III presents a new topic, the stagnation pressure zone in the region close to the leading edge of the blade. The flow both inside and outside of the gap must be modelled. This part also includes two chapters. In chapter 7, an analytical one-dimensional model to estimate the effect of the stagnation pressure on pressure pulses is developed. In the following chapter a two-dimensional free surface model is developed and added to the two-dimensional model of flow in the gap of Chapter 3.

Chapter 9 summarizes all the findings of these studies and Chapter 10 presents recommendations for future work. These studies significantly improve our understanding of the hydrodynamics of papermachine gap formers. This in turn gives us a potential tool for estimating how blades affect sheet formation and other paper properties.

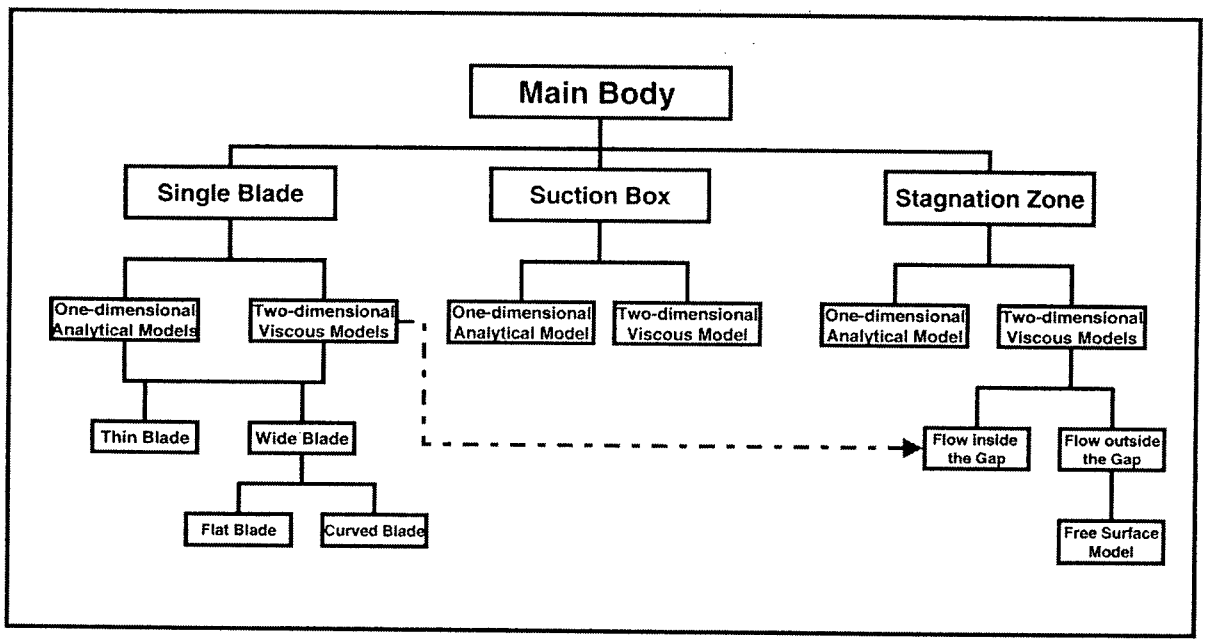

Figure 1.11: The main body of the thesis.

Part I

Modelling of a Single Blade

Chapter 2

Analytical Solution of Single Blades

As mentioned in the previous chapter, Zhao and Kerekes [28] used a linearization method to develop an analytical one-dimensional model for predicting the pressure pulse generated by a single thin blade (ZK model). In this chapter, the same method with some modifications, is employed to extend the model to determine the pressure pulses generated by first infinitely thin, then flat, then curved blades. The first part of this chapter (infinitely thin blade) can be considered as a confirmation of previously developed model using a modified approach.

2.1 Modified Approach

This modified approach gives a general second order differential equation directly for the pressure rather than the shapes of fabrics (ZK model). The new model can be used to calculate the pressure pulse upstream of the blade and between two adjacent blades with less effort. We consider two forming fabrics passing over a blade, as shown in Figure 2.1. This geometry is a simplified representation of a single blade former. We assume that the machine direction is horizontal, although the analysis that follows is in no way so limited. Some of the important variables shown are:

- y_t: The vertical position of the top fabric.
- y_b: The vertical position of the bottom fabric.
- h_o: The gap size between two fabric far upstream of the blade.
- V_o: The velocity of the fabrics.
- α_1: The wrap angle far upstream of the blade.

- α_2: The wrap angle far downstream of the blade.

As shown in Figure 2.1, the bottom fabric is in contact with the blade and both fabrics wrap the blade at given angles. These angles are assumed to be sufficiently small for x to represent the distance along the fabric from the origin. The pressure induced between the fabrics is created by fabric tension and fluid flow. We model the pulp suspension between the fabrics as a fluid bounded by moving, flexible, and permeable walls.

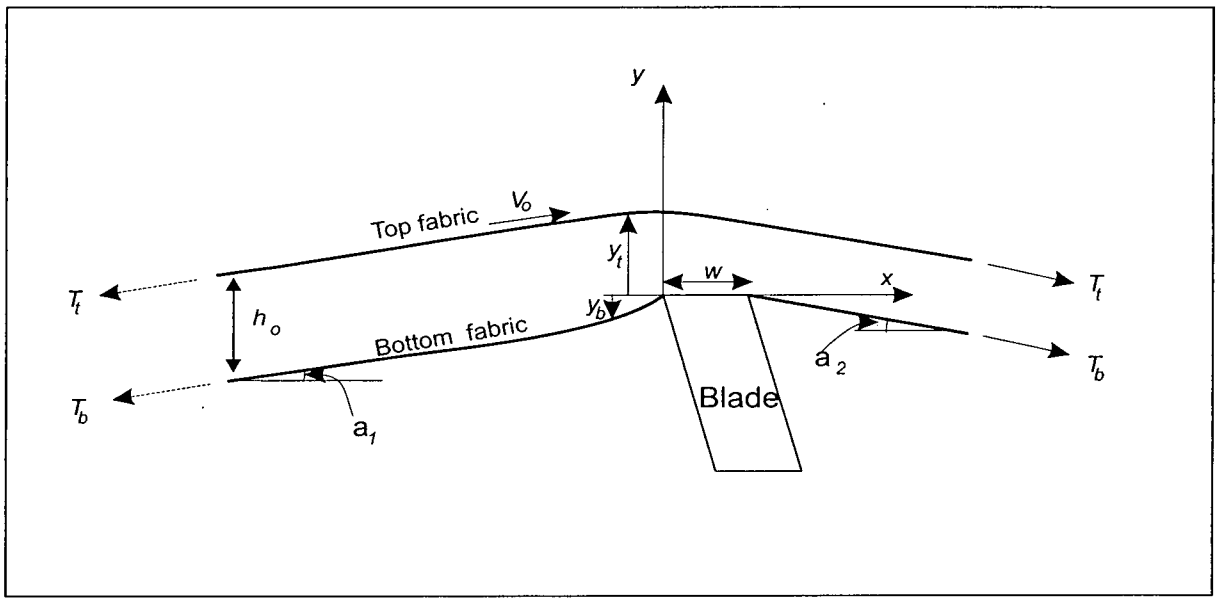

Figure 2.1: Schematic of a single blade with important physical parameters involved in the blade forming problem.

In order to obtain a closed-form expression for the pressure, we make the following assumptions:

1. The flow is steady and one-dimensional.
2. All effects of fibres, in the suspension, are neglected.
3. The pulp suspension is an inviscid fluid.
4. Darcy's Law describes the flow through the fabrics and fibre mat.
5. The permeability of the fabric and fibre mat is constant.
6. There is no centrifugal force, and thus $p = p_t = p_b$.

7. The bending stiffness of the fabric is negligible.
8. The momentum of the fabric is negligible.
9. The fabric is considered to be a thin membrane.
10. The blade and the bottom fabric surfaces are smooth.
11. Two fabrics are parallel downstream of the blade.

The flow rate per unit area from the top and bottom fabrics can be written as:

$$w_t = \overline{k}_t p \tag{2.1}$$

$$w_b = \overline{k}_b (p - p_{ext}) \tag{2.2}$$

where:

- w_t: The flow rate per unit area (in the positive y direction) though the top fabric.
- w_b: The flow rate per unit area (in the negative y direction) through the bottom fabric.
- p: The pressure in the fluid between the fabrics.
- p_{ext}: The pressure underneath the fabric passing over the blade.
- $\overline{k}_t$: The average permeability of the top fabric and fibre mat deposited on it.
- $\overline{k}_b$: The average permeability of the bottom fabric and fibre mat deposited on it.

If the gap between the fabrics, $h(x)$ is defined as $y_t - y_b$, the equation of continuity for an element dx can be written as,

$$\frac{d}{dx}(Vh) = -(\overline{k}_t + \overline{k}_b)p + \overline{k}_b p_{ext} \tag{2.3}$$

where V is the local average fluid velocity in the x direction.

For pulp suspension, the x-momentum equation is:

$$\frac{dp}{dx} + \rho V \frac{dV}{dx} = 0 \tag{2.4}$$

where ρ is the density of the fibre suspension.

The relationship between fabric tension and the pressure between the fabrics is determined by a force balance in the y-direction. Neglecting the stiffness and the momentum of the fabrics, we have the following set of fabric tension equations [28]:

$$\frac{d^2 y_t}{dx^2} = -\frac{p}{T_t} \tag{2.5}$$

$$\frac{d^2 y_b}{dx^2} = \frac{p}{T_b} - \frac{p_{ext}}{T_b} \tag{2.6}$$

where:

- T_t: The tension per unit width in the top fabric.
- T_b: The tension per unit width in the bottom fabric.

The continuity equation 2.3 can be linearized by writing, $V = V_o + \triangle V$, $h = h_o + \triangle h$, and neglecting the second order terms as:

$$h_o \frac{d}{dx}\Delta V + V_o \frac{d}{dx}\Delta h = -(\overline{k_t} + \overline{k_b})p + \overline{k}_b p_{ext} \tag{2.7}$$

We can combine 2.3 and 2.4 as:

$$-\frac{h_o}{\rho V_o}\frac{dp}{dx} + V_o(\frac{dy_t}{dx} - \frac{dy_b}{dx}) = -(\overline{k_t} + \overline{k_b})p + \overline{k}_b p_{ext} \tag{2.8}$$

Taking the derivative of the above equation and substituting the fabric tension equations 2.5 and 2.6, we obtain a general second order equation for the pressure using the

Table 2.1: Typical operating conditions.

Fabric Velocity	V_o	14	m/s
Initial Gap Size	h_o	4	mm
Tension on top Fabric	T_t	7000	N/m
Tension on bottom Fabric	T_b	7000	N/m
Wrap Angle	α_1	0.0124	$rad.$
Wrap Angle	α_2	-0.0124	$rad.$
Average permeability	$\overline{k_t}$	5×10^{-5}	$m^3/N/s$
Average permeability	$\overline{k_b}$	5×10^{-5}	$m^3/N/s$
Density	ρ	1000	kg/m^3

modified approach:

$$\frac{d^2p}{dx^2} - \frac{V_o\rho(\overline{k}_t + \overline{k}_b)}{h_o}\frac{dp}{dx} + \frac{\rho V_o^2}{h_o}\frac{T_t + T_b}{T_tT_b}p - \frac{\rho V_o^2}{h_oT_b}p_{ext} + \frac{\rho V_o\overline{k}_b}{h_o}\frac{dp_{ext}}{dx} = 0 \tag{2.9}$$

We may now calculate values of $p(x)$ for some typical cases under the typical operating conditions, shown in Table 2.1.

2.2 Infinitely Thin blade ($w = 0$)

First, we consider the simplified case where the blade is thin. We assume that the average permeability of the top and the bottom fabrics are the same, $\overline{k_t} = \overline{k_b} = \overline{k}$, and the pressure underneath the bottom fabric is zero, $p_{ext} = 0$, as assumed by Zhao and Kerekes [28]. The general Equation 2.9 can be written as:

$$\frac{d^2p}{dx^2} - \frac{2V_o\rho\overline{k}}{h_o}\frac{dp}{dx} + \frac{\rho V_o^2}{h_o}\frac{T_t + T_b}{T_tT_b}p = 0 \tag{2.10}$$

or in the simpler form:

$$\frac{d^2p}{dx^2} - a\frac{dp}{dx} + bp = 0 \tag{2.11}$$

where:

$$a = \frac{2V_o\rho\overline{k}}{h_o} \qquad and \qquad b = \frac{\rho V_o^2}{h_o}\frac{T_t + T_b}{T_t T_b} \tag{2.12}$$

The solution of the above equation yields the explicit solution for pressure:

$$p = c_1 e^{n_1 x} + c_2 e^{n_2 x} \qquad x \leq 0 \tag{2.13}$$

where:

$$n_1 = \frac{(a + \sqrt{a^2 - 4b})}{2} \tag{2.14}$$

$$n_2 = \frac{(a - \sqrt{a^2 - 4b})}{2} \tag{2.15}$$

We know that the integrated pressure is the product of the top fabric tension and the total wrap angles around the blade [32]. We also force both fabrics to make a prescribed angle to the horizontal far downstream of the blade. Then, the constants c_1 and c_2 can be determined from the following conditions:

$$p(0) = 0 \qquad and \qquad \int_{-\infty}^{0} p dx = T_t(\alpha_1 - \alpha_2)$$

Thus:

$$c_1 = -c_2 = \frac{-n_1 n_2 T_t(\alpha_1 - \alpha_2)}{n_1 - n_2} \tag{2.16}$$

The location of maximum pressure can be determined by solving $dp/dx = 0$ for x:

$$x_{max} = \ln(\frac{n_2}{n_1})(n_1 - n_2)^{-1} \tag{2.17}$$

The shape of the bottom fabric can be found from equation 2.6:

$$y_b = \frac{1}{T_t}\left(\frac{c_1}{n_1^2}e^{n_1 x} + \frac{c_2}{n_2^2}e^{n_2 x}\right) + c_3 x + c_4 \tag{2.18}$$

The constants c_3 and c_4 can be determined from the following boundary conditions:

$$y_b(0) = 0 \qquad and \qquad \frac{dy_b}{dx}(-\infty) = \alpha_1$$

The shape of the top fabric can be found from equation 2.5:

$$y_t = -\frac{1}{T_t}\left(\frac{c_1}{n_1^2}e^{n_1 x} + \frac{c_2}{n_2^2}e^{n_2 x}\right) + c_3 x + c_4 \tag{2.19}$$

The constants c_3 and c_4 can be determined from the following boundary conditions:

$$y_t(-\infty) = y_b(-\infty) + h_o \qquad and \qquad \frac{dy_t}{dx}(0) = \alpha_2$$

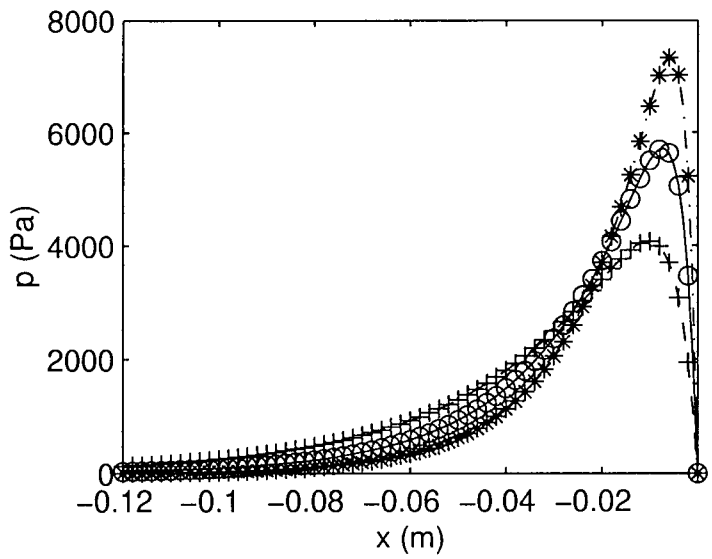

Figure 2.2: Pressure distribution in the gap for a thin blade, $V_o = 14\ m/s$ (− modified model, o ZK model), $V_o = 10\ m/s$ (−− modified model, + ZK model), $V_o = 18\ m/s$ (−.− modified model, * ZK model), other variables from Table 2.1.

Infinity was taken to be far enough from the blade that the pressure in the gap approaches to zero; typically about 120 mm upstream for the operating conditions given

in Table 2.1. Figure 2.2 shows that the pressure distributions predicted by this modified approach agree well with the ZK model. Both models predict that the pressure in the gap increases in the machine direction as the blade approached, reaches its maximum at x_{max}, and drops to zero at the blade location. Increasing the fabric velocity increases the peak pressure, but the integrated pressure remains unchanged, as expected.

2.3 Finite Width Blade

In order to determine the pressure distribution over the blade, we make the reasonable assumption that the bottom fabric makes physical contact with the blade. In consequence, in this region it is not possible for there to be flow out through the bottom fabric. We apply the same linearziation approach to obtain an explicit expression for pressure pulses over and upstream of finite flat and curved blades. In the following subsection we assume that $\overline{k_t} = \overline{k_b} = \overline{k}$.

2.3.1 Flat Blade

Since we assumed that the dewatering takes place from the top fabric over the blade, we can combine equations 2.5 and 2.8 and write:

$$\frac{d^3y_t}{dx^3} - \frac{\overline{k}\rho V_o}{h_o}\frac{d^2y_t}{dx^2} + \frac{\rho V_o^2}{h_o T_t}\frac{dy_t}{dx} = 0 \tag{2.20}$$

or in simpler form:

$$\frac{d^3y_t}{dx^3} - \acute{a}\frac{d^2y_t}{dx^2} + \acute{b}\frac{dy_t}{dx} = 0 \tag{2.21}$$

where:

$$\acute{a} = \frac{\overline{k}\rho V_o}{h_o} \qquad and \qquad \acute{b} = \frac{\rho V_o^2}{h_o T_t} \tag{2.22}$$

The second and first derivatives of y_t are:

$$\frac{d^2y_t}{dx^2} = -\frac{p}{T_t} = c_1 m_1^2 e^{m_1 x} + c_2 m_2^2 e^{m_2 x} \qquad 0 \le x \le w \tag{2.23}$$

$$\frac{dy_t}{dx} = c_1 m_1 e^{m_1 x} + c_2 m_2 e^{m_2 x} \qquad 0 \le x \le w \tag{2.24}$$

where:

$$m_1 = \frac{(\acute{a} + \sqrt{\acute{a}^2 - 4\acute{b}})}{2} \tag{2.25}$$

$$m_2 = \frac{(\acute{a} - \sqrt{\acute{a}^2 - 4\acute{b}})}{2} \tag{2.26}$$

If the blade width is w, the constant c_1 and c_2 can be determined from boundary conditions at $x = w$, where:

$$\frac{d^2y_t}{dx^2} = -\frac{p}{T_t} = 0, \qquad and \qquad \frac{dy_t}{dx} = \alpha_2$$

Thus,

$$c_1 = \frac{\alpha_2 m_2}{m_1 \exp(m_1 w)(m_2 - m_1)} \tag{2.27}$$

$$c_2 = -\frac{\alpha_2 m_1}{m_2 \exp(m_2 w)(m_2 - m_1)} \tag{2.28}$$

The pressure upstream of the blade can be determined from following equation:

$$p = c_1 e^{n_1 x} + c_2 e^{n_2 x} \qquad x \le 0 \tag{2.29}$$

The constants c_1 and c_2 are:

$$c_1 = \frac{n_1(p_m - n_2 T_t(\alpha_1 - \alpha_m))}{(n_1 - n_2)} \tag{2.30}$$

$$c_2 = -\frac{n_2(p_m - n_1 T_t(\alpha_1 - \alpha_m))}{(n_1 - n_2)} \tag{2.31}$$

where p_m and α_m are the pressure and the slope of the top fabric at the leading edge of the blade determined from Equations 2.23, 2.24, respectively. Figure 2.3 illustrates the effect of blade width on the pressure pulse development. Wide blades, as predicted by the numerical model of Green et al. [33], generate two distinguishable pulses, one associated with deflection of the fabric at the leading edge of the blade, and one corresponding with the fabric deflection at the trailing edge of the blade.

Figures 2.4 and 2.5 show the effect of the top fabric tension on pressure distributions. As with the thin blade, increasing the tension in the top fabric increases the peaks over the blade and upstream of the blade.

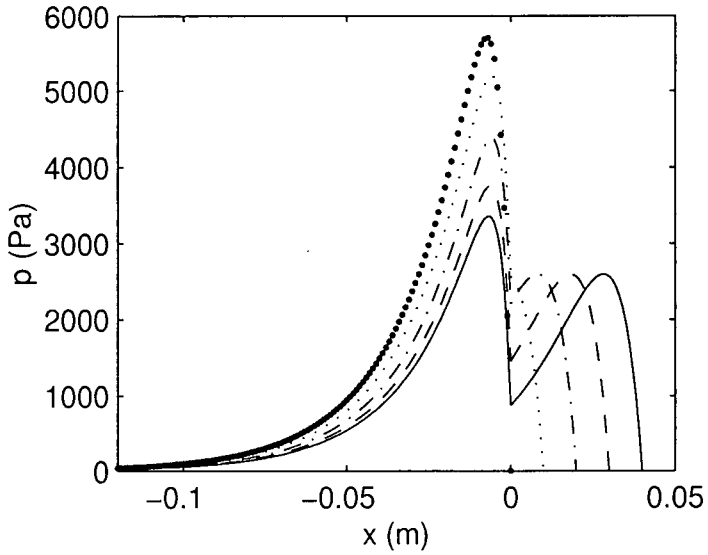

Figure 2.3: Effect of blade width on pressure distribution in the gap for the flat blades $-w = 0.04\,m$, $--\,w = 0.03\,m$, $-.-\,w = 0.02\,m$, $....\,w = 0.01\,m$, $\bullet\, w = 0$, variables from Table 2.1.

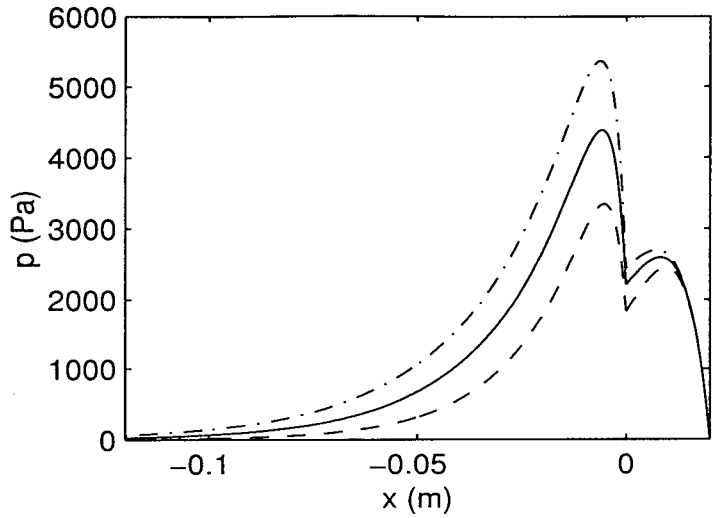

Figure 2.4: The effect of tension in the top fabric on pressure distribution in the gap, w = 0.02 m, $-T_t$= 7000 N/m, $--T_t$= 5000 N/m, $-.-T_t$= 9000 N/m, other variables from Table 2.1.

2.3.2 Curved Blade

In the following sections two analytical models are developed for two typical curved blades.

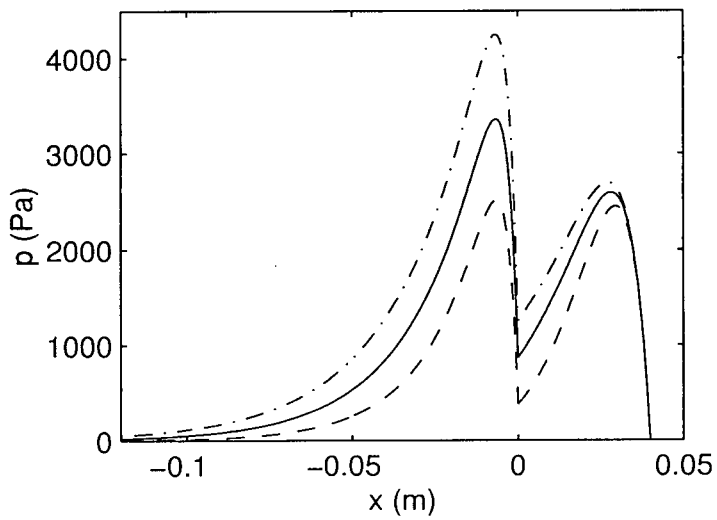

Figure 2.5: The effect of tension in the top fabric on pressure distribution in the gap, w = 0.04 m, $-T_t$= 7000 N/m, $--T_t$= 5000 N/m, $-.-T_t$= 9000 N/m , other variables from Table 2.1.

Second Order Approximation of Blade Surface

Here we assume that the surface of the curved blade can be approximated by:

$$y = f_1 x + f_2 x^2 \tag{2.32}$$

If θ_1 and w are the nose angle (angle relative to the blade land at the blade leading edge), and blade width, respectively, f_1 and f_2 are (Figure 2.6):

$$f_1 = \theta_1,\ f_2 = -\frac{\theta_1}{w}$$

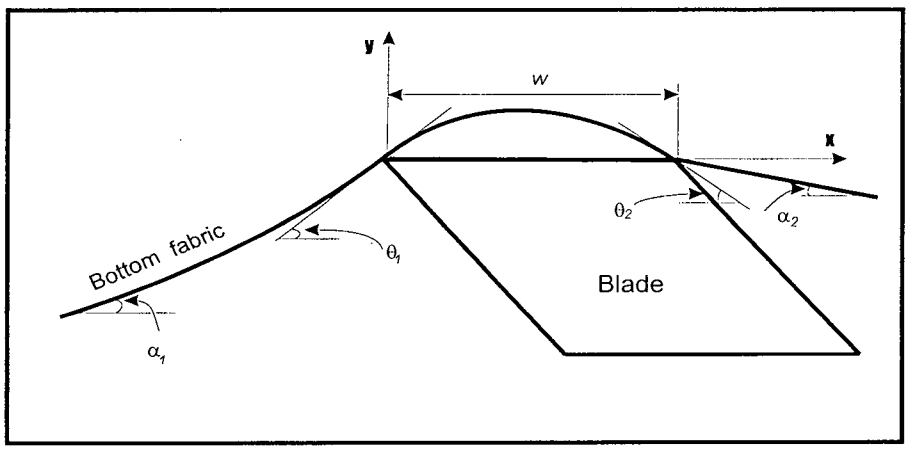

Figure 2.6: Second order approximation of blade surface shapes.

For the top fabric over the blade we can write:

$$\frac{d^3 y_t}{dx^3} - \frac{2\bar{k}\rho V_o}{h_o}\frac{d^2 y_t}{dx^2} + \frac{\rho V_o^2}{h_o T_t}\frac{dy_t}{dx} - \frac{\rho V_o^2}{h_o T_t}\frac{dy}{dx} = 0 \tag{2.33}$$

or:

$$\frac{d^3 y_t}{dx^3} - \acute{a}\frac{d^2 y_t}{dx^2} + \acute{b}\frac{dy_t}{dx} - \acute{b}\frac{dy}{dx} = 0 \tag{2.34}$$

The solution yields the following equations for the second and first derivatives of y_t:

$$\frac{d^2 y_t}{dx^2} = -\frac{p}{T_t} = 2f_2 + c_1 m_1^2 e^{m_1 x} + c_2 m_2^2 e^{m_2 x} \qquad 0 \le x \le w \tag{2.35}$$

$$\frac{dy_t}{dx} = \frac{2\acute{a}f_2}{\acute{b}} + f_1 + 2f_2x + c_1m_1e^{m_1x} + c_2m_2e^{m_2x} \qquad 0 \leq x \leq w \tag{2.36}$$

As for the flat blade, the constants c_1 and c_2 can be determined from boundary conditions at $x = w$,

$$\frac{d^2y_t}{dx^2} = -\frac{p}{T_t} = 0, \qquad and \qquad \frac{dy_t}{dx} = \alpha_2$$

The constant c_1 and c_2 are:

$$c_1 = -\frac{m_2\acute{b}y'(w) + (m_2\acute{a} - \acute{b})y''(w) - m_2\acute{b}\alpha_2}{m_1\acute{b}\exp(m_1w)(m_2 - m_1)} \tag{2.37}$$

$$c_2 = \frac{m_1\acute{b}y'(w) + (m_1\acute{a} - \acute{b})y''(w) - m_1\acute{b}\alpha_2}{m_2\acute{b}\exp(m_2w)(m_2 - m_1)} \tag{2.38}$$

The pressure upstream of the blade can be determined from equation 2.29. Figure 2.7 shows three curved blade shapes. Corresponding pressure distributions are shown in Figure 2.8. Blades for which all or most of the wrap is taken at the blade nose and heel (e.g. $\theta_1 \leq 0.005$ *rad.*) develop two distinct pressure pulses on the blade, one associated with fabric wrap at the blade nose, and one with fabric wrap at the blade heel. As the blade nose and heel angles increase, the pressure pulse over the blade becomes more flat and two pressure pulses merge together. Finally, when the leading and trailing blade angles match the far field fabric angle, the central pressure pulse is dominant; the leading and tailing edge pulses are subsumed within the central pulse.

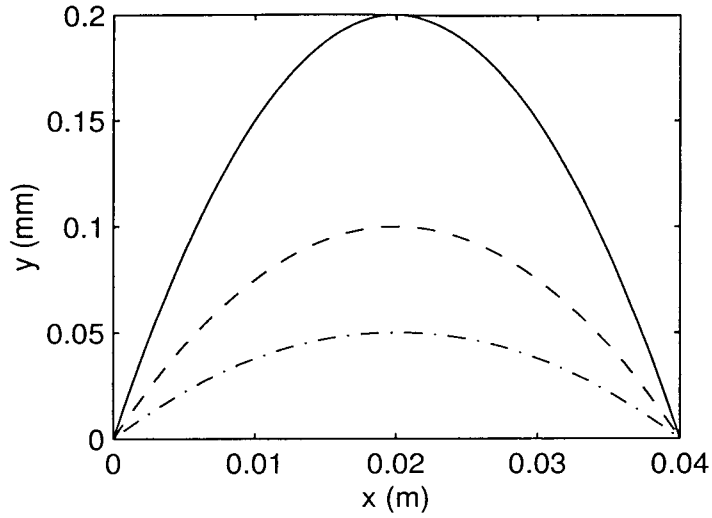

Figure 2.7: Blade surface shapes, corresponding pressure distributions are shown in the next figure, $w = 0.04\ m$, $-\theta_1 = 0.02\ rad.$, $--\theta_1 = 0.01\ rad.$, $-.-\theta_1 = 0.005\ rad.$, $\alpha_1 = -\alpha_2 = 0.02\ rad.$, other variables from Table 2.1.

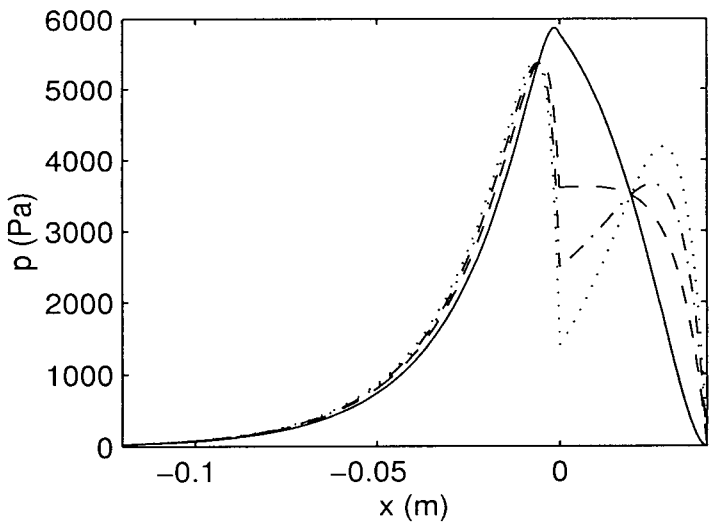

Figure 2.8: Pressure distributions for curved blades, $w = 0.04\ m$, $-\theta_1 = 0.02\ rad.$, $--\theta_1 = 0.01\ rad.$, $-.-\theta_1 = 0.005\ rad.$, $\alpha_1 = -\alpha_2 = 0.02\ rad.$, ... flat blade, other variables from Table 2.1.

Fourth Order Approximation of Blade Surface

It is also possible to quantify the curved blade by measuring the blade crown, c (height above the line joining the blade leading and trailing edges), even if the blade nose and tail angles are fixed. For this case, the surface of the blade can be described by:

$$y = f_1 x + f_2 x^2 + f_3 x^3 + f_4 x^4 \tag{2.39}$$

where the coefficients can be determined by fixing the blade width w, the nose angle θ_1, and the crown c:

$$f_1 = \theta_1,\ f_2 = \frac{16c - 5\theta_1 w}{w^2},\ f_3 = 8\frac{\theta_1 w - 4c}{w^3},\ f_4 = 4\frac{4c - \theta_1 w}{w^4}$$

For this case the solution of 2.33 yields the following equations for the first and the second derivatives of y_t:

$$\frac{d^2 y_t}{dx^2} = y'' + \frac{\acute{a} y'''}{\acute{b}} + \frac{(\acute{a}^2 - \acute{b}) y^{(4)}}{\acute{b}^2} + c_1 m_1^2 e^{m_1 x} + c_2 m_2^2 e^{m_2 x}\ \ 0 \le x \le w \tag{2.40}$$

$$\frac{dy_t}{dx} = y' + \frac{\acute{a} y''}{\acute{b}} + \frac{(\acute{a}^2 - \acute{b}) y'''}{\acute{b}^2} + \frac{(\acute{a}^3 - 2\acute{a}\acute{b}) y^{(4)}}{\acute{b}^3} +$$

$$c_1 m_1 e^{m_1 x} + c_2 m_2 e^{m_2 x}\ \ 0 \le x \le w \tag{2.41}$$

The constants c_1 and c_2 are:

$$c_1 = \frac{m_2 \acute{b}^3 y'(w) + (m_2 \acute{a}\acute{b}^2 - \acute{b}^3) y''(w) + (m_2 \acute{a}^2 \acute{b} - m_2 \acute{b}^2 - \acute{a}\acute{b}^2) y'''(w)}$$

$$\frac{+(m_2 \acute{a}^3 - 2m_2 \acute{a}\acute{b} + \acute{b}^2 - \acute{a}^2 \acute{b}) y^{(4)}(w) - m_2 \alpha_2 \acute{b}^3}{m_1 \acute{b}^3 \exp(m_1 w)(m_1 - m_2)} \tag{2.42}$$

$$c_2 = -\frac{m_1\acute{b}^3 y'(w) + (m_1\acute{a}\acute{b}^2 - \acute{b}^3)y''(w) + (m_1\acute{a}^2\acute{b} - m_1\acute{b}^2 - \acute{a}\acute{b}^2)y'''(w)}{+(m_1\acute{a}^3 - 2m_1\acute{a}\acute{b} + \acute{b}^2 - \acute{a}^2\acute{b})y^{(4)}(w) - m_1\alpha_2\acute{b}^3}{m_2\acute{b}^3\exp(m_2 w)(m_1 - m_2)} \tag{2.43}$$

where:

$$y'(w) = -\theta_1,\ y''(w) = \frac{32c - 10\theta_1 w}{w^2}$$

$$y'''(w) = 48\frac{4c - \theta_1 w}{w^3},\ y^{(4)}(w) = 96\frac{4c - \theta_1 w}{w^4}$$

The influence of the blade crown variations is illustrated in Figure 2.9. Figure 2.10

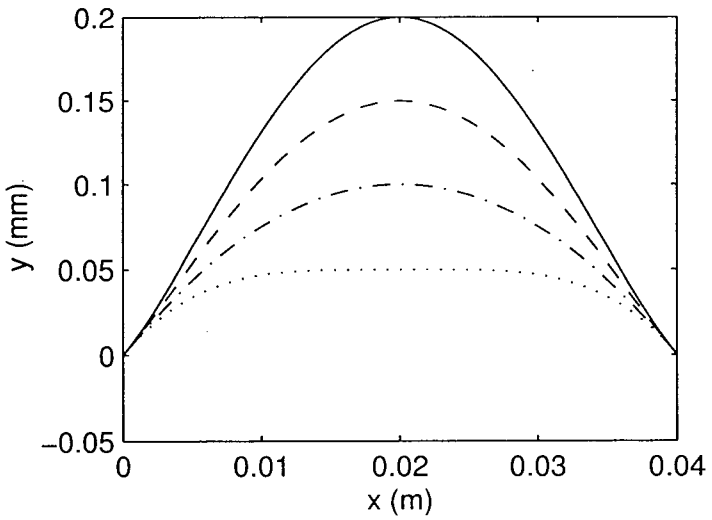

Figure 2.9: Blade surface shapes, corresponding pressure distributions are shown in the next figure, $w = 0.04\ m$, $-c = 0.2\ mm$, $- - c = 0.15\ mm$, $-. - c = 0.1\ mm$, ... c = $0.05\ mm$, $\theta_1 = -\theta_2 = 0.01\ rad.$, $\alpha_1 = -\alpha_2 = 0.02\ rad.$, other variables from Table 2.1

shows the corresponding pressure distributions. With small blade crown e.g. $c = 0.05$ mm, the blade shape has two regions of small radius of curvature near the leading and trailing edges. Consequently, one pressure pulse is generated in each of these locations. By increasing the crown the central pulse forms. Finally, for large blade crown , e.g. $c =$

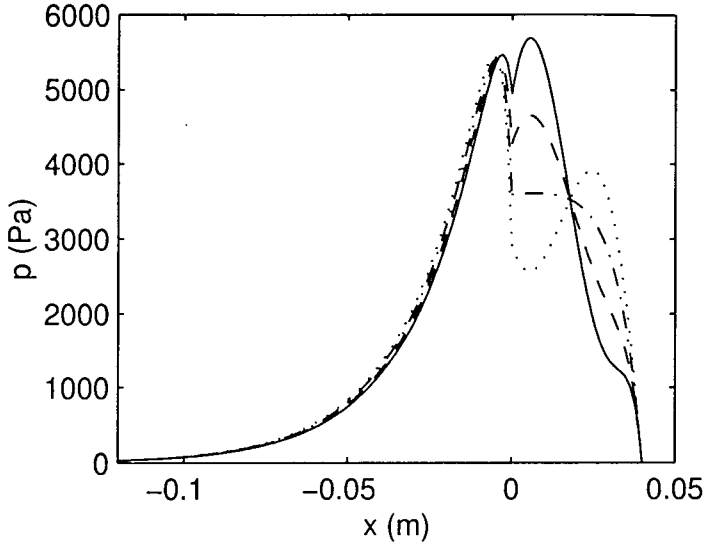

Figure 2.10: Pressure distributions for curved shaped blades, $w = 0.04\ m$, $-c = 0.2\ mm$, $- - c = 0.15\ mm$, $-. - c = 0.1\ mm$, ... c = $0.05\ mm$, $\theta_1 = -\theta_2 = 0.01\ rad.$, $\alpha_1 = -\alpha_2 = 0.02\ rad$, other variables from Table 2.1.

$0.2\ mm$, the central pulse dominates pulses at the leading and trailing edges.

2.4 Summary

The discussion and analysis of this chapter have shown how pressure pulses can be calculated for several cases of practical interest. The modified approach which gives directly a second order differential equation for the pressure provides the same results for single thin blades as the original and experimentally verified model of Zhao and Kerekes [28] does. Upon confirming the modified approach with their model, the finite width blades were considered and it was shown that the thin blade model was a special case of the more general model of finite width blades.

The results from these models will serve as initial guesses for a two-dimensional viscous model of single blade that will be presented in the next chapter.

Chapter 3

Two Dimensional Viscous Model of Single Blades

In Chapter 2 the analytical one-dimensional model of Zhao and Kerekes [28] for a thin blade was extended to study a single curved blade. It was assumed that the pulp suspension to be an inviscid fluid. Based on the same assumption, Zahari and Bark [31] developed a two-dimensional potential model of a single blade. The objective of this chapter is to develop a two-dimensional viscous model and study the hydrodynamics of blade gap formers in more detail. Thus this chapter presents the analysis, method of solution, and the results of such a model. The numerical method developed in this chapter involves an iterative process. The analytical one-dimensional models developed in Chapter 2 always provide very good initial guesses to start this process.

3.1 Analysis

Figure 2.1 shows a schematic of a single blade with the important physical parameters involved in the blade forming problem. As mentioned, the objective of this chapter is to develop a two-dimensional model of blade gap forming that solves the full Navier-Stokes equations for the fluid flow and force balance equations for the location of fabrics. The following assumptions are made to simplify the governing equations:

1. The flow is steady and two dimensional.
2. All effects of fibres are neglected.
3. The pulp is considered to be an incompressible Newtonian fluid (pure water).
4. Darcy's Law can be used to model the flow through the fabrics.
5. Far upstream and far downstream of the blade the fabrics are straight and parallel with angles α_1 (far upstream) and α_2 (far downstream) relative to the horizontal.

6. The permeability and the thickness of the fabric and fibre mat to it is constant.
7. There is no external under-fabric pressure or doctoring pressure.
8. The edge of the blade is sharp and the bottom fabric follows the shape of the blade surface.
9. Fabrics have no mass and stiffness.
10. The blade and bottom fabric surfaces are smooth.

In view of the above assumptions, the governing equations can be considered. To model the blade gap former, five equations must be used. Three of the equations model the behavior of the fluid. Continuity and two momentum equations (Navier-Stokes for flow in the gap and Darcy's Law for flow through the fabrics). Two force balance equations can be used to calculate the shape of the fabrics. In order to simplify the problem these five equations can be de-coupled. Thus the effects of the flow and fabrics can be considered separately.

3.1.1 Fluid Flow Equations

The continuity equation is:

$$\frac{\partial u}{\partial x} + \frac{\partial v}{\partial y} = 0 \tag{3.1}$$

The steady two-dimensional Navier-Stockes (fluid momentum) equations are:

$$\rho(u\frac{\partial u}{\partial x} + v\frac{\partial u}{\partial y}) = -\frac{\partial p}{\partial x} + \mu(\frac{\partial^2 u}{\partial x^2} + \frac{\partial^2 u}{\partial y^2}) \tag{3.2}$$

$$\rho(u\frac{\partial v}{\partial x} + v\frac{\partial v}{\partial y}) = -\frac{\partial p}{\partial y} + \mu(\frac{\partial^2 v}{\partial x^2} + \frac{\partial^2 v}{\partial y^2}) \tag{3.3}$$

Equations 3.2 and 3.3 are replaced by Darcy's Law in the porous media part of the

domain, where fibre mat and fabrics are present:

$$\frac{\partial p}{\partial x} = -\frac{R_x}{F_t}u \tag{3.4}$$

$$\frac{\partial p}{\partial y} = -\frac{R_y}{F_t}v \tag{3.5}$$

where F_t is thickness of the fibre mat and fabric, and R_x and R_y are the resistances of the porous media (fibre mat and fabric) in the x, and y directions, respectively. The above equations determine the following three unknowns:

- The fluid velocity $u(x, y)$,
- The fluid velocity $v(x, y)$,
- The pressure in the fluid $p(x, y)$.

3.1.2 Force Balance Equations

The relation between fabric tension and pressure between the fabrics was obtained in [28]. The force balance equations for the top and bottom fabrics are:

$$\frac{d^2y_t}{dx^2} + \frac{p_t}{T_t} = 0 \tag{3.6}$$

$$\frac{d^2y_b}{dx^2} - \frac{p_b}{T_b} = 0 \tag{3.7}$$

where p_t and p_b are the pressure distributions on the top and the bottom fabrics, respectively. Given the acting fluid pressure on the top and bottom fabrics, the above two equations determine the following two unknowns:

- The shape of the top fabric $y_t(x)$,
- The shape of the bottom fabric $y_b(x)$.

3.2 Method of Solution

The method of solution of the governing equations is as follows. First, the location of the fabrics is calculated using the analytical one-dimensional model (Chapter 2). Then, the governing equations for the fluid are solved using FLUENT CFD code [49]. FLUENT uses a control volume based technique [50] to convert the differential conservation equations 3.1-3.5 to algebraic equations that can be solved numerically. In the porous media part of the domain, the permeability of the porous media in the x- direction $k_x = 1/R_x$ is set to a large value. Also, the u-component of velocity is fixed to the fabric velocity. These conditions guarantee that the fabrics have no effect on the fluid velocity through the porous media in the x direction. The second order upwind interpolation scheme was employed. The solution was considered to converge when normalized residuals fell below 5×10^{-4}. The pressure calculated by FLUENT on the top and bottom fabrics were then applied to the force balance equations to find the new shapes of the fabrics. The force balance equations were solved by using a standard finite difference method. A three-point approximation on a uniform grid size ($\Delta x = 0.5\ mm$) was used for interior nodes. For boundary conditions a three-point approximation was applied to the slope. The whole process was repeated by supplying the new fabric locations to FLUENT and solving the new fluid field in the new fixed geometry. These iterations were repeated until the pressure satisfies both the fluid flow and force balance equations, as indicated by an L_2 (1×10^{-4}) global norm of difference convergence criterion on the fabric displacement. Because the fabric shapes obtained from the one-dimensional model provide a good initial guess, usually only few iterations were necessary to converge on a correct solution.

3.3 Boundary Conditions

The above equations can be solved subject to the following boundary conditions.

3.3.1 Fluid Flow Boundary Conditions

The following fluid flow boundary conditions were used. We know that the velocity of fluid far upstream of a blade is equal to the fabric velocity. Also, the fluid gauge pressure

downstream of the blade approaches zero, which is consequence of the parallelism of the two fabrics. The gauge pressure on the outer surface of the fabrics is zero as well. In the case of a finite width blade, it was assumed that the bottom fabric follows the blade surface. Thus, the blade surface acts as a frictionless wall. In solving for the fluid flow, the curved physical space was mapped onto a rectangular computational domain. In view of the above discussion, the boundary conditions on this domain are:

- Inflow normal velocity upstream equal to the fabric velocity.
- Zero static pressure at downstream boundary.
- Zero static pressure at top boundary.
- Zero static pressure at bottom of domain.
- Slip wall where there is contact between the bottom fabric and the blade surface.

3.3.2 Fabric Boundary Conditions

The Equation 3.7 applies over the regions upstream and downstream of the blade, where the bottom fabric is not in contact with the blade. To solve each force balance equation, two boundary conditions are needed. The first boundary condition is the location of the bottom fabric right at the leading and trailing edges of the blade. The second boundary condition is the slope of the fabric far upstream and downstream of the blade (wrap angle). Over the blade, the surface of the blade represents the shape of the bottom fabric. These boundary conditions can be written as follows:

$$Upstream \qquad y_b(0) = 0, \quad \frac{dy_b}{dx}(-\infty) = \alpha_1 \tag{3.8}$$

$$Downstream \qquad y_b(w) = 0, \quad \frac{dy_b}{dx}(\infty) = \alpha_2 \tag{3.9}$$

where the blade runs between $x = 0$ and $x = w$.

Table 3.1: Typical operating conditions

Velocity of fabric	V_o	16	m/s
Upstream gap size	h_o	3	mm
Top fabric tension	T_t	7000	N/m
Bottom fabric tension	T_b	7000	N/m
Upstream wrap angle	α_1	0.71	$degree$
Downstream wrap angle	α_2	-0.71	$degree$
Resistance of fibre mat + fabric	R_t	20000	$Pa-s/m$
Resistance of fibre mat + fabric	R_b	20000	$Pa-s/m$
Blade width	w	30	mm
Density of suspension	ρ	1000	kg/m^3
Viscosity of suspension	μ	0.001	$Pa-s$

For the top fabric, the location of the fabric far upstream of the blade and its slope far downstream of the blade are applied. These boundary conditions can be written as follows:

$$y_t(-\infty) = y_b(-\infty) + h_o \tag{3.10}$$

$$\frac{dy_t}{dx}(\infty) = \alpha_2 \tag{3.11}$$

where h_o is the far upstream gap size. In the simulations, infinity was taken to be far enough from the blade that the pressure in the gap approaches to zero; typically about 120 mm upstream and 30 mm downstream of the blade, respectively.

3.4 Results

In this section, first the results of thin blade and then the results of finite width blade simulations are presented. The typical operating conditions of a gap former, shown in Table were considered as primarily fixed variables in all subsequent simulations.

3.4.1 Infinitely Thin Blade ($w = 0$) Results

Comparison of Analytical One-Dimensional and Two-Dimensional Viscous Results

In order to compare the new viscous model with the analytical one-dimensional model, three cases are considered with different fabric tensions. Comparisons between pressure pulses obtained from the analytical one-dimensional and two-dimensional viscous models are shown in Figures 3.1, 3.2, and 3.3. In these figures the generated pressures between the two fabrics are plotted as a function of distance upstream and downstream of the thin blade. The point $x = 0$ corresponds with the location of the thin blade. The pressures p_m, p_t, and p_b represent the pressure distributions along the gap centre line, on the top fabric, and on the bottom fabric. The pressure p_{1D} is the pressure distribution obtained from the one-dimensional model. Both models predict that the pressure pulse forms primarily in front of the blade location. The two-dimensional model predicts pressure pulses with a somewhat lower amplitude than the one-dimensional model, but with a broader pulse peak. Both this two-dimensional viscous model and the two-dimensional potential flow model of Zahrai and Bark [31] predict a negative pressure on the bottom fabric just downstream of the blade. The rapid turning of the fluid at the sharp blade edge accounts for this negative pressure on the bottom fabric.

The Influence of Grid Size

In order to examine the effect of grid size on pressure pulses, different grid sizes were used. The number of cells, originally 45000, was increased in both directions to 180000. The computed pressure pulses were found to be almost identical and independent of the grid size. Figure 3.4 and 3.5 show the effect of grid size on pressure pulses generated by a thin blade. Note that almost the dashed curves lie atop the solid curves, and thus are not visible.

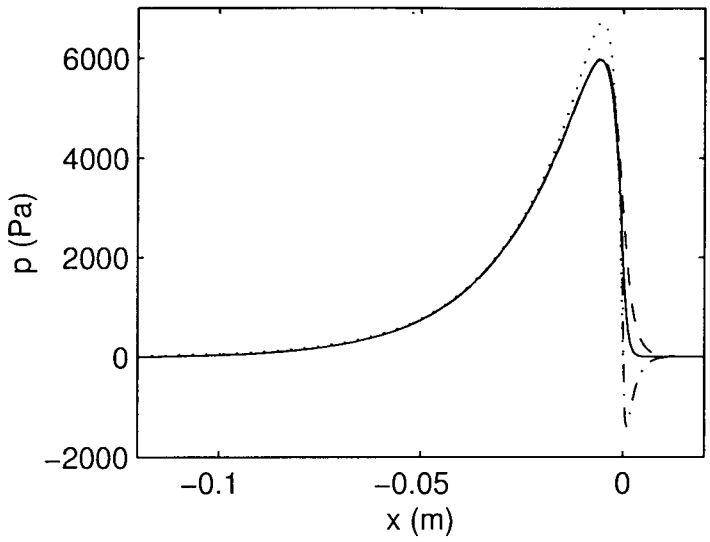

Figure 3.1: Comparison of analytical one-dimensional and two-dimensional viscous pressure pulses, $-p_m$, $--p_t$, $-.-p_b$, ... p_{1D}, variables from Table 3.1.

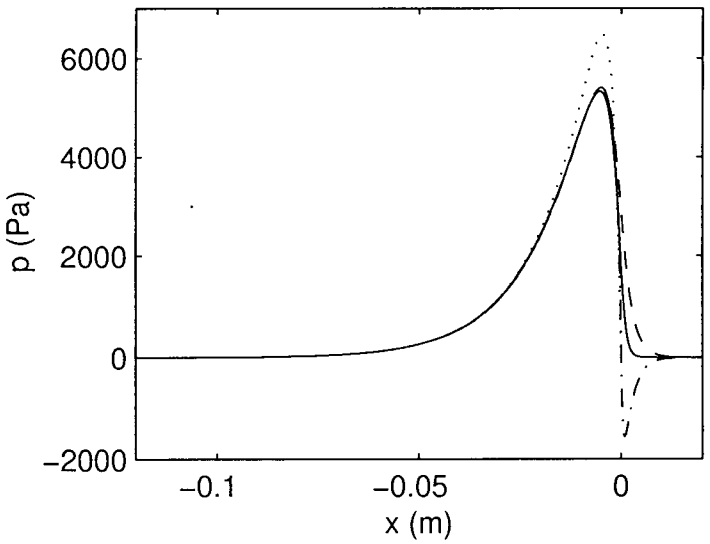

Figure 3.2: Comparison of analytical one-dimensional and two-dimensional viscous pressure pulses $T = 5000\ N/m$, $-p_m$, $--p_t$, $-.-p_b$, ...p_{1D}, other variables from Table 3.1.

The Effect of Viscosity

To determine the effect of fluid viscosity on pressure pulse, two different cases were run. The viscosity was set first to $10^{-3}\ Pa-s$ (viscosity of water) and then to $5\times10^{-3}\ Pa-s$.

In both cases the permeability of the fabric and fibre mat were adjusted in order to simulate water flow through them. The pressure pulses along the centre line of the gap, p_m, are shown in Figure 3.6. It is apparent that the effect of viscosity on the pressure pulses is negligible.

Effect of Fabric Tension

Figure 3.7 shows the effect of fabric tension on the centre line pressure pulses, p_m induced by the blade. The solid-curve represents the pressure distribution obtained from a simulation using the variables in Table 3.1. Fixing all other variables and increasing the fabric tension from 7000 N/m to 9000 N/m increases the peak pressure by 8.4% and the size of the pressure zone upstream of the blade by about 20%. As a result, the integrated pressure in the fluid in contact with the top fabric increases by almost 26%, from 173.6 $Pa - m$ to 219.9 $Pa - m$. On other hand, reducing the fabric tension to 5000 N/m, decreases the peak pressure and the size of the pressure pulse zone by 10.8%, and about 20%, respectively. For this case the integrated pressure drops by almost 30% to 122.1 $Pa - m$.

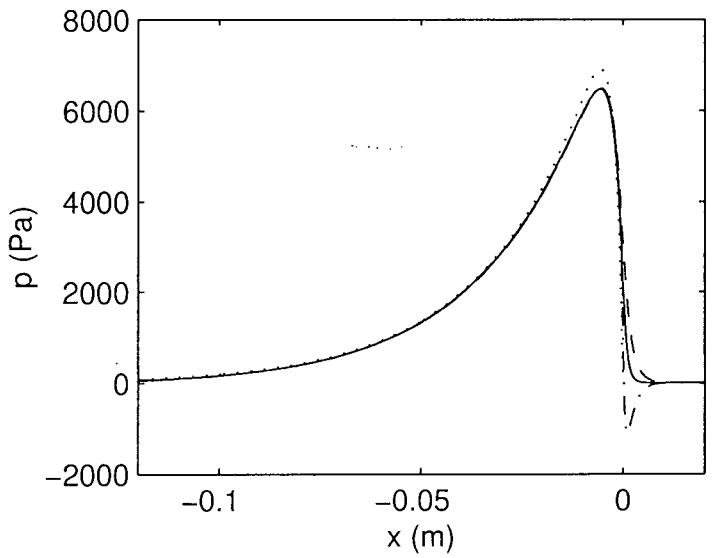

Figure 3.3: Comparison of analytical one-dimensional and two-dimensional viscous pressure pulses $T = 9000\ N/m$, $-p_m$, $- - p_t$, $-. - p_b$, $....p_{1D}$, other variables from Table 3.1.

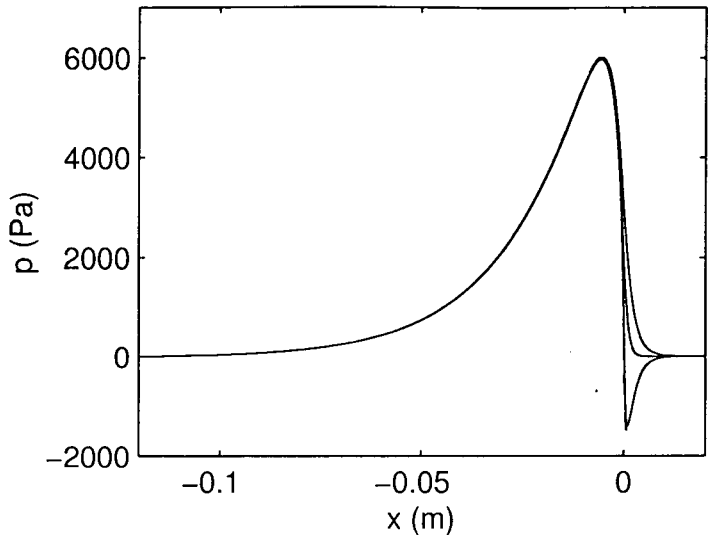

Figure 3.4: The influence of grid size on the pressure pulse, variables from Table 3.1. The pressure at the top, middle, and bottom of the gap are shown, −45000 cells, − − 180000 cells. Note that the dashed curves lies almost atop the solid curves.

Effect of Fabric Wrap Angles

The integrated pressure in the fluid at the top fabric is directly proportional to the total wrap angles. Therefore one might anticipate that both the integrated pressure and the

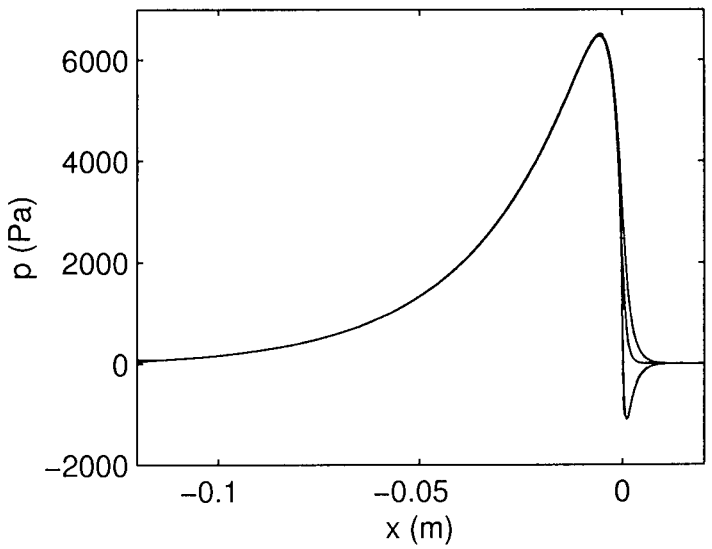

Figure 3.5: The influence of grid size on the pressure pulse, −45000 cells, − −180000 cells, $T = 9000N/m$, other variables from Table 3.1.Note that the dashed curves lies almost atop the solid curves.

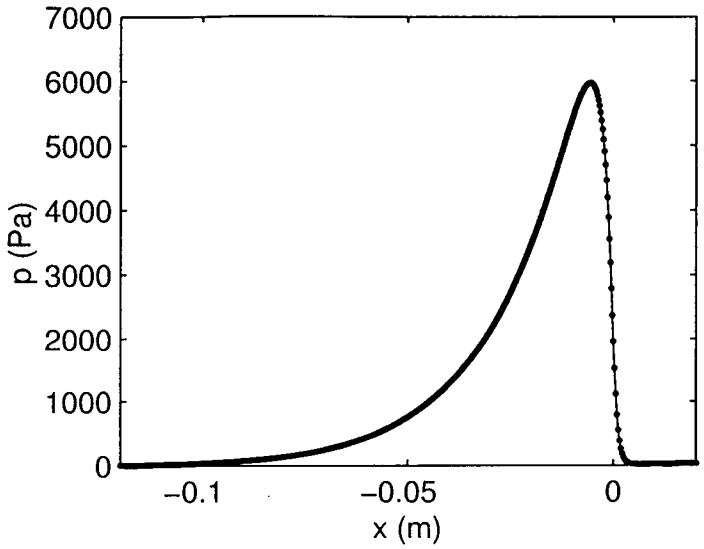

Figure 3.6: The influence of viscosity on the pressure pulse, -10^{-3} $(Pa-s)$, • 5×10^{-3} $(Pa-s)$ other variables from Table 3.1.

pressure distribution are affected by the wrap angles. The influence of three different wrap angles on the pressure distributions are illustrated in Figure 3.8. As expected, increasing the wrap angles both upstream and downstream of the blade from 0.71 *degree* to 1.4 *degree*, increases the integrated pressure on the top fabric by a factor of almost 2, from 173.6 $Pa-m$ to 342.2 $Pa-m$. The peak pressure also increases about 110% to 12600 Pa. The region of elevated pressure is extended about 10% upstream of the blade relative to the low angle case. On the other hand, reducing the fabric wrap angles upstream and downstream of the blade from 0.71 *degree* to 0.35 *degree* has the opposite effects. The integrated pressure at the top fabric reduces by a factor of almost 2 to 85.1 $Pa-m$. Peak pressure and pressure distribution range decrease by 51.4%, and about 8%, respectively.

Effect of Average Resistance of Fibre Mat and Fabric

The resistance of fibre mat increases in the downstream of direction as a result of fibre buildup on the fabric. In this section we do not attempt to model the variation of the fibre mat and its resistance in the machine direction. Rather, we assume that the resistance is constant and equal to the average of the resistance over the range of the pressure pulse. Figure 3.9 shows the effect of the average resistance of the fibre mat and fabric on pressure

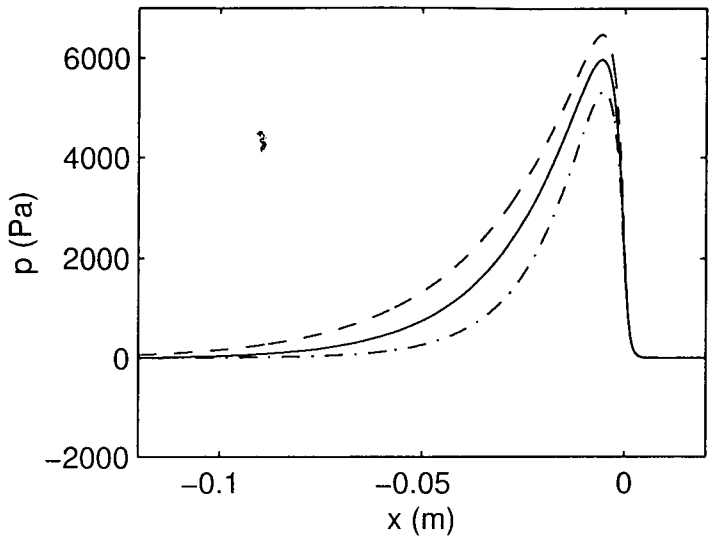

Figure 3.7: Effect of tension on pressure pulse, $-T = 7000\,(N/m)$, $--T = 9000\,(N/m)$, $-.-T = 5000\,(N/m)$, other variables from Table 3.1.

distributions. For the low resistance case, it was necessary to extend the computational domain farther upstream to ensure that the pressure in the gap approaches the gauge pressure. In general, higher resistance is associated with higher peak pressure. Increasing the average resistance to 30000 $Pa - s/m$ yields a peak pressure of 7990 Pa; about 34% higher compared to the peak pressure obtained with an average resistance of 20000 $Pa-s/m$. The other effect of the higher average resistance is the narrowing of the pressure distribution. Reducing the average resistance from a typical value of 20000 $Pa - s/m$ to 10000 $Pa - s/m$ extends the pressure distribution range about 200% upstream of the blade and reduces the peak pressure by about 40%.

Effect of Fabric Velocity

The effect of fabric velocity on the pressure pulse is shown in Figure 3.10. If the fabric velocity increases from 16 m/s to 24 m/s, the peak pressure increases by 38%. Higher fabric velocity narrows the pressure distribution. Reducing the fabric velocity from 16 m/s to 10 m/s extends the pressure distribution range by about 200% and reduces the peak pressure by about 32% to 4080 Pa.

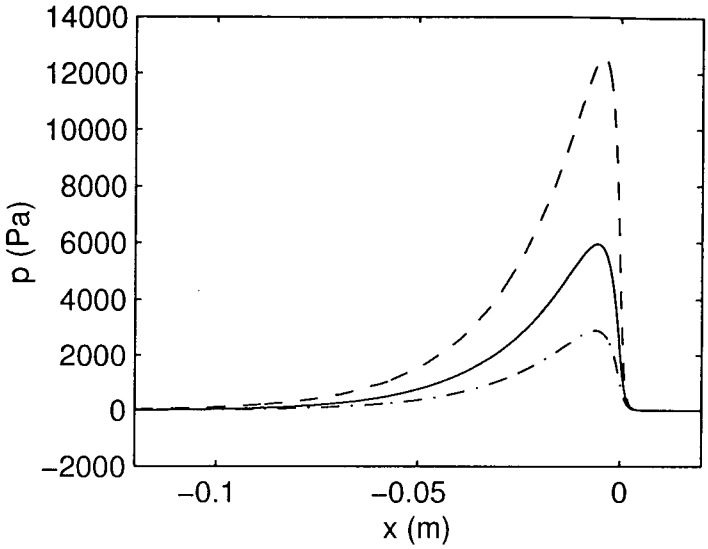

Figure 3.8: Effect of wrap angles on pressure pulse, $-\alpha_1 = -\alpha_2 = 0.71\,degree$, $--\ \alpha_1 = -\alpha_2 = 1.4\,degree$, $-.-\ \alpha_1 = -\alpha_2 = 0.35\,degree$, other variables from Table 3.1.

Velocity Profile

Figure 3.11 shows the velocity profiles in different cross section in the gap. As shown, the difference between the fluid and fabric velocities causes thin boundary layers to be formed

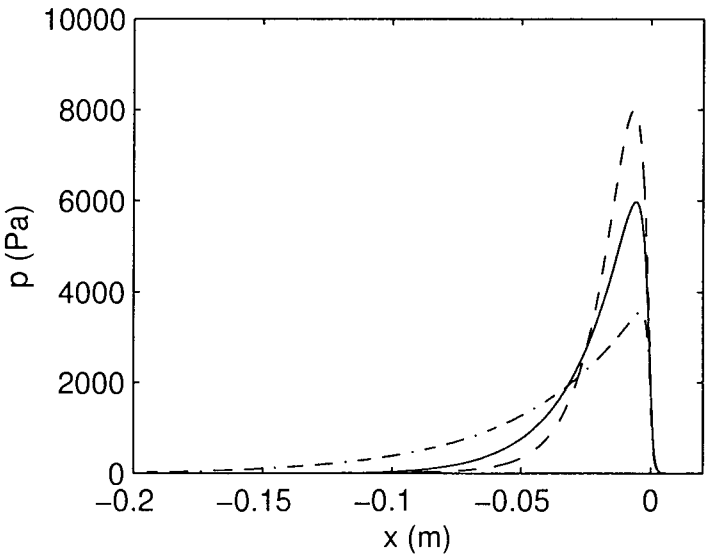

Figure 3.9: Effect of average fibre mat and fabric on pressure pulse, $-R = 20(kPa-s/m)$, $--\ R = 30\ (kPa-s/m)$, $-.-\ R = 10\ (kPa-s/m)$, other variables from Table 3.1.

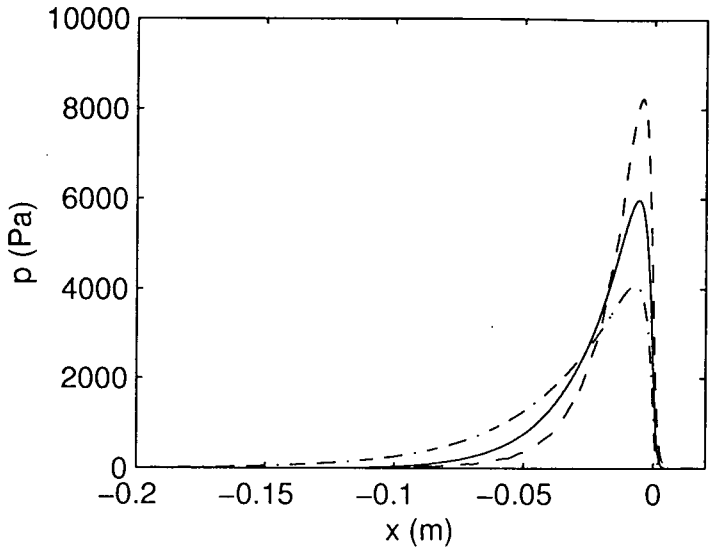

Figure 3.10: Effect of fabric velocity on pressure pulse, $-V_o = 16(m/s)$, $--V_o = 24(m/s)$, $-.-V_o = 10\ (m/s)$, other variables from Table 3.1.

on the fabrics. The variation of fluid velocity outside the boundary layer is small. The velocity gradient in the vertical direction produces a shearing stress in the fluid, which is believed to result in improved paper formation. The fluid velocity inside of the fabrics

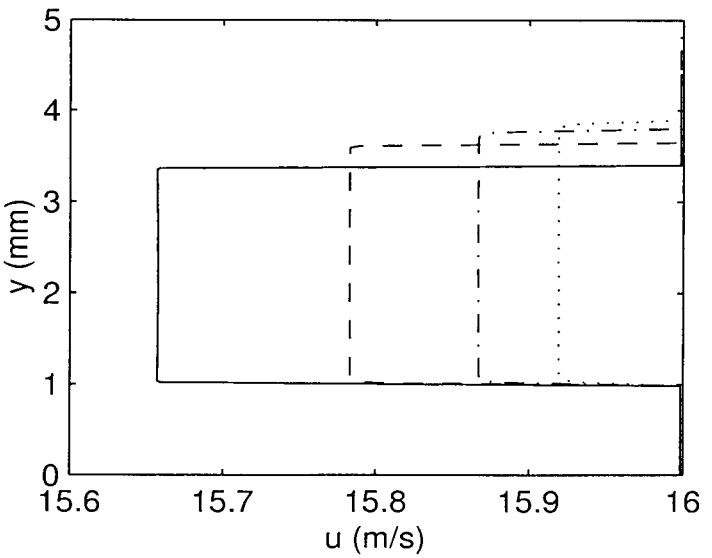

Figure 3.11: u component of the fluid velocity, $-$ 10 mm upstream of the blade, $--$ 20 mm upstream of the blade, $-.-$ 30 mm upstream of the blade, ... 40 mm upstream of the blade, variables from Table 3.1.

(of 1 mm thickness) is equal to the fabric velocity.

Figures 3.12 and 3.13 show the fluid velocity variations in the vertical direction 1.5 mm upstream and downstream of the thin blade for different fabric tensions. The variation of fluid velocity outside the boundary layer upstream of the blade is still small. Downstream of the blade the fluid moves faster than the fabric in the region close to the bottom fabric, which is consistent with the low pressure near the bottom fabric. For a short distance downstream of the blade, pulp suspension outside of the boundary layer experiences shear stress as well.

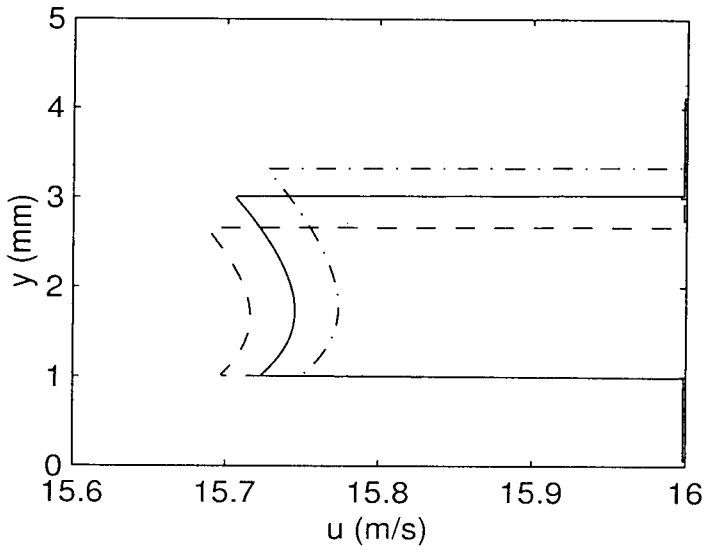

Figure 3.12: u component of the fluid velocity 1.5 mm upstream of the thin blade for different fabric tensions, $-T_t$= 7000 N/m, $--T_t$= 9000 N/m, $-.-T_t$= 5000 N/m, other variables from Table 3.1.

3.4.2 Finite Width Blade Results

For the case of a blade of finite width, it was assumed that over the blade the bottom fabric makes physical contact with the blade. In consequence, in this region it is not possible for there to be flow out through the bottom fabric. Equation 3.7 applies over the two regions upstream and downstream of the finite blade, where the bottom fabric is not in contact with it. Figure 3.14 shows a comparison between pressure pulses obtained from the analytical one-dimensional model developed in Chapter 2 and two-dimensional viscous

model for a 30 *mm* wide flat blade. Both models predict two pressure pulses, associated with fabric bending around the leading and trailing edges. The peak pressures upstream of the blade and over the blade are about 11% and 15% lower than those predicted by the one-dimensional model. The two-dimensional model predicts two negative pressures on the bottom fabric, one just upstream of the blade leading edge, and the second just downstream of the blade trailing edge. The first sudden pressure drop is a result of the no-stiffness assumption made earlier. In reality the fabric stiffness causes the bottom fabric to have a finite radius of curvature around the blade leading edge. Therefore the fluid can turn smoothly in that region and consequently this rapid change in pressure on the bottom fabric would be partially suppressed. In order to examine the effect of grid size on pressure pulses, the number of cells, originally 33000, was increased to 131000. The computed pressure pulses were found to be almost identical and independent of the grid size. Figure 3.15 shows the effect of grid size on pressure pulses generated by a flat blade.

Figure 3.16 illustrates the effect of blade width on pressure pulses. Three different relatively wide flat blades were considered. The magnitude of the pressures over the blade remains relatively unchanged. However, upstream of the blade, the 20 *mm* wide blade

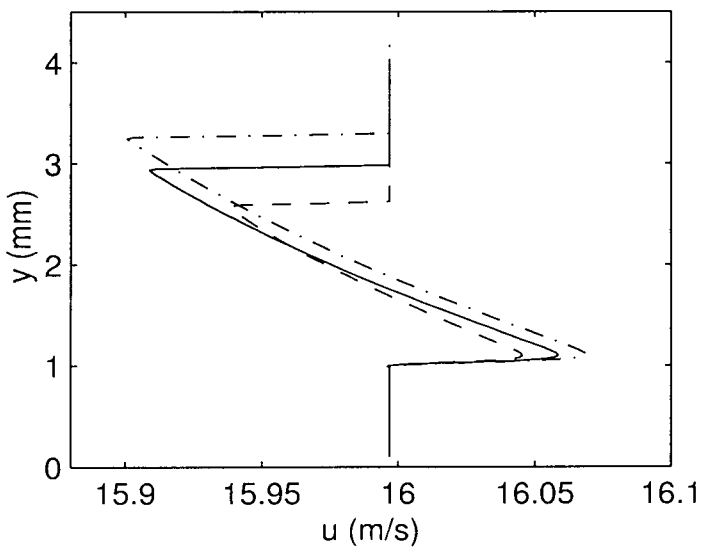

Figure 3.13: u component of the fluid velocity 1.5 mm downstream of the thin blade for different fabric tensions, $-T_t$= 7000 N/m, $--T_t$= 9000 N/m, $-.-T_t$= 5000 N/m, other variables from Table 3.1.

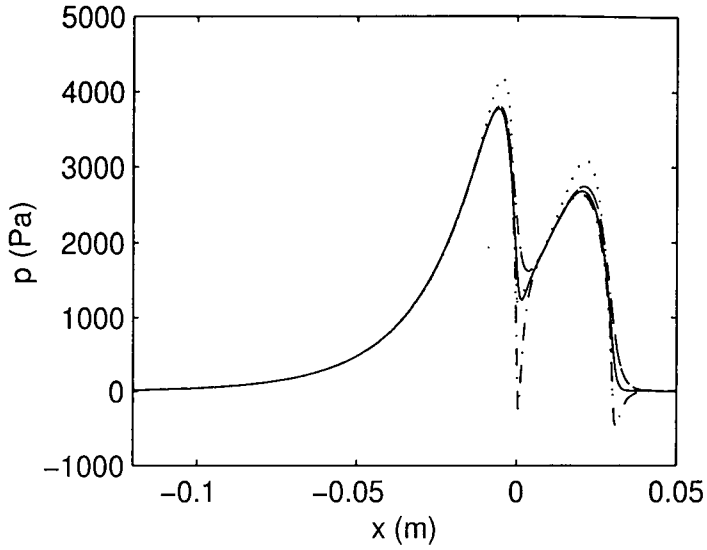

Figure 3.14: Comparison between one-dimensional analytical and two-dimensional viscous models of pressure generated by a 30 mm wide flat blade, $-p_m$, $--p_t$, $-.-p_b$, $....p_{1D}$, other variables from Table 3.1.

produces about a 30% higher peak pressure than does the 40 mm blade.

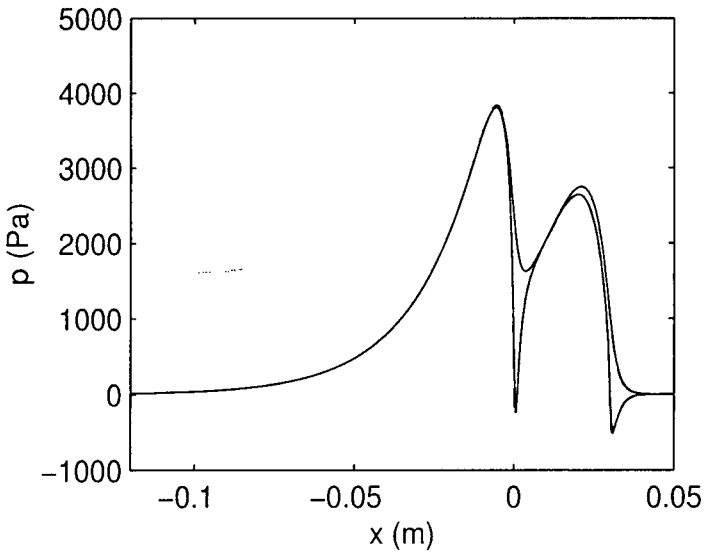

Figure 3.15: The influence of grid size on pressure pulses. Pressure at the top and bottom fabrics are shown,−33000 cells, −− 131000 cells.

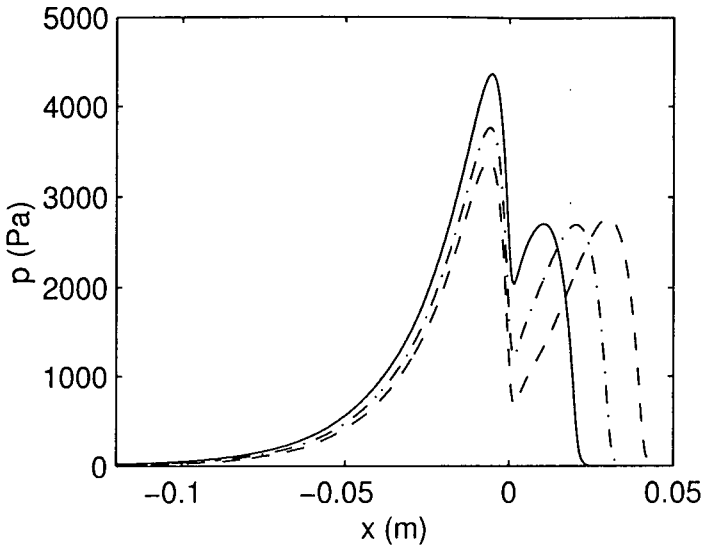

Figure 3.16: Effect of flat blade width on pressure pulses, $-w = 0.02\,m$, $-.-w = 0.03\,m$, $--w = 0.04\,m$.

3.5 Summary

In this chapter, a viscous model was developed to predict pressure pulses created between fabrics in blade gap formers. The continuity and full two-dimensional Navier-Stokes equations and Darcy's Law were solved to model the fluid flow. The results show the effect of viscosity on pressure pulses in the former is negligible. The pressure pulses were compared with the previously developed analytical one-dimensional model. As expected, the integrated pressure pulses in the fluid in contact with the top fabric are in good agreement with the simple analytical expression.

$$\int_{-\infty}^{\infty} p dx = T_{top}(\alpha_1 - \alpha_2) \tag{3.12}$$

It was also found that the pressure pulse over a thin blade obtained from the two-dimensional viscous model was in good agreement with the pressure pulse obtained from analytical one-dimensional analytical model [28]. Table 3.2 summarizes the integrated pressure for all cases presented in previous sections. All primary variables were obtained from Table 3.1. Some of the results have been published in [51].

In the following part, the single blade models will be extended to include the effect of

Table 3.2: Integrated pressure pulse(s) in the fluid in contact with the top fabric

case	secondary variable			$\int pdx Pa-m$	Error (%)
1	Tension	5000	N/m	122.1	1.5
2	Tension	9000	N/m	219.9	1.5
3	Viscosity	0.005	$Pa-s$	171.8	1.0
6	Wrap angles	0.35	*degree*	85.1	0.5
7	Wrap angles	1.4	*degree*	342.2	0.0
8	Average resistance	10000	$Pa-s/m$	170.2	2.0
9	Average resistance	30000	$Pa-s/m$	182.8	5.3
10	Fabric velocity	10	m/s	173.2	0.2
11	Fabric velocity	24	m/s	184.2	6.1
12	Flat blade width	20	mm	173.9	0.2
13	Flat blade width	30	mm	173.3	0.2
14	Flat blade width	40	mm	173.8	0.1
15	Curved blade crown	0.05	mm	167.3	3.6
16	Curved blade crown	0.10	mm	167.3	3.6
17	Curved blade crown	0.15	mm	166.9	3.9

suction boxes on pressure pulse development.

Chapter 4

Fluid Inertial Effect on Drainage Resistance

In our consideration of pressure pulses, first a one-dimensional analytical model was developed in Chapter 2. Then, the model was extended to the two-dimensional viscous model in Chapter 3. In both models, a number of assumptions were made to simplify the analysis. One of the them was that Darcy's Law can be used to model the flow through the fabrics. We now address the question what would be the internal effect on pressure pulses and the predicted results? The purpose of this chapter is to answer to this question.

4.1 Inertial Effect

A more general flow equation may describe the flow correctly. Forcheimer [52] suggested that Darcy's Law be modified at high velocities to account for inertia by a second order velocity term, in keeping with experimental data. Forcheimers equation is:

$$\Delta p = av + bv^2 \tag{4.1}$$

where Δp is the pressure drop through a porous medium, v is the flow velocity through the media, a and b are the viscous resistance and the inertial resistance coefficients, respectively. In this study the total pressure drop through a fabric and fibre mat is considered to be the superposition of pressure through the fabric and mat:

$$\Delta p = \Delta p_{fabric} + \Delta p_{mat} \tag{4.2}$$

The pressure loss across the fabric can be described by the following equation:

$$\Delta p_{fabric} = a_{fabric} v + b_{fabric} v^2 \tag{4.3}$$

Table 4.1: Characteristics of three types of forming fabrics.

Constants		Fabric A [41]	Fabric B [41]	Fabric C [40]
a	$Pa-s/m$	3.4×10^3	1.8×10^3	4.8×10^3
b	$Pa-s^2/m^2$	24.5×10^3	10.3×10^3	16.1×10^3

where a_{fabric} and b_{fabric} are the respective viscous and inertial drainage resistance coefficients of the fabric. In order to determine the viscous and inertial coefficients of a particular fabric, the pressure drop across the fabric can be measured at several flow rates. The pressure drop-velocity curve from the experiments is non linear, and is well represented by equation 4.3.

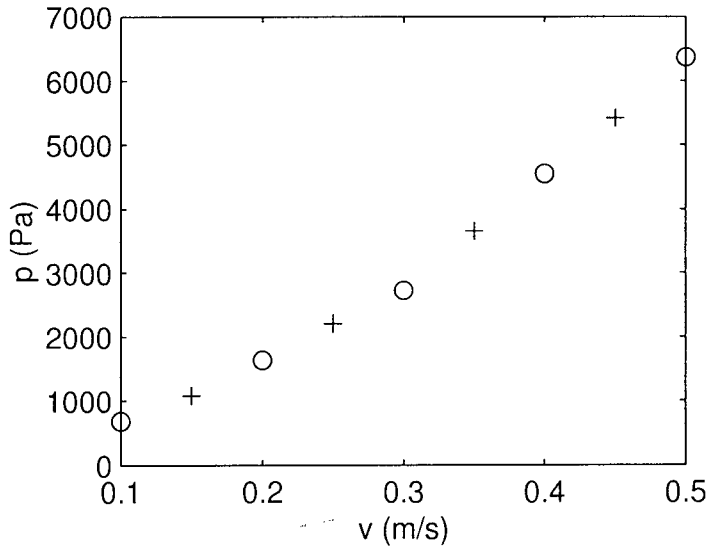

Figure 4.1: Pressure drop across a fabric as a function of the approach flow velocity, o experimental results [40], + numerical results.

The fibre mat resistance is a function of its basis weight and the compressibility characteristics of the fibres. The pressure loss across the mat can also be described by an equation that includes both viscous and inertial terms:

$$\Delta p_{mat} = a_{mat}v + b_{mat}v^2 \tag{4.4}$$

where a_{mat} and b_{mat} are functions of the fibre furnish. Jong et al. [41] conducted

an experiment to determine the variation of pressure drop with velocity. They created mats of different basis weight in their facility. They showed that the net pressure drop across the mat behaves distinctively as the basis weight was varied. For basis weights less than 18 g/m^2 the pressure drops increases almost linearly with basis weight. Herzing and Johnson [40] also showed that the relation between pressure drop across mat and velocity is linear over the basis weight range investigated of up to $\simeq$ 17 g/m^2 for Groundwood (Newsprint and Directory Grade). It is import to note that when a sheet is formed on a gap former, two sheets are really made, one on each fabric. The two sheets merge into one when all the free water is drained out of one side or the other. For example, a newsprint sheet ($\simeq$ 49 g/m^2) is really comprised of two ($\simeq$ 24.5 g/m^2) sheets assuming symmetrical drainage occurring. Based on the above experimental results for low basis weight, the mat resistance over the blades tends to increase linearly as the basis weight increases. In equation 4.4 , b_{mat} is normally small and can be neglected. In view of the linear dependence of Δp on basis weight, equation 4.4 can be written to include the basis weight (BW) and Specific Filtration Resistance (SFR):

$$\Delta p_{mat} = \mu \times BW \times SFR \times v \tag{4.5}$$

4.2 Method of Solution

The fluid flow equations were similar to those of the single blade model of Chapter 3, except in the porous media part of the domain Darcy's Law was replaced by the following equations:

$$\frac{dp}{dx} = \frac{\mu}{\alpha_x} u + \frac{1}{2} c_x \rho |u| u \tag{4.6}$$

$$\frac{dp}{dy} = \frac{\mu}{\alpha_y} v + \frac{1}{2} c_y \rho |v| v \tag{4.7}$$

where α and C are permeability and inertial resistance factors, corresponding to each of the component directions. The boundary conditions are the same as those of the thin blade model where:

Table 4.2: Fixed variables in simulations

Velocity of fabrics	V_o	16	m/s
Tension on fabrics	T	5000	N/m
Wrap angle	$\alpha_1 = -\alpha_2$	1	$degree$
Specific filtration resistance	SFR	2×10^9	m/kg
Fabric thickness	F_t	1	mm

- Inflow normal velocity upstream equal to the fabric velocity.
- Zero static pressure at downstream boundary.
- Zero static pressure at top boundary.
- Zero static pressure at bottom of boundary.

The pressure calculated by the code at the top and bottom fabrics must satisfy the fabric force balance. The fabric shapes thus deduced were used in a second two-dimensional viscous model that solved Darcy's Law and a converged flow field was achieved. The average resistance obtained from this two-dimensional model then was compared with the resistance calculated from a simple theoretical equation [32]:

$$R = \frac{2T_{top}(\alpha_1 - \alpha_2)}{V_o(h_{in} - h_{out})} \tag{4.8}$$

4.2.1 Results

The parameters shown in Table 4.2 were fixed in the simulations. The viscous resistance of the fibre mat was calculated based on the Specific Filtration Resistance (SFR) of Groundwood pulp [40] with water flow at 0.22 m/s approaching velocity. Two cases were considered. Case I represents what occurs when pulp suspension passes over a blade right after the jet impingement region. The average basis weight for this case was assumed to be 7 g/m^2 as might be the case in a pure blade former. Case II simulates the case where the basis weight is 10 g/m^2 over the blade, after partial dewatering of suspension over a roll former. The upstream gap size were considered 5 mm and 3 mm for the case I and case II, respectively. Generally this model, as the thin blade model, predicts that the

pressure increases in the machine direction, reaches its maximum close to the thin blade and immediately after the blade drops to zero. Figure 4.2 shows pressure distributions at the top fabric and at the bottom fabric for Fabric A. The solid curves represent the case for which the effect of both viscous and inertial resistances of the fabric were included (Forcheimers model). The dash-dot curves show the results obtained, using a Darcy's Law model, based on the average viscous resistance for the same dewatering. Note that some parts of the dash-dot curve lie atop the solid curves, and thus are not visible. The integrated pressures at the top fabric for both cases are within 2% of the theoretical value given by:

$$\int_{-\infty}^{\infty} p_{top} dx = T_{top}(\alpha_1 - \alpha_2) \tag{4.9}$$

The new two-dimensional model (Forcheimers) yields a slightly higher peak pressure. There is a difference 9.5% between the two-dimensional average viscous resistance and the average resistance obtained from Equation 4.8.

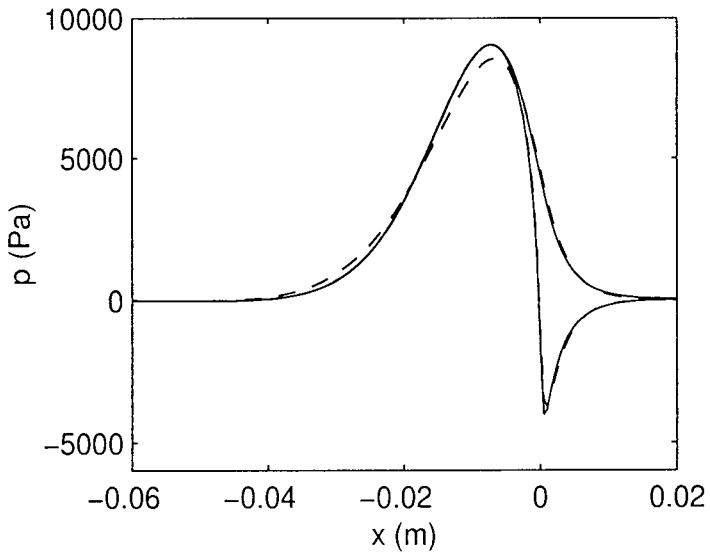

Figure 4.2: Pressure distribution at top and at bottom fabric A case I (– Forcheimers model, –– Darcy's Law model).

Figures 4.3 and 4.4 show the pressure distributions at the top and the bottom fabrics for Fabric B and Fabric C (case I), respectively. In both cases, the Forcheimers model predicts a slightly higher peak pressure than does the Darcy's Law model. The differences

between the average resistance in the two-dimensional models and the average obtained from Equation are about 7.5% and 9.2%.

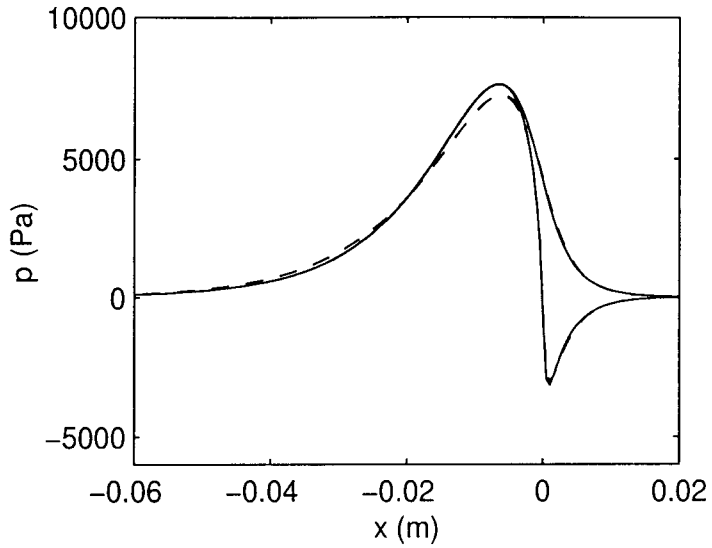

Figure 4.3: Pressure distribution at top and at bottom fabric B case I (– Forcheimers model, −− Darcy's Law model).

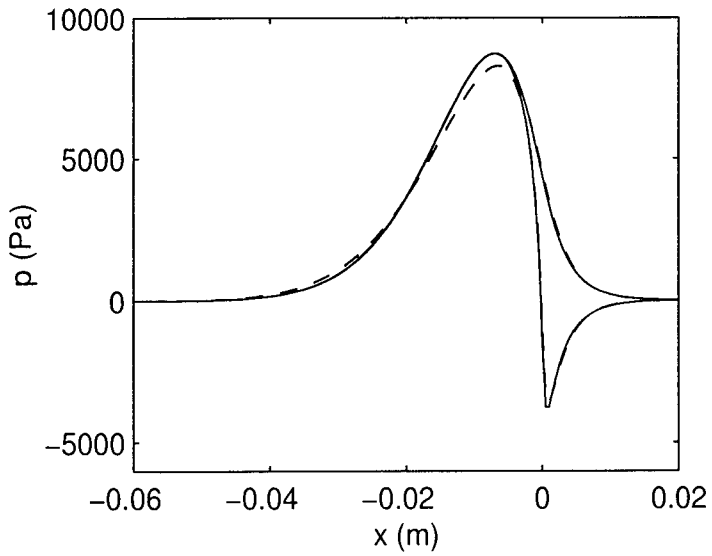

Figure 4.4: Pressure distribution at top and at bottom fabric C case I (– Forcheimers model, −− Darcy's Law model).

It is difficult to compare the different graphs because they represent fabrics with different average resistances. In particular, Fabric A has the highest peak pressure and

Table 4.3: One-dimensional and two-dimensional average viscous resistances, case I.

Fabric	R_{1D} $(Pa-s/m)$	$R_{2D}(Pa-s/m)$	Difference
A	26300	23800	9.5%
B	20000	18500	7.5%
C	25000	22700	9.2%

Table 4.4: Integrated pressure at the top fabrics and the difference from Eq. 4.8, case I.

Fabric	Forcheimers Eq.$(Pa-m)$	Difference	Darcy's Law $(Pa-m)$	Difference
A	175.7	0.7%	174.6	0.1%
B	177.5	1.7%	177.0	1.4%
C	177.5	1.7%	175.2	0.4%

Fabric B has the lowest, since they have respectively the highest and lowest resistances. Some of the results are summarized in Tables 4.3 and 4.4.

Figures 4.5, 4.6, and 4.7 show the pressure distributions at the top and at the bottom fabrics for case II. The integrated pressures at the top of all three fabrics are within 1% of

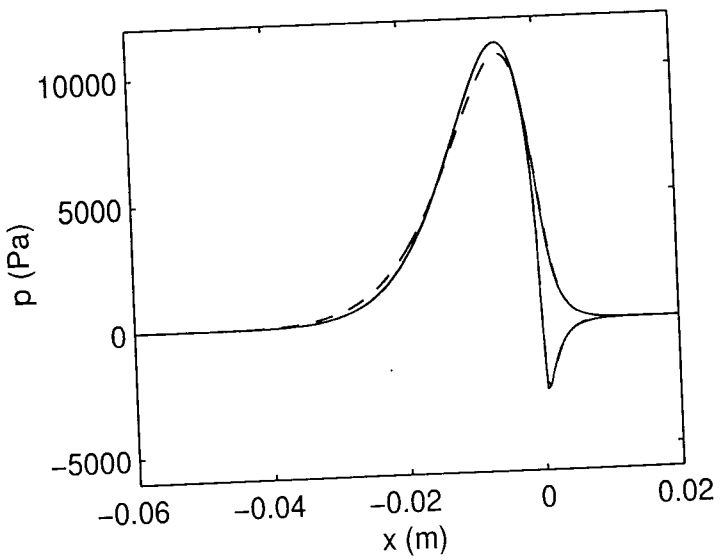

Figure 4.5: Pressure distribution at top and at bottom fabric A case II (– Forcheimers model, –– Darcy's Law model).

the expected value. As case I, the Forcheimers model predicts a slightly higher pressure

than does the Darcy's Law model. The difference between the two-dimensional average viscous resistance and the average resistance predicted by Equation 4.8 for this case is less than 5%.

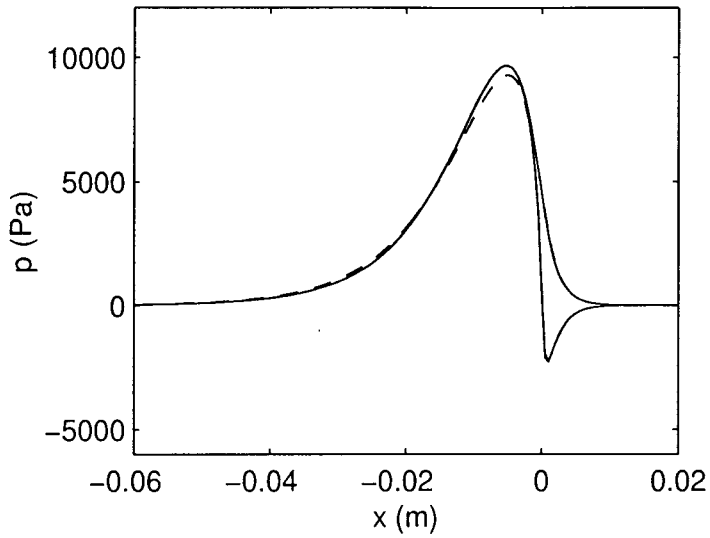

Figure 4.6: Pressure distribution at top and at bottom fabric B case II (– Forcheimers model, −− Darcy's equation model).

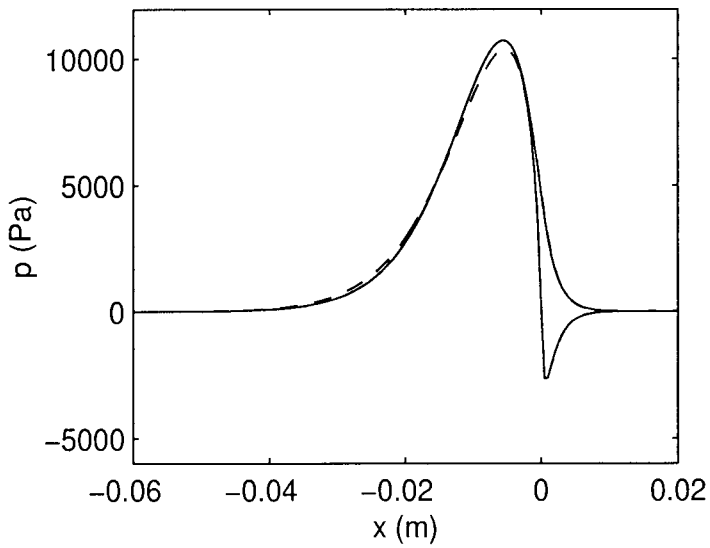

Figure 4.7: Pressure distribution at top and at bottom fabric C case II (– Forcheimers model, −− Darcy's Law model).

The results for case II are summarized in Tables 4.5 and 4.6.

Table 4.5: One-dimensional and two-dimensional average viscous resistances, case II.

Fabric	R_{1D} $(Pa-s/m)$	$R_{2D}(Pa-s/m)$	Difference
A	31450	29900	4.9%
B	25600	24400	4.7%
C	30300	29000	4.3%

Table 4.6: Integrated pressure at the top fabrics and the difference from Eq. 4.8, case II.

Fabric	Forcheimers Eq.$(Pa-m)$	Difference	Darcy's Law $(Pa-m)$	Difference
A	173.4	0.6%	174.3	0.1%
B	174.6	0.1%	173.7	0.5%
C	175.1	0.3%	175.5	0.6%

4.3 Summary

Based on the results, it is apparent that even at the low mat basis weight of 7 g/m^2, the influence of Forcheimers drainage characteristics are modest. In particular, the Forcheimers equation drainage model yields slightly higher peak pressures. Once a higher basis weight accumulates on the fabrics and the fibre mat basis weight reaches 10 g/m^2 even this modest Forcheimers equation behavior will cease to be evident and the differences between the average viscous resistances for one-dimensional and two-dimensional Darcy's Law models fall below 5%. Therefore for industrially relevant fibre mats and forming fabrics, the effect of Forcheimers equation drainage resistance on the integrated gap pressure and the pressure distributions is small. Some of the results of this study have been published in [53].

Part II

Modelling of Two Blades With Applied Suction

Chapter 5

Analytical Solution of Suction Boxes

In the previous part, a single blade was analyzed. In practice, in blade gap formers more than one blade is used. Also, suction is applied between the blades on the side of the moving fabric in contact with the blades by using elements called *Suction Boxes*. This negative pressure increases dewatering through the fabric in contact with the blades. A one-dimensional numerical model of suction shoes was developed by Green [36-37]. The objective of this chapter is to develop an analytical one-dimensional model that provides an explicit equation for pressure distribution over the suction box based on the same linearization used in the Chapter 2.

5.1 Analysis

For simplification, we assume that the two adjacent blades are thin. Figure 5.1 shows a schematic of the two thin blades and some of the physical parameters involved in the problem. Note that in order to obtain a closed form for the pressure distribution, the gap size at blade 1, h_m, is considered to be known. The following second order differential equation for the pressure over the suction box can be obtained from Equation 2.9:

$$\frac{d^2p}{dx^2} - \frac{V_o\rho(\overline{k}_t + \overline{k}_b)}{h_o}\frac{dp}{dx} + \frac{\rho V_o^2(T_t + T_b)}{h_o T_t T_b}p - \frac{\rho V_o^2}{h_o T_b}p_{suct} = 0 \tag{5.1}$$

where p_{suct} is the applied suction on the fabric passing the blade. This yields the following solution for the pressure distribution over the suction box:

$$p = \frac{p_{suct}}{2} + c_1 e^{n_1 x} + c_2 e^{n_2 x} \qquad 0 \le x \le s \tag{5.2}$$

where s is the separation of the two blades. The constants c_1 and c_2 are determined from following conditions:

$$p(s) = 0, \qquad and \qquad \int_0^s p dx = T_t(\alpha_m - \alpha_2)$$

The constants c_1 and c_2 are:

$$c_1 = \frac{n_1}{2} \frac{p_{suct}(1 + e^{n_2 s}(n_2 s - 1)) - 2n_2 e^{n_2 s} T_t(\alpha_m - \alpha_2)}{n_1 e^{n_1 s}(\exp(n_2 s) - 1) - n_2 e^{n_2 s}(\exp(n_2 s) - 1)} \tag{5.3}$$

$$c_2 = -\frac{n_2}{2} \frac{p_{suct}(1 + e^{n_1 s}(n_1 s - 1)) - 2n_1 e^{n_1 s} T_t(\alpha_m - \alpha_2)}{n_1 e^{n_1 s}(\exp(n_2 s) - 1) - n_2 e^{n_2 s}(\exp(n_2 s) - 1)} \tag{5.4}$$

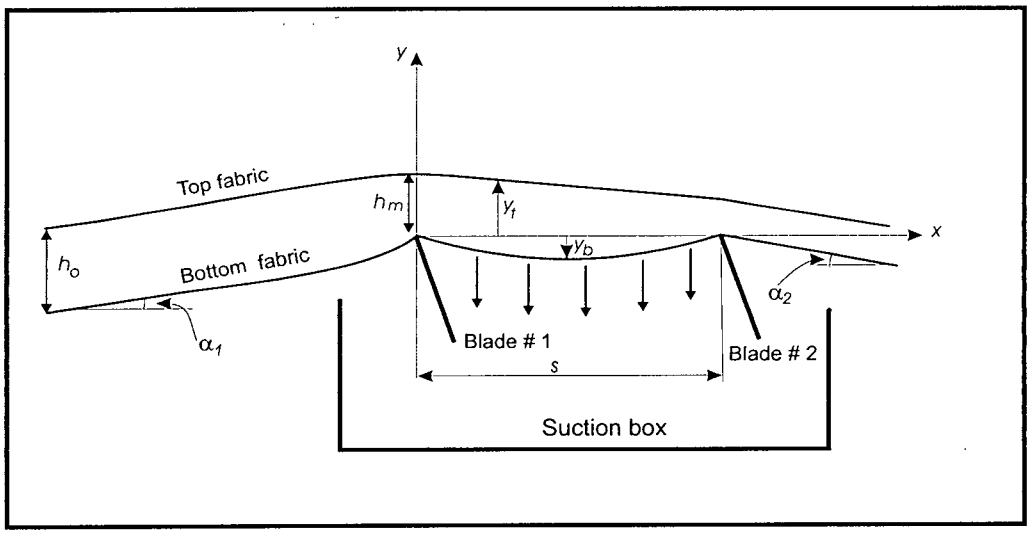

Figure 5.1: Schematic of two thin blades and a suction box.

In the above two equations, α_m is the slope of the top fabric at the first blade which is not known. An iterative process is applied to determine its value as follows:

First, the pressure in the gap at the first blade, p_m, is assumed to be known, e.g. $p_{suct}/2$. Applying the Bernoulli equation in the gap, from somewhere far upstream of the first blade (about 120 mm for the typical operating conditions given in Table 2.1), where

Table 5.1: Converged values of p_m, V_m, and α_m.

Case	p_{suct} (Pa)	s (m)	p_m (Pa)	V_m (m/s)	α_m $(rad.)$
I	-7000	0.06	-2648	14.1879	-0.0065
II	-5000	0.06	-1857	14.1320	-0.0068
III	-3000	0.06	-1066	14.0759	-0.0072
IV	0	0.06	120	13.9914	-0.0076
V	-7000	0.10	-3315	14.2348	-0.0066
VI	-5000	0.10	-2363	14.1678	-0.0063
VII	-3000	0.10	-1411	14.1004	-0.0070
VIII	0	0.10	16	13.9989	-0.0076

$p \approx 0$ and $V \approx V_o$, to the location of the first blade gives:

$$V_m = \sqrt{V_o^2 - 2\frac{p_m}{\rho}} \tag{5.5}$$

Writing the continuity equation over the same interval yields:

$$\alpha_m = \alpha_1 - \frac{h_o V_o - h_m V_m}{(\overline{k_t} + \overline{k_b})T_t} \tag{5.6}$$

Now, c_1, c_2, and p over the suction box can be determined from Equations 5.3, 5.5, and 5.2. Now, if the pressure at the first blade, $p(0)$, differs from the assumed p_m, then the iteration continues using new $p_m = p(0)$. Usually, a few iterations converge to the right p_m, and α_m, which are then used to determine the pressure upstream of the first blade using equation 2.29. Table 5.1 shows some of the variables and converged values.

5.1.1 Effect of Applied Suction

Figure 5.2 shows the effect of applied suction on pressure distributions over suction box and upstream of the first blade. Generally, this model predicts that the pressure between two blades has its minimum downstream of the first blade, increases in the machine direction as the second blade is approached, and drops to zero at the second blade. By applying more suction, the pressure downstream of the first blade is decreased, while the peak pressure close to the second blade is increased. The reason for this is the increased

fabric deflection around the second blade with higher applied suction.

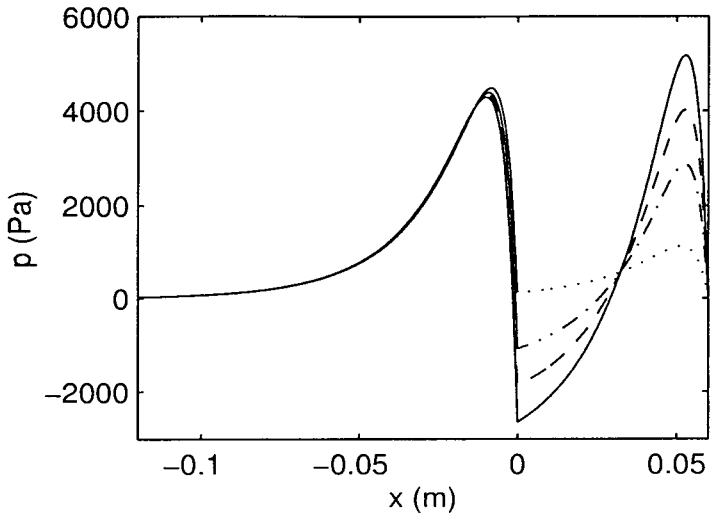

Figure 5.2: Effect of applied suction on the pressure distributions, $h_o = 5\ mm$, $h_m = 4\ mm$, blade locations $x = 0$ and $x = 0.06\ m$, – Case I, –– Case II, –.– Case III, ... Case IV, other variables from Table 2.1.

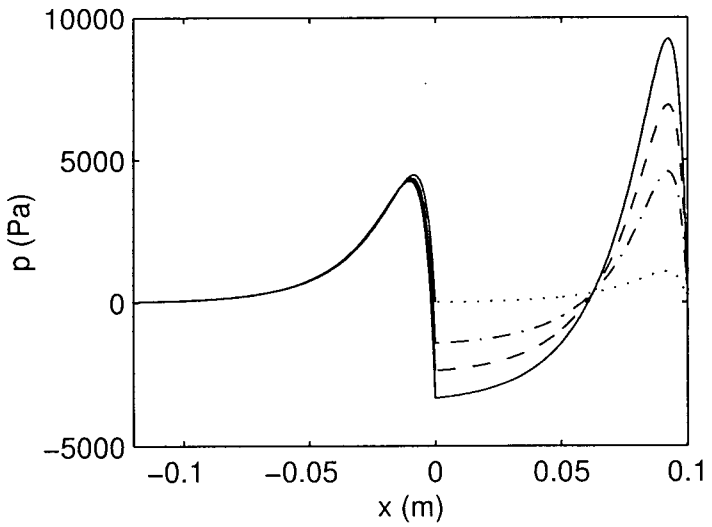

Figure 5.3: Effect of the blade separation on pressure distributions $h_o = 5\ mm$, $h_m = 4\ mm$, blade locations $x = 0$ and $x = 0.1\ m$, – Case V, –– Case VI, –.– Case VII, ... Case VIII, other variables from Table 2.1.

5.1.2 Effect of Blade Separation

Figure 5.3 shows the effect of the blade separation. For this case, more of the pulp suspension is exposed to negative pressure owing to the larger separation between blades. The bottom fabric is drawn down more deeply between the blades, which causes it to wrap the second blade to a greater extent, and increases the pressure pulse. With the large separation the pressure approaches to half of the applied suction immediately downstream the first blade. If we assume that the separation of blades is large enough to avoid interaction between blades, and set the suction to zero, we obtain the same pressure distribution to that of Zhao and Kerekes [28] for a single thin blade. This shows that the analytical one-dimensional ZK model can be considered as a special case of this more general model.

5.2 Summary

In this chapter, the one-dimensional analytical model of the suction boxes was developed. It is found that for constant fabric and fibre mat permeability, applying more suction decreases the suspension pressure close to the first blade, and increases the peak-to-peak pressure. The fabric draw down enhances the positive pressure peak generated at the second blade, compensating for the lower pressure between the blades. Increasing blade separation likewise causes a greater draw down of the bottom fabric, which produces a sharper pressure gradient close to the second blade. The results of this model will provide the initial guess for the two-dimensional viscous model of suction boxes in the following chapter.

Chapter 6

Two Dimensional Viscous Model of Suction Boxes

In the previous chapter the analytical one-dimensional model of the suction boxes was developed. The objective of this chapter is to develop a two dimensional viscous model of suction shoes. This model is based on solving the Navier-Stokes equations for the flow between the fabrics and Darcy's Law for the flow through the fabrics. One equation of motion for each fabric and one equation for the fabric and fibre mat drainage resistance of each fabric are solved as well.

6.1 Analysis

Figure 5.1 shows a schematic of the two thin blades and some physical parameters involved in the problem. Suction is applied between the two blades, which causes the bottom fabric to have an arced shape.

Compared to previous two-dimensional viscous model of a single blade presented in this thesis, the effects of fabric mass and mat resistance variations in the machine direction were added. Therefore, to develop a mathematical model for this process, three sets of physical behaviors must be considered: the fluid flow, the fabric deflection, and the mat resistance variation. The following assumptions were made to simplify the physical aspects of the problem to obtain mathematical relations:

1. The flow is steady and two-dimensional.
2. The suspension is dilute and can be treated as a pure water.
3. Darcy's Law describes the flow through the fabrics and fibre mat.
4. The drainage resistance of a fibre mat is proportional to the number of fibres accumulated in the mat.

5. The fabrics have zero stiffness.

Considering the above assumptions, seven coupled differential equations must be solved in order to cover all three sets of physical behaviors. Three equations (continuity and two momentum equations) describe the fluid flow field; two equations of motion model the fabric shapes; and two fabric and fiber mat resistance equations relate the permeability variation of the fibre mat to dewatering. These equations are discussed below.

6.1.1 Fluid Flow Equations

In the suspension flow, the steady continuity and Navier-Stokes equations are:

$$\frac{\partial u}{\partial x} + \frac{\partial v}{\partial y} = 0 \tag{6.1}$$

$$\rho(u\frac{\partial u}{\partial x} + v\frac{\partial u}{\partial y}) = -\frac{\partial p}{\partial x} + \mu(\frac{\partial^2 u}{\partial x^2} + \frac{\partial^2 u}{\partial y^2}) \tag{6.2}$$

$$\rho(u\frac{\partial v}{\partial x} + v\frac{\partial v}{\partial y}) = -\frac{\partial p}{\partial y} + \mu(\frac{\partial^2 v}{\partial x^2} + \frac{\partial^2 v}{\partial y^2}) \tag{6.3}$$

In the porous media Darcy's Law represents the last two of these equations:

$$\frac{\partial p}{\partial x} = -\frac{R_x}{F_t}u \tag{6.4}$$

$$\frac{\partial p}{\partial y} = -\frac{R_y}{F_t}v \tag{6.5}$$

In the above equations $u(x, y)$ and $v(x, y)$ are respectively the x and y velocities, $p(x, y)$ is the pressure, ρ is the pulp suspension density, μ is the suspension viscosity, F_t is the fabric thickness, and R is the drainage resistance of the fabric and fibre mats.

6.1.2 Equations of Motion for Fabric

The equations of motion can be obtained by writing a force balance on each fabric. For the top and bottom fabrics we can write:

$$\frac{d^2y_t}{dx^2} + \frac{p_t}{T_t - mV_o^2} = 0 \tag{6.6}$$

$$\frac{d^2y_b}{dx^2} - \frac{p_b - p_{suct}}{T_b - mV_o^2} = 0 \tag{6.7}$$

The shapes of the top and bottom fabrics are given by $y_t(x)$ and $y_b(x)$, the fabric tensions are T_t and T_b, the fabric mass per unit area is m, the fabric velocity is V_o, and the pressure in the pulp suspension at the top and bottom fabrics are respectively p_t and p_b. p_{suct} is the suction applied between the blades.

6.1.3 Fabric and Fibre Mat Resistance Equations

The drainage resistance of the fabric and fibre mat increases along the machine direction. Because of uneven dewatering caused by the application of suction, the drainage resistance of the top and bottom fibre mats differ. If one neglects the compressibility of the fibre mats, assumes that the fibre concentration in the suspension is constant, and assumes that the resistance of a fibre mat is proportional to the number of fibres deposited on the fabrics, then, as shown by Green [36], the drainage resistance variation can be found from equations 6.8 and 6.9.

$$\frac{dR_t}{dx} = \frac{c_r p_t}{R_t V_o} \tag{6.8}$$

$$\frac{dR_b}{dx} = \frac{c_r p_b}{R_b V_o} \tag{6.9}$$

where c_r is a constant. All equations have been presented in Cartesian co-ordinates (given small fabric angles relative to the x axis). However, curvilinear co-ordinates can also be

used to describe this physical problem.

6.2 Boundary Conditions

The above equations must be solved subject to certain boundary conditions. The boundary conditions just upstream and downstream of the double-blade are not obvious. Therefore, the fabrics are extended far upstream of the first blade and forced to be parallel downstream of the second blade. This means that we isolate the double-blade from any other elements in the gap former, which makes it easier to study the effect of applied suction independent of upstream dewatering. Considering the above argument, we used the following boundary conditions for the fluid flow equations:

- Constant applied suction p_{suct} on the outer surface of the bottom fabric, between the two blades.
- Uniform velocity V_o far upstream of the first blade.
- The gauge pressure p_{atm} at all other boundaries.

To solve each equation of motion we need two boundary conditions. For the bottom fabric, the locations right at the blades are known. For the top fabric, the location at the first blade and the slope at the second blade are known. These boundary conditions can be written as follow:

$$y_b(0) = y_b(s) = 0$$

$$y_t(0) = h_m$$

$$\frac{dy_t}{dx}(\infty) = \alpha_2$$

The first blade in this model is located at $x = 0$, and the second downstream blade at $x = s$. Physically, infinity is defined to be 20 mm downstream of the second blade.

Table 6.1: Fixed variables in simulations.

Fabric Velocity	V_o	16	(m/s)
Tension on Fabric	T	7000	(N/m)
Initial Gap Size	h_m	5	(mm)
Wrap Angle	α_2	-0.03	$(radian)$
Fabric Thickness	F_t	1	(mm)
Mass/Area of Fabric	m	1.6	(kg/m^3)
Drainage Resistance Constant [36]	c_r	2×10^7	$(Pa - s/m^2)$

Only one boundary condition is needed to solve each drainage equation, namely that the drainage resistance at blade 1 is known for each fibre mat.

6.3 Method of Solution

The method of solution of the equations is the same as that used in Chapter 3, except the permeability variation equations are added to the model. In this method, equations describing the fluid flow are decoupled from the other equations, and solved by an iterative method in the following manner.

First, the one-dimensional model is solved to obtain fabric locations, y_t and y_b, and the drainage resistance of the fibre mats, R_t and R_b. Having defined the physical boundaries of the flow, the governing equations for the fluid are solved using the FLUENT CFD code. In the porous media parts of the domain, representing the fabrics, Darcy's Law is applied. The pressure calculated by the CFD code is then used to solve the fabric and fiber mat resistance equations to find the new fabric locations and mat permeabilities. These equations are solved using a finite difference method.

In the next iteration, the new fluid field is obtained by using the new fabric locations and mat permeabilities. These iterations are repeated until the pressure and fabric locations satisfy all seven equations which describe the problem. The solution was considered converged when the residual of the fluid flow equations and L_2 global norm of the equations of motion and fabric and fibre mat resistance fell below 5×10^{-4}.

Table 6.2: Other variables used in simulations.

Case	$p_s(Pa)$	$R(Pa-s/m)$	$s(m)$	No. of cells
I	-7000	20000	0.05	23000
II	-10000	20000	0.05	23000
III	-7000	20000	0.10	32000
IV	-7000	Eq. (6.8,6.9)	0.05	23000
V	-7000	20000	0.05	90000
VI	-7000	20000	0.05	36000

6.4 Results

As in the single blade model, there are a number of variables to be considered in modelling of the suction box, such as fabric tension, fabric velocity, upstream gap size, etc. In addition, the applied suction, separation distance between the blades, and starting drainage resistances on the two fabrics are all variables. In order to study two blades with associated suction, a number of variables, shown in Table 6.1, are fixed in simulations. Table 6.2 shows the variable parameters and the number of cells used for four simulations.

The Influence of Applied Suction

Figure 6.1 shows the shapes of the fabrics for cases I and II. The bottom fabric is sucked down between the two fixed blades located at $x = 0$ and $x = 0.05\ m$. The top fabrics, in contrast, have nearly linearly shapes.

Figures 6.2, 6.3 show pressure distributions along the centre line in the gap p_m, as well as pressure at the top fabric p_t, and bottom fabric p_b. Generally, this model predicts, as does the one dimensional model, that the pressure between two blades reaches its minimum shortly downstream of the first blade, and increases in the machine direction as the second blade is approached. The model also predicts that the fluid pressure in the gap at the top fabric is less than the pressure at the bottom fabric, except in regions close to the blades. This differential is caused by the curved streamlines of the flow that produce a centrifugal pressure gradient. A comparison of Figures 6.2 and 6.3 shows the effect of applied suction. By applying more suction the pressure downstream of the first blade

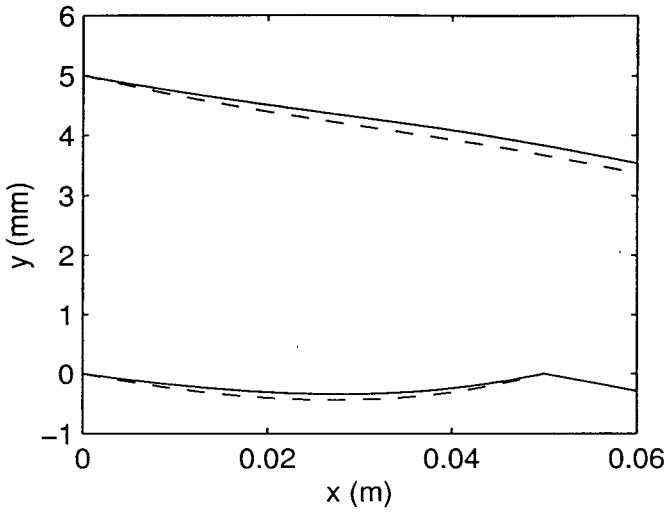

Figure 6.1: The effect of applied suction on fabric shapes, – cases I, –– Case II.

is reduced, as expected. Also, as a result of the larger suction, the radius of curvature of the bottom fabric decreases, resulting in a greater pressure differential in the gap. It is also predicted that the maximum positive pressure close to the second blade for both cases I and II is almost equal. The reason for this is that the increased fabric deflection around Blade 2 with higher suction results in a higher local pressure pulse there, which compensates for the higher applied suction.

The Influence of Blade Separation

For case III, the location of the second blade shifts from $x = 0.05\ m$ to $x = 0.1\ m$. Figure 6.4 shows the effect of the blade separation on the fabric shapes. For this case, more of the pulp suspension is exposed to negative pressure owing to the larger separation between blades. With the larger blade separation the bottom fabric is drawn down more deeply between the blades, which causes it to wrap the downstream blade to a greater extent and produce a sharper pressure gradient close to the second blade. The effect of larger blade separation on pressure distributions is shown in Figure 6.5. This large blade wrap increases the pressure pulse at the downstream blade from 4000 Pa to almost 8000 Pa.

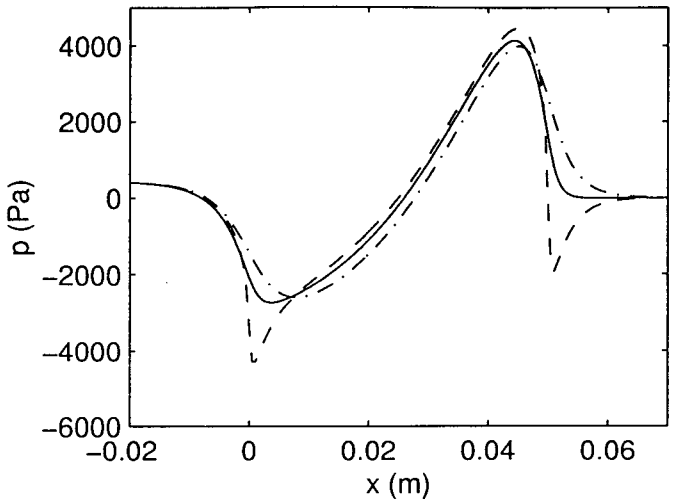

Figure 6.2: Pressure distributions in the gap for Case I ($-p_m, -. - p_t, - - p_b$).

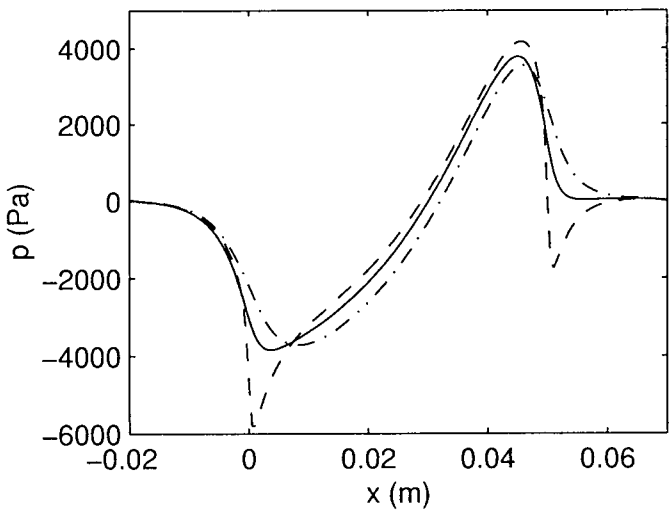

Figure 6.3: Pressure distributions in the gap for Case II ($-p_m, -. - p_t, - - p_b$).

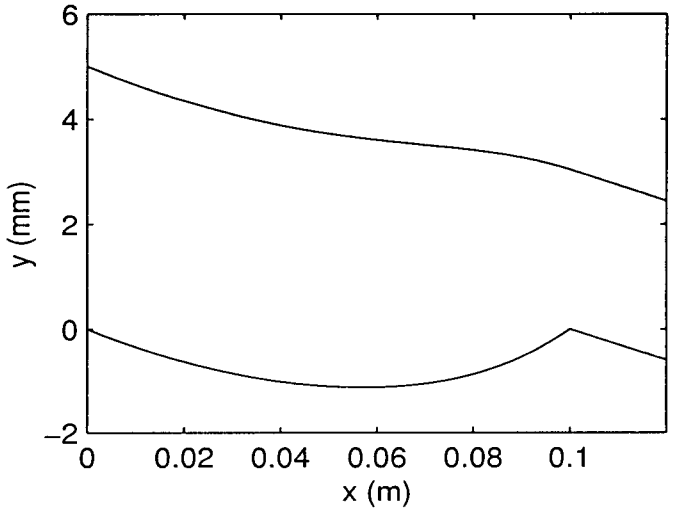

Figure 6.4: Effect of blade separation on fabric shape, cases III.

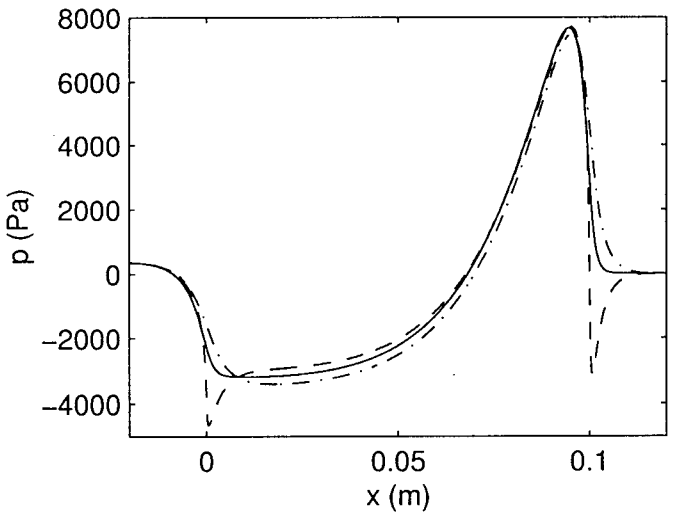

Figure 6.5: Pressure distributions in the gap for case III ($-p_m, -.-p_t, --p_b$).

The Influence of Fibre Mat Resistance

Allowing the permeability to vary along the machine direction increases the amplitude of both negative and positive pressure peaks. It most affects the pressure distribution, close to the second blade, where the resistance to dewatering is high. The effect of permeability variation is shown in Figure 6.6. The primary effect of fibre mat build up is observed close to the second blade, where the peak positive pressure upstream is about 25% higher and

peak negative pressure is about 120% lower compared with case I. Figure 6.7 shows the increase in fabric and mat resistance in the machine direction. The resistance increases more rapidly on the blade side fabric than the other fabric owing to the greater dewatering on that side.

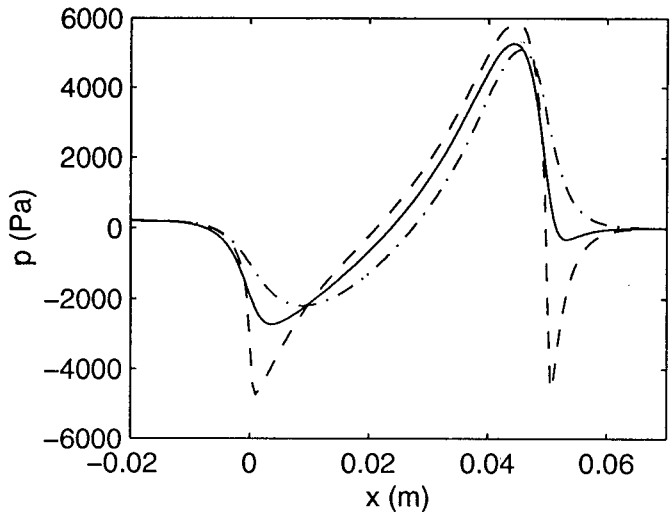

Figure 6.6: Pressure distributions in the gap for case IV ($-p_m, -. - p_t, - - p_b$).

Velocity Profiles

Figures 6.8 and 6.9 show the profile of the u component of velocity in the gap for three cases. As expected in view of Bernoulli equation effects, the fluid moves faster than the fabrics downstream of the first blade where the pressure is low, and slower than the fabrics upstream of the second blade, where the pressure is high. In both regions the fluid close to the top fabric moves faster than the fluid close to the bottom fabric, owing to the higher pressure at the bottom fabric than at the top fabric. The fluid velocity inside of the fabrics (of 1 *mm* thickness) is equal to the fabric velocity.

The Influence of Upstream Blade

In the above simulations, in order to simplify the forming geometry, the fabrics were assumed to take no wrap around the upstream blade. To examine the implications of

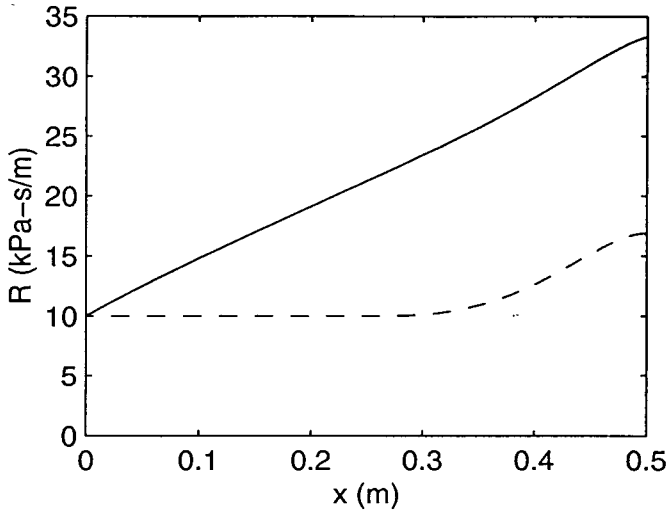

Figure 6.7: Fabric and mat resistance variation for Case IV (– bottom fabric, –– top fabric.

this simplified geometry, one case was studied (Figure 6.10) with upstream wrap. For this case the upstream wrap angle and the upstream gap size were 1 *degree* and 7.9 *mm*, respectively. The gap size right at the first blade was thus 5 *mm*, to simulate the same conditions as case I. As shown, the pressure distributions for cases I and VI over the suction shoe are similar except in the region very close to the first blade. This shows that

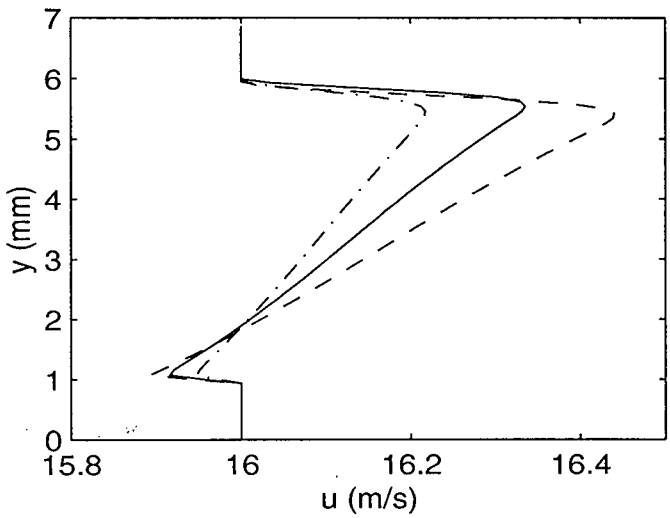

Figure 6.8: u Component of velocity 15 *mm* downstream of Blade 1 (–Case I,–– Case II, –.– Case IV).

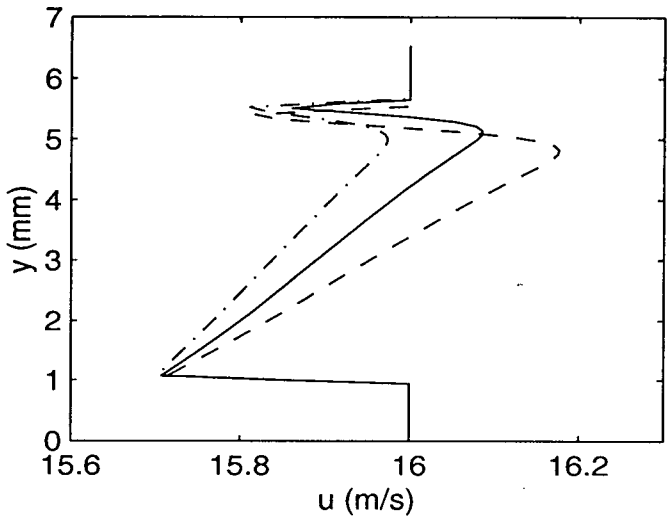

Figure 6.9: u Component of velocity 15 mm upstream of Blade 2 (– Case I, –– Case II, –.– Case IV).

the pressure in the gap over the suction box is mainly affected by the applied suction rather than by far-upstream conditions.

The Influence of Grid Size

In order to examine the effect of grid size on pressure pulses, two different grid sizes were used. The number of cells (originally 23000) was increased in both co-ordinate directions to 90000. The computed pressure pulses were found to be almost identical and independent of the grid size. Figure 6.11 show the effect of grid size on pressure pulses. Note that most parts of the dashed curve lie atop the solid curves, and thus are not visible.

6.5 Summary

In this chapter, the two-dimensional viscous model of the suction boxes was developed. The model predicts pressure distributions as well as velocity profiles in the pulp suspension. The effect of applied suction, blade separation, and fabric and fiber mat permeability variations were studied. It is found that for constant fabric and fibre mat permeability, applying more suction decreases the suspension pressure close to the first blade, but it

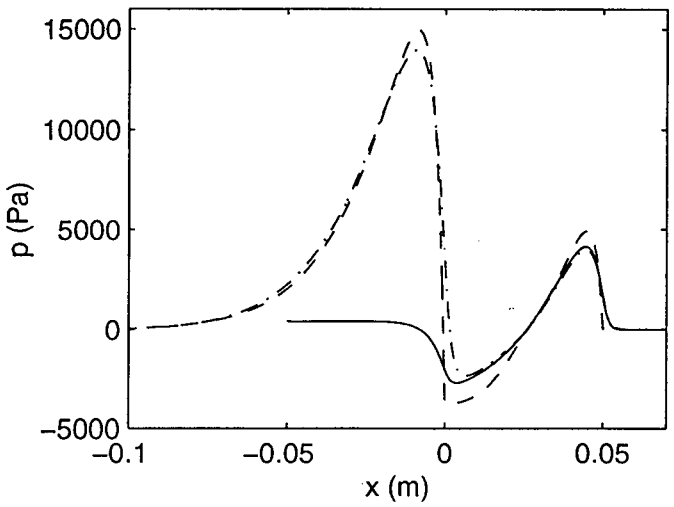

Figure 6.10: Pressure distribution along the centre line of the gap ($-p_m$ Case I, $-.-p_m$ Case VI, $--p_{1D}$ [36]). The upstream blade is at $x = 0.05\ m$ and the downstream blade is at x=0.

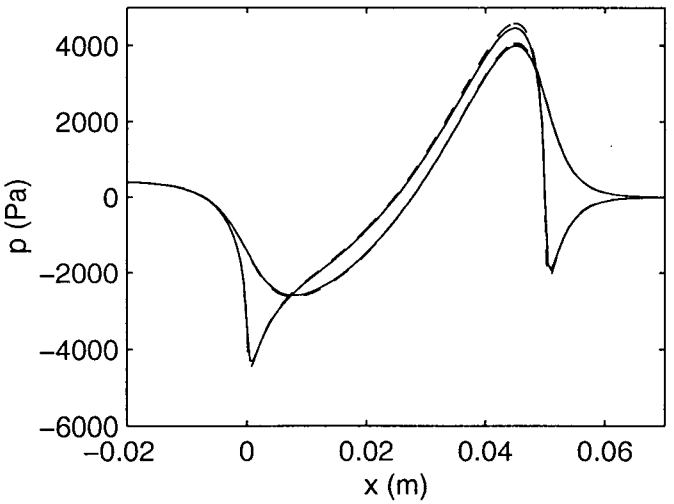

Figure 6.11: The influence of grid size on the pressure pulse for case I.

does not significantly change the positive peak pressure for a given fabric deflection at the second blade. The fabric draw down enhances the positive pressure peak generated at the second blade, compensating for the lower pressure between the blades. Increasing blade separation likewise causes a greater draw down of the bottom fabric, which produces a sharper pressure gradient close to the second blade. Variable permeability increases the amplitude of both negative and positive pressure peaks. Some of the results have been

published in [54].

Having considered the effect of applied suction between two adjacent blades, the effect of external pressure generated as a result of deflecting of white water from the fabric close to the blade, will be considered in the following part.

Part III

Modelling of the Stagnation Zone

Chapter 7

One-Dimensional Analysis of Stagnation Zone

In previous parts of this thesis, one-dimensional analytical models were developed to study first single blades and then two blades with applied suction between them. Those models provide very useful tools to understand the dewatering process and serve as initial guesses for two-dimensional viscous models. Following the same route in this part, first a one-dimensional analytical model and then a two-dimensional viscous model of the stagnation zone close to the blade will be developed. In all blade gap formers, dewatering produces a thin water layer adhering to the outside of the moving fabrics. This water layer approaches the stationary blade supporting the fabric with the same velocity as the fabric. The water layer then impinges on the blade and is deflected by it. A pressure distribution is generated in the stagnation zone very close (on the order of a few millimeters) to the upstream of the leading edge of the blade. This pressure distribution is called the *Doctoring Pressure*. It is the objective in this chapter to develop an analytical model for estimating the effect of the doctoring pressure generated as a result of dewatering.

7.1 Analysis

Figure 7.1 shows the region close to the blade where water is doctored by the blade. Complete one-dimensional and two-dimensional models of a single blade former that neglects the doctoring pressure are given in Part I. In both models a constant pressure boundary condition p_{atm} was applied on the blade-side of the fabric where it is not in contact with blade. This boundary condition must be modified as a result of the doctoring pressure distribution close to the blade. As a first approximation, in the numerical one-dimensional model, Green and Kerekes [34], represented the doctoring pressure by an exponential function. They assumed that the doctoring pressure reaches to its maximum, $p_o = \rho V_o^2/2$, at the tip of the leading edge of the blade. In the following section an analytical model is

developed to estimate the doctoring effect on pressure pulse in the gap. We assume that the doctoring pressure can be approximated by:

$$p_{doc} = f_1 e^{f_2 x/h_w} \tag{7.1}$$

where f_1 and f_2 are two constants, and h_w is the thickness of the water layer adhering to the outside of the fabric approaching the blade. The water layer approaches the blade with the same speed as the bottom fabric. The thickness of the water layer can be calculated as:

$$h_w \approx \frac{T_t(\alpha_1 - \alpha_m)\overline{k_b}}{V_o} \tag{7.2}$$

From the general differential equation 2.9, we can write:

$$\frac{d^2p}{dx^2} - a\frac{dp}{dx} + bp + (\frac{af_2}{2h_w} - \frac{b}{2})p_{doc} = 0 \tag{7.3}$$

The solution of the above equation yields the following:

$$p = n_3(c_1 e^{n_1 x} + c_2 e^{n_2 x}) + n_4 p_{doc} \qquad x \leq 0 \tag{7.4}$$

where:

$$n_3 = \frac{4(bh_w^2 - ah_w f_2 + f_2^2)}{n_5} \tag{7.5}$$

$$n_4 = \frac{2(bh_w^2 - ah_w f)2}{n_5} \tag{7.6}$$

$$n_5 = (h_w a + h_w(a^2 - 4b)^{0.5} - 2f_2)(h_w a - h_w(a^2 - 4b)^{0.5} - 2f_2) \tag{7.7}$$

The constants c_3 and c_4 can be determined from the following boundary conditions:

$$p(0) = p_w \qquad and \qquad \int_{-\infty}^{0} p dx = T_t(\alpha_1 - \alpha_w)$$

$$c_1 = -\frac{2f_1(h_w^2 b - h_w a f_2)(n_2 h_w - f_2) + f_2 n_5 (p_w - n_2 T_t(a_1 - a_w))n_1}{4f_2(n_1 - n_2)(a h_w f_2 - b h_w^2 - f_2)^2)} \tag{7.8}$$

$$c_2 = \frac{2f_1(h_w^2 b - h_w a f_2)(n_1 h_w - f_2) + f_2 n_5 (p_w - n_1 T_t(a_1 - a_w))n_2}{4f_2(n_1 - n_2)(a h_w f_2 - b h_w^2 - f_2)^2)} \tag{7.9}$$

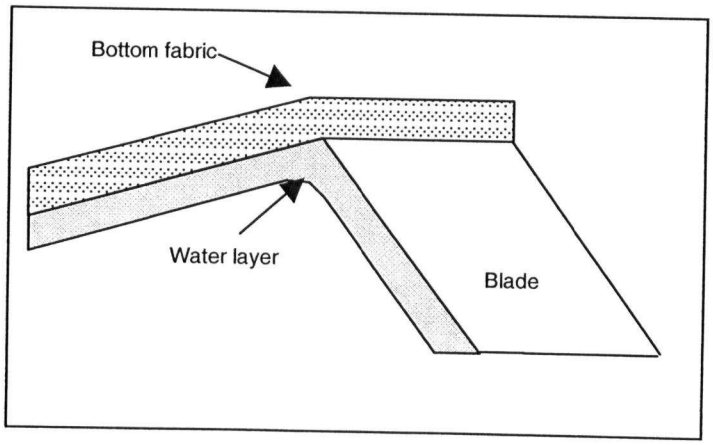

Figure 7.1: Region close to the sharp blade.

7.1.1 Estimated Effect of Doctoring Pressure for a Infinitely Thin Blade

Figure 7.2 shows the estimated effect of the doctoring on pressure pulse for a thin blade. According to this model, the maximum possible peak pressure between the fabrics can be obtained if the doctoring pressure reaches its maximum value, $p_o = \rho V_o^2/2$ at the tip of the blade. For this case the peak pressure between the fabrics is about 50% higher than that of the case with no doctoring effect. Due to the passage of water through the bottom

fabric, the maximum doctoring pressure is less than p_o. The results show the doctoring can increase the peak pressure in the gap even if its maximum is only $p_o/2$.

7.1.2 Estimated Effect of Doctoring Pressure for a Flat Blade

The effect of the doctoring pressure for a flat blade is shown in Figure 7.3. For this case, as for a thin blade, the doctoring effect increases the pressure pulse immediately upstream of the blade leading edge. The relative increase in peak pressure pulse in this case is higher than that of a thin blade. The peak pressure between the fabrics can become as high as 70% greater than of that of the case with no doctoring. Thus, the effect of the doctoring is more important for a finite width blade than a thin blade.

7.2 Summary

In this chapter a one-dimensional model to estimate the doctoring pressure in the stagnation zone was developed. It was shown that the doctoring effect increases the peak pressure pulse right upstream of the leading edge of the blade. Unlike the analytical one-dimensional models of a single blade and two blades with applied suction, which predict pressure pulses, this model provides an estimate of the effect of doctoring on the pressure pulse between the fabrics. In order to obtain more accurate result, the flow in the stagnation zone must be be modelled. The following chapter presents such a model.

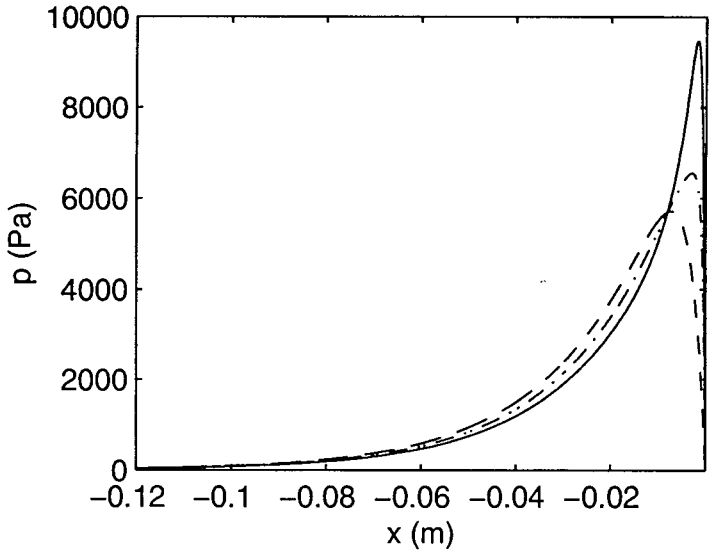

Figure 7.2: Effect of the doctoring pressure on pressure distributions, $-f_1 = p_o, -.- f_1 = p_o/2, -- f_1 = 0$, variables from Table 2.1.

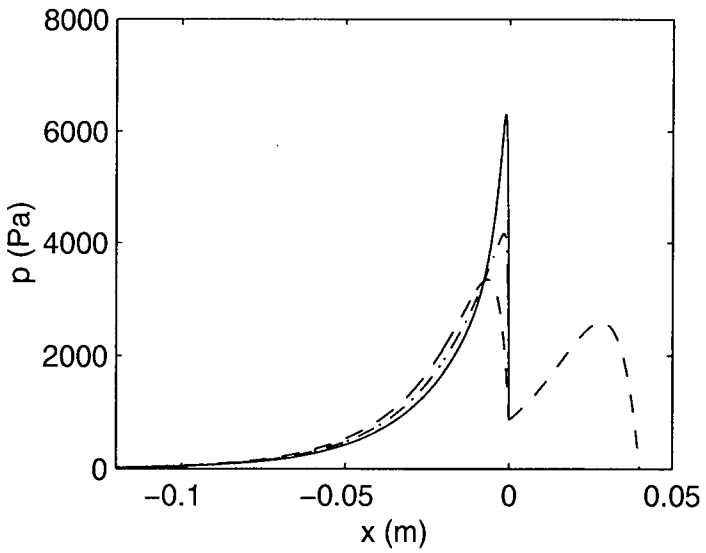

Figure 7.3: Effect of the doctoring pressure on pressure distributions, $w = 0.04\ m, -f_1 = p_o, -.- f_1 = p_o/2, -- f_1 = 0$, variables from Table 2.1.

Chapter 8

Two Dimensional Model of Stagnation Pressure Zone

The model developed in the previous chapter showed that the pressure generated in the water film in the stagnation zone has a significant effect on pressure pulse(s) in the gap. The doctoring pressure was approximated by an exponential function. It did not take into account blade geometry variables, such as radius of curvature of the leading edge. Such factors may affect the prediction. To determine this, in this chapter we examine the effect of the blade nose radius on the doctoring pressure distribution, and then the effect of doctoring on pressure pulses in gap forming for some practical blade geometries. To achieve this objective a two-dimensional free-surface model will be developed and added to the previously developed the two-dimensional viscous model of the flow in the gap (Chapter 3).

8.1 Analysis

Figure 8.1 shows the region close to the blade where water is doctored by the blade. In order to develop a mathematical model for this process, the following assumptions are made:

1. The flow is steady and two dimensional.
2. All effects of fibres, in the suspension, are neglected.
3. The pulp suspension is considered to be an incompressible Newtonian fluid (pure water).
4. Darcy's Law can be used to model the flow through the fabrics.
5. The permeability of the fibre and mat is constant.

6. The water layer moves with the same velocity as the fabric far upstream of the blade.

7. The water layer contains no fibres and additives (retention is 100%).

8. The fabrics have no stiffness and mass.

9. The bottom fabric follows the shape of the blade surface.

10. The blade and the bottom fabric surfaces are smooth.

11. The blade angle is 60°.

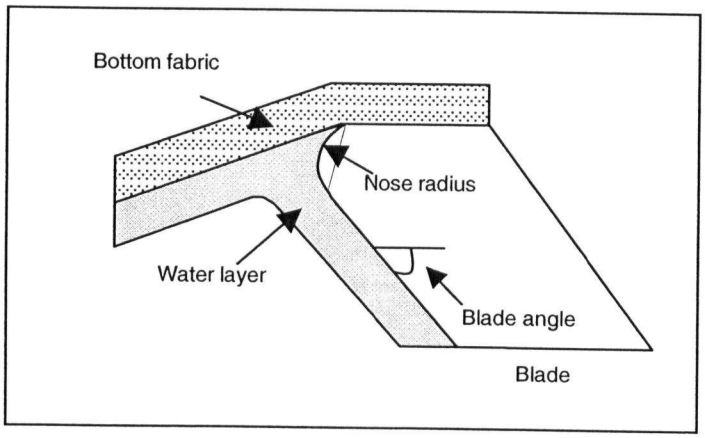

Figure 8.1: The region close to the blade where water is doctored by the blade.

8.2 Method of Solution

The method of solution of this free surface flow involves an iterative process. In the first step, the analytical one-dimensional model developed in Chapter 2 is solved to obtain the pressure pulses and fabric locations for a single blade. We recall this model has been developed based on a linearization approach [28] to derive two ordinary differential equations whose solutions are the pressure pulses upstream and over a finite width blade. In this step the effect of doctoring pressure is neglected. The variables used are shown in Table 8.1. In the next step, the thickness of the water layer approaching the blade, h_w,

Table 8.1: Fixed variables used in this Chapter.

Tension on fabrics	T	8000	N/m
Velocity of fabrics	V_o	14	m/s
Wrap angles	$\alpha_1 = -\alpha_2$	1	$degree$
Upstream gap size	h_o	3.5	mm
Average fibre+mat resistance	R	20000	$Pa-s/m$
Blade width	w	40	mm

is estimated by integrating the dewatering velocity upstream to somewhere close to the blade x_o, taken as a few times the water layer thickness. Since the dewatering velocity is $W_1 = p/R$, where R is the drainage resistance and p is the local pressure in the gap, the water film thickness is:

$$h_w = \frac{\int_{-\infty}^{x_o} p dx}{V_o R} \tag{8.1}$$

In order to determine the distance x_o over which the doctoring pressure applies, the inviscid theory of flow around a corner can be used. According to this theory, the pressure applies over a distance about 6 times the fluid thickness [55]. Considering the low viscosity of water, and the high velocity of the water layer, inertial effect dominate and therefore the inviscid theory should be approximately correct. We use this theory to select x_o and define the domain in which two phase flow modelling is done. In the third step, knowing the velocity and thickness of the water layer approaching the blade, the Volume of Fluid (VOF) model [56] is employed to find the doctoring pressure in the region close to the blade.

In the VOF model, for additional phase, a variable is introduced, which is the volume fraction of that phase. In each cell volume in the domain, the volume fractions of the two phases add to unity. If the volume fraction of the k^{th} fluid in a multi-phase flow is denoted ϵ_k, then:

- $\epsilon_k = 0$ the cell is empty of the k^{th} fluid

- $\epsilon_k = 1$ the cell is full of the k^{th} fluid
- $0 < \epsilon_k < 1$ the cell contains the interface between the fluids

The properties and variables are assigned to each cell, based on the local value of ϵ_k. The tracking of the interfaces between the N phases is accomplished by the solution of a continuity equation for the volume fraction of $N-1$ phases,

$$u_j \frac{\partial \epsilon_k}{\partial x_j} = 0 \tag{8.2}$$

In our system, air and water are the two fluids. The fluids share a single set of momentum equations. The properties (e.g. density and viscosity) in the transport equations are determined based on the amount of each phase present in each control volume, for example:

$$\rho = \epsilon_{water}\rho_{water} + (1 - \epsilon_{water})\rho_{air} \tag{8.3}$$

The FLUENT CFD code is used to solve the VOF model. Quadratic upwind interpolation was used to obtain sharper interface. Figure 8.2 shows a typical free surface profile obtained from the VOF model. The boundary conditions used in this modelling are given in Table 8.2.

Boundary conditions 5 and 6 are no slip and slip walls respectively. The solution is considered converged when residuals of pressure, velocities, and volume fraction of water fall below 1×10^{-4}. The doctoring pressure changes the pressure pulses obtained in step one, and therefore an iterative method is necessary to correct the pressure pulses and the resulting doctoring pressure. The doctoring pressure, is then approximated by an exponential function as:

$$p_{doc} = f_1 e^{f_2 x/h_w} \tag{8.4}$$

where f_1 and f_2 are two constants. Then, the analytical one-dimensional model with doctoring effect, developed in the previous chapter, can be used to determine the pressure

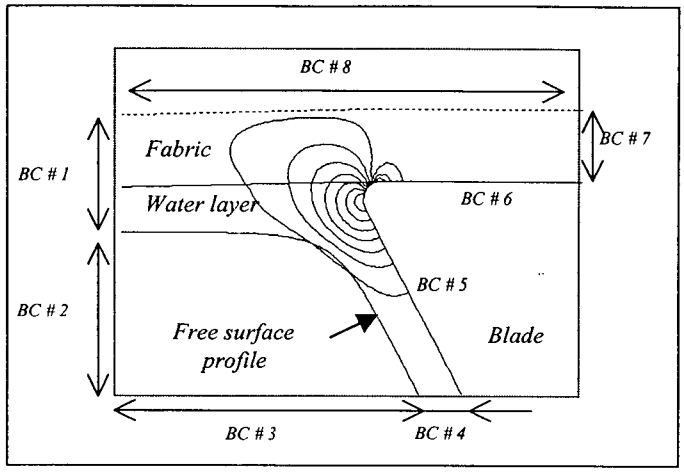

Figure 8.2: A typical free surface profile and pressure contours obtained from the VOF model. One pressure contour crosses the free surface owing to the interface definition, which is based on the local value of ϵ_k.

Table 8.2: Boundary conditions used in simulations.

Boundary number	Normal velocity	Static pressure	Volume fraction of water
1	constant	– – – – – –	1
2	– – – – –	constant	0
3	– – – – –	constant	0
4	– – – – –	constant	1
7	– – – – –	constant	1
8	– – – – –	piecewise	1

pulses in the gap. Iteration continues until the pressure pulses and resulting doctoring stop changing from one iteration to the next (normally 2-3 iterations).

After finding the right doctoring pressure from the VOF model, the doctoring pressure is then applied as a new pressure boundary condition in the two-dimensional viscous model of a single blade. Details of this model were described in Chapter 3.

Finally, the doctoring pressure used in the two-dimensional model can be checked by applying the pressure on the bottom fabric as a boundary condition (BC #8) in the VOF model.

8.3 Validation Case

In order to test the accuracy of the VOF model, we assume that the resistance of the fiber mat and fabric approaches infinity and the sum of the wrap angle and the blade angle is 90 *degree*. Physically, this means that we replace the fabric with a solid wall. Figure 8.3 shows the computed pressure distribution acting on the upper wall produced by a 0.5 mm water layer approaching the corner with a velocity at 14 m/s. The agreement between the analytical results [55] and the VOF modelling is very good, which lends support to the use of VOF modelling for the blade doctoring problem

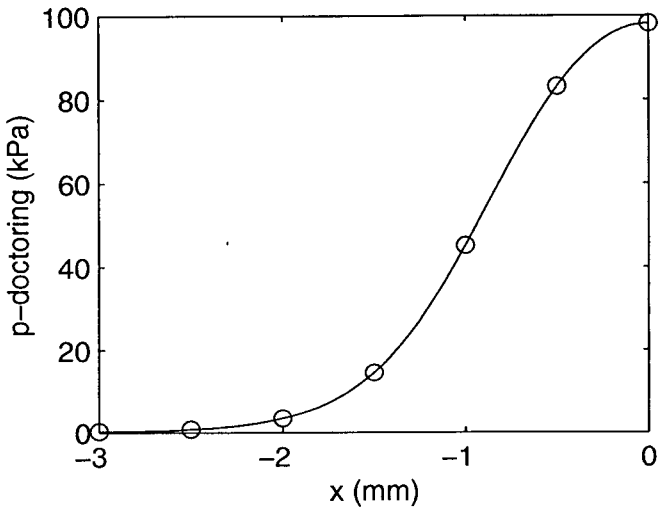

Figure 8.3: Pressure distribution along upper wall (– VOF model, o analytical solution [55]).

8.4 Results

In this section first the effect of the blade nose on the doctoring pressure, and then the effect of doctoring on the pressure pulse, will be presented.

8.4.1 2D Free Surface Model; Effect of Nose Radius on Doctoring Pressure

In order to study the effect of blade nose radius on the doctoring pressure, a number of blades were considered. Table 8.3 shows the blade characteristics used in simulations.

Table 8.3: Forming blade geometry [57].

No	Nose radius (mm)
1	0
2	0.254
3	0.635
4	1.016

Blade #1

Figure 8.4 shows a comparison between the assumed doctoring pressure and the resulting doctoring pressure for Blade #1. The thickness of the water layer is 0.5 mm and moves at 14 m/s upstream of the blade. The maximum pressure obtained is about 60% of the stagnation pressure. The doctoring pressure applies over a region about 2.5 mm upstream the blade which is about 2% of the distance over which the first pressure pulse applies.

Blade #4

Figure 8.5 shows the (initially) assumed and the converged doctoring pressure from the VOF model. The maximum doctoring pressure for this blade is about the same as that of Blade #1. For Blade # 4, the doctoring pressure applies over a wider range than that of Blade #1, however this range is still less than 3% of the range of the pressure pulse upstream of the blade.

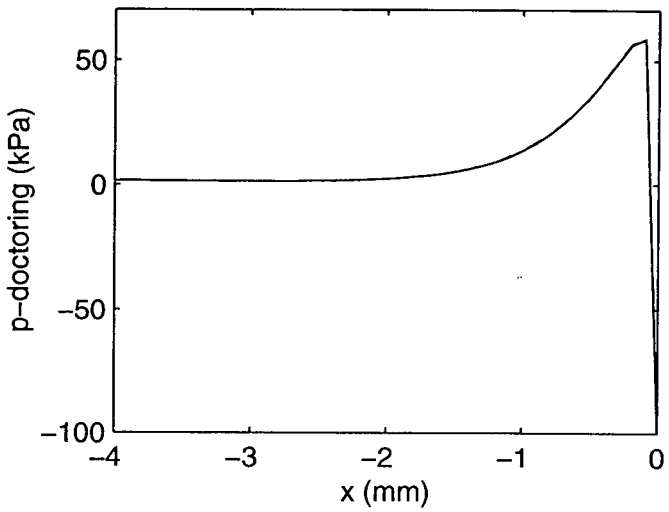

Figure 8.4: Doctoring pressure for Blade #1, −− assumed (previous iteration) and − converged doctoring pressures.

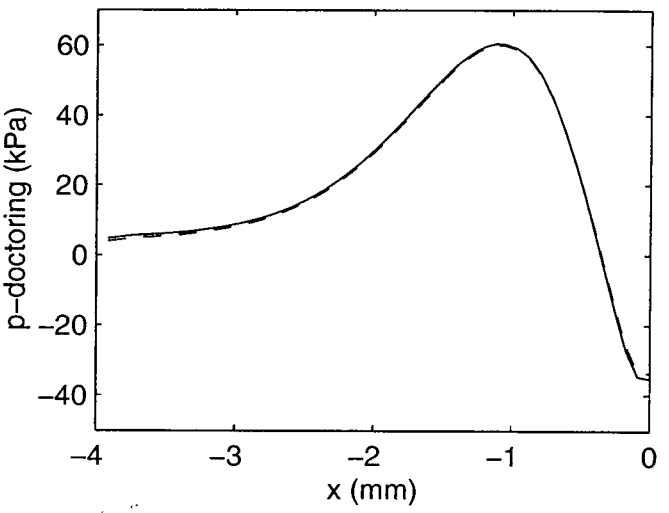

Figure 8.5: Doctoring pressure for Blade #4, −− assumed (previous iteration) and − converged doctoring pressures.

Figure 8.6 and Table 8.4 summarize the effect of nose radius on doctoring pressure. Figures 8.7, 8.8, 8.9 and 8.10 show the pressure and volume fraction contours for Blades #2 and #4, respectively.

As shown in pressure contours, the location of the stagnation pressure, p_o, is some small distance away from the contact point between the fabric and blade, which is expected owing the porosity of the forming fabric. For all cases, the peak doctoring pressure is about 50% - 60% of the stagnation pressure. However, as the nose radius increases, the doctoring pressure applies over a wider region upstream of the blade and the location of the peak doctoring pressure, $x_{(doc,max)}$, shifts away from the leading edge of the blade. The larger nose radius also lets the fluid turn smoothly and reduces the peak negative pressure acting on the blade.

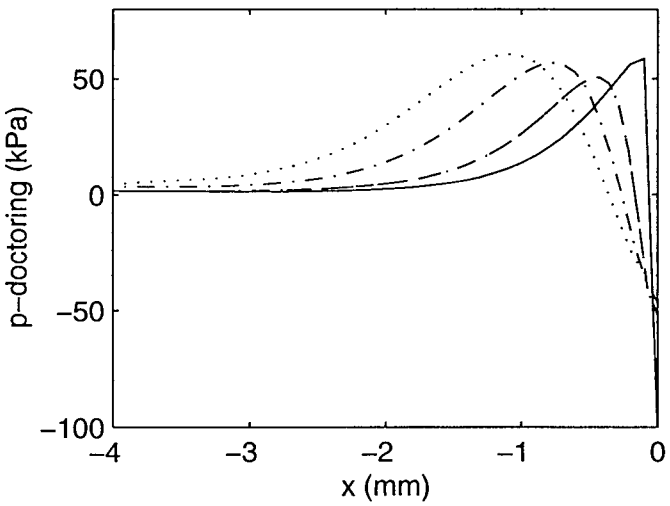

Figure 8.6: Effect of nose radius on doctoring pressure (− Blade #1, −− Blade #2, −.− Blade #3, and ... Blade #4).

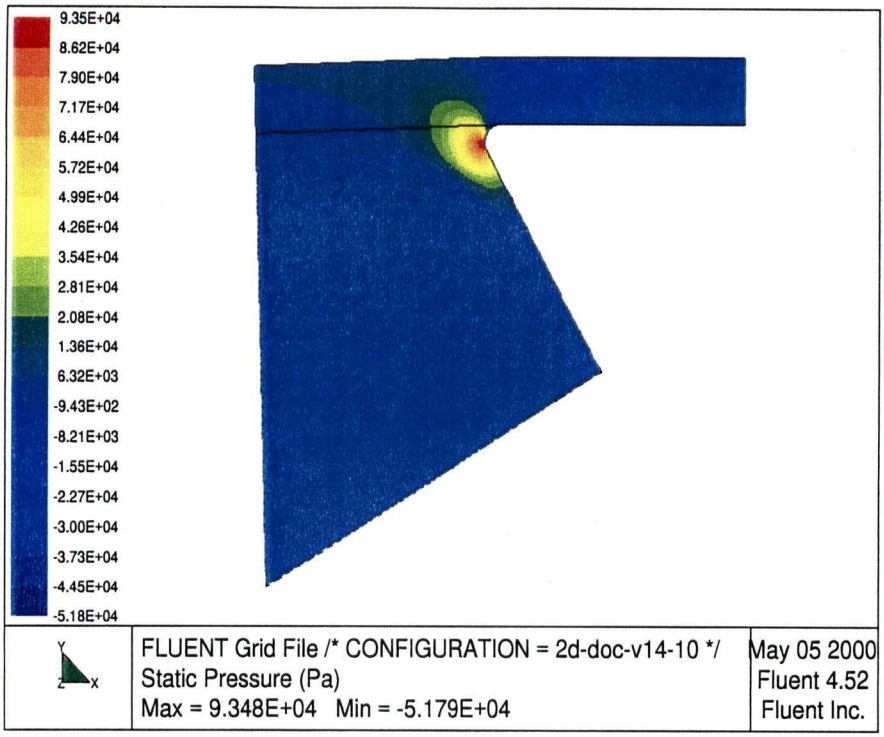

Figure 8.7: Pressure contour for Blade #2.

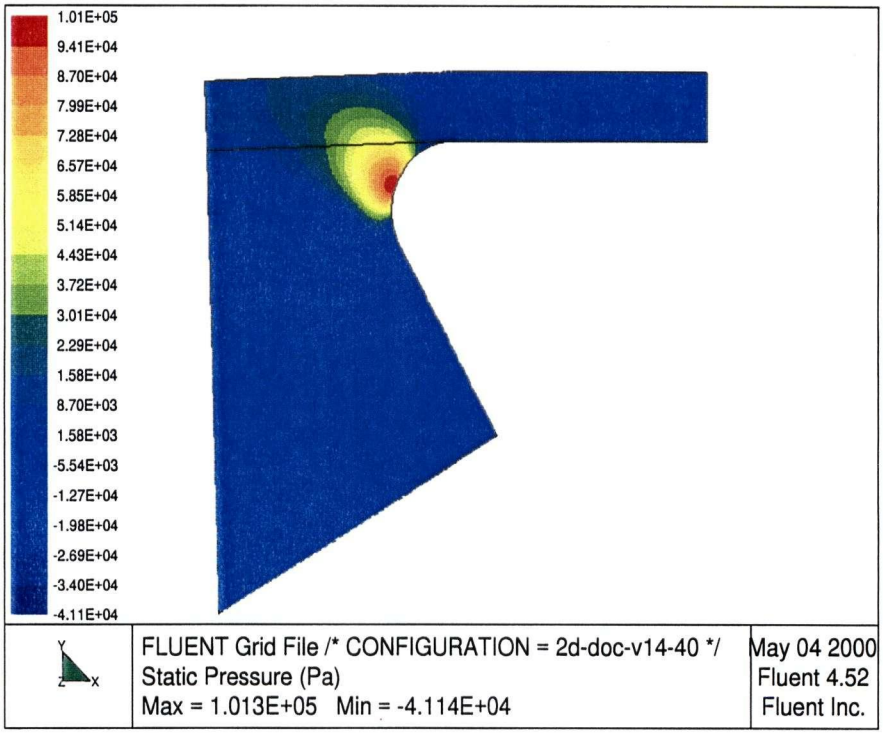

Figure 8.8: Pressure contour for Blade #4.

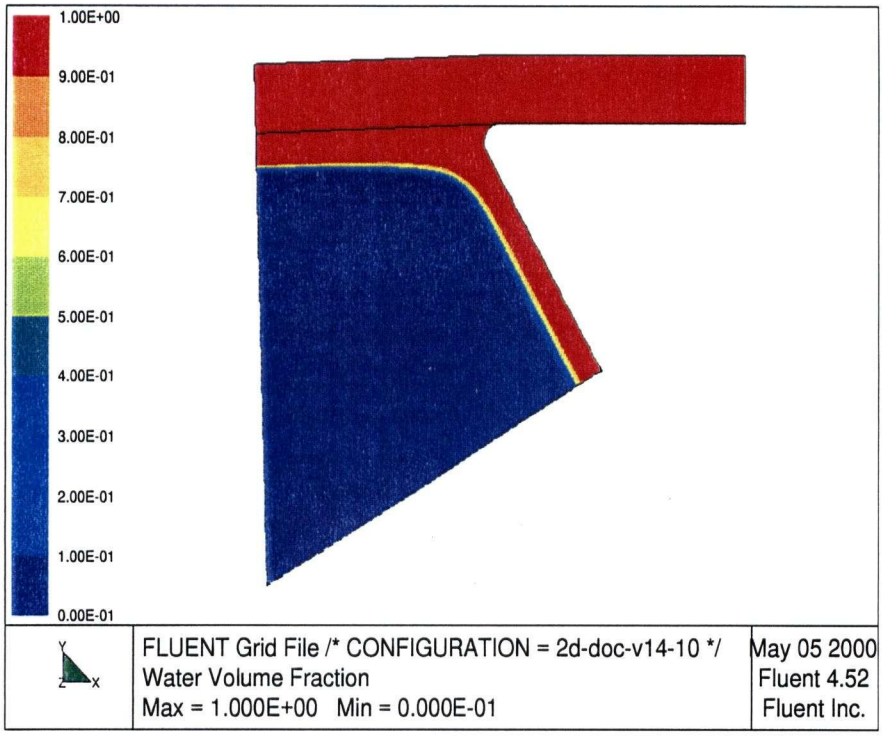

Figure 8.9: Volume fraction of water contour for Blade #2.

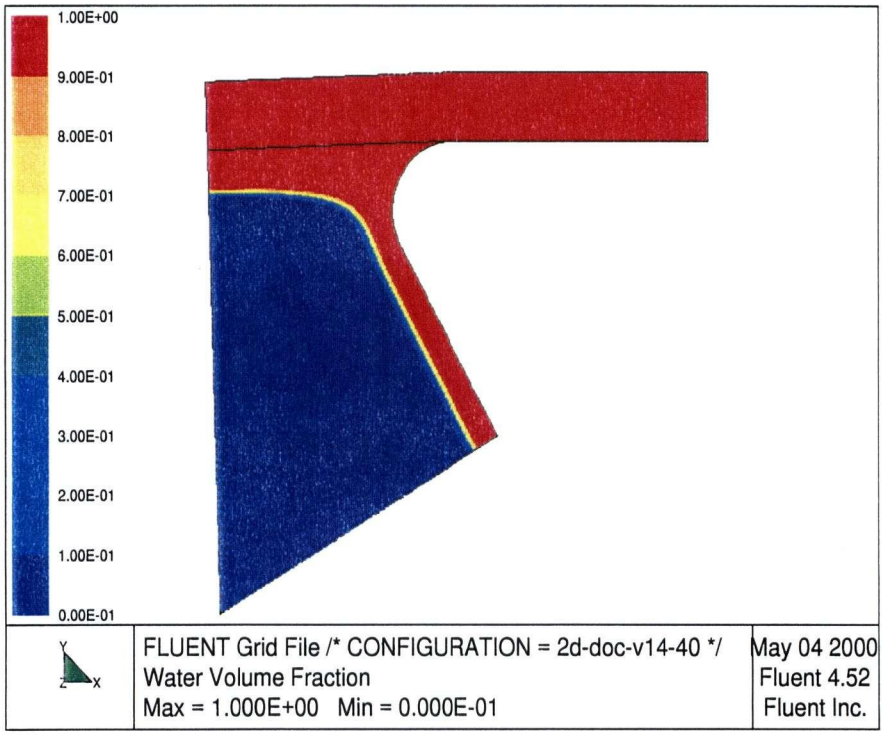

Figure 8.10: Volume fraction of water contour for Blade #4.

Table 8.4: Summarized results of two-dimensional free surface model.

Blade	No. of cells	$p_{doc,max}$ kPa	$x_{doc,max}$ mm
1	7600	60	-0.11
2	8800	51	-0.43
3	9970	57	-0.78
4	10440	61	-1.12

8.4.2 2D Model of Flow in the Gap; Effect of Doctoring on Pressure Pulses

Blade #1

Figure 8.11 shows the pressure pulses in the gap, at the bottom fabric p_b, in the middle p_m, and at the top fabric p_t. As expected, the effect of the doctoring pressure is important over a region a few millimeters upstream of the blade leading edge. As shown, the maximum pressure on the bottom fabric (8600 Pa) can exceed the pressure between the fabric (in the middle) by as much as 30% more than that in the middle of the gap (6600 Pa). Also the pressure on the bottom fabric falls below atmospheric pressure (-3500 Pa for this case). This model also predicts a negative pressure on the bottom fabric just downstream of the trailing edge of the blade.

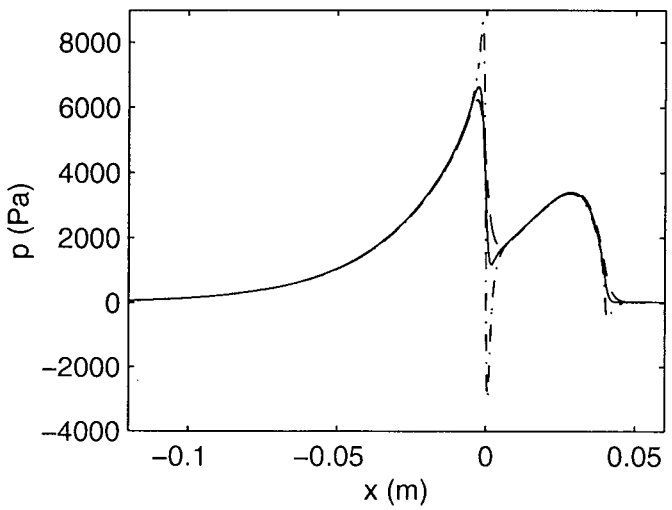

Figure 8.11: Pressure pulse in the gap for Blade #1 ($-$ p_m, $--$ p_t, $-.-$ p_b).

Blade #4

Figure 8.12 shows pressure distributions in the gap for Blade #4. The maximum pressure on the bottom fabric can reach as high as 17900 Pa, about 50% higher than the maximum pressure in the middle of the gap.

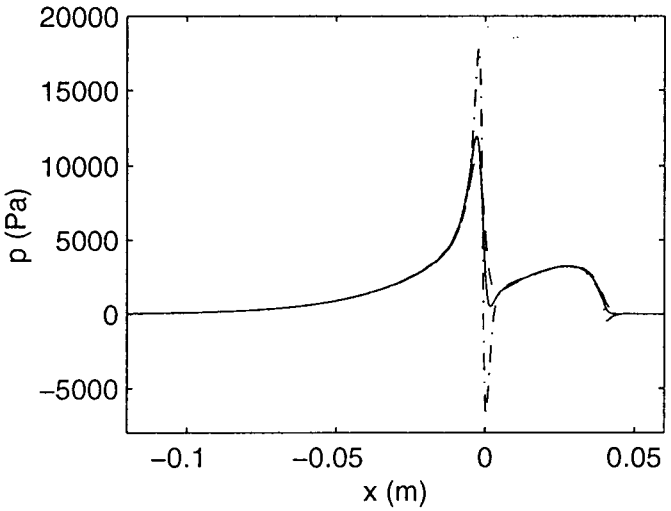

Figure 8.12: Pressure pulse in the gap for Blade #4 ($-$ p_m, $--$ p_t, $-.-$ p_b).

Table 8.5 summarize some results from the two-dimensional viscous pressure pulse model. It shows that for all cases the integrated pressure in the fluid in contact with the top fabric is within 7% of the simple theoretical value, $T_t(\alpha_1 - \alpha_2)$, which is conformation that the simulation is behaving reasonably. A comparison between the pressure pulses in the middle of the gap, produced by different blades, is shown in Figure 8.13. As shown, the peak pressure pulse in the gap increases with increasing nose radius. If the magnitude of the doctoring pressure were responsible for this increase in pressure pulse magnitude, then Blade #1 and Blade #4 should predict almost the same peak pressure (Blade #1 and Blade #4 produce doctoring pressures as high as 60 kPa). As shown in Figure 8.6, with increasing nose radius the location of maximum doctoring pressure shifts away from the leading edge of the blade and toward the location of the peak pressure pulse in the gap upstream of the blade. For example, for Blade #4 the location of the peak doctoring pressure (at -1.12 mm) is the closest to the location of peak pressure pulse in the gap upstream of the blade (at -2.85 mm). Thus, this model predict that the magnitude of the

pressure pulse in the gap is affected more by the location of the peak doctoring pressure than by its magnitude, Figure 8.13.

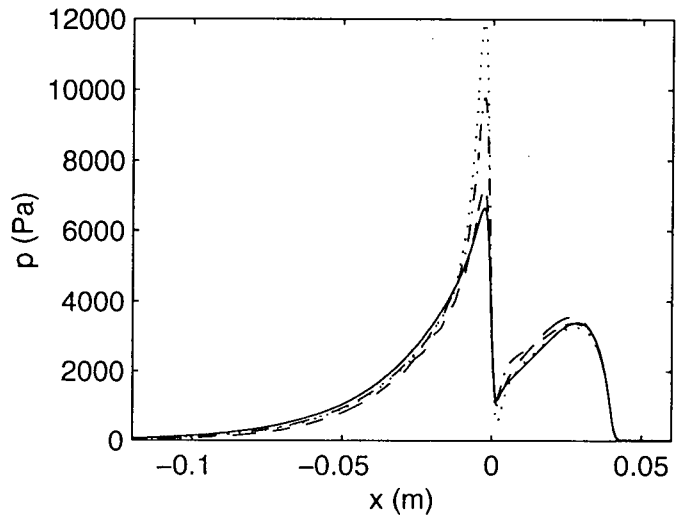

Figure 8.13: Pressure pulses in the middle of the gap (− Blade #1, −− Blade #2, −.− Blade #3, and ... Blade #4).

Based on the above findings, one can estimate that a portion (about 10%) of the drained water layer is forced back into the gap as a result of the doctoring pressure.

Figure 8.13 also shows that increasing the nose radius not only increases the peak pressure pulse right upstream of the leading edge of the blade, but decreases the pressure just downstream of the leading edge of the blade. It has been observed experimentally [27] that under some operating conditions the water adhering to the top fabric is sucked back between the fabics just downstream of the leading edge of the blade. This means that over this portion of the blade, the pressure of fluid at the top fabric drops below atmospheric pressure. The one-dimensional model of a single blade fail to predict any negative pressure over the blade. The two-dimensional free surface model might predict negative pressures in the gap under some operating conditions. In order to investigate this possibility, some of the operating conditions given in Table 8.1 are modified as given in Table 8.6.

Figure 8.14 shows the pressure distributions at the top fabric obtained from different models. As shown, the two-dimensional viscous (without doctoring effect) models predict

Table 8.5: Summarized results of the two-dimensional viscous model.

Blade	No. of cell	$\int p_t dx\ (Pa-m)$	Error%	$p_{m,max}\ (Pa)$	$x_{max}\ (mm)$
1	109200	287.2	2.9	6640	-2.69
2	84800	272.4	2.4	7250	-2.74
3	84800	298.4	6.7	9770	-2.69
4	84800	299.1	7.1	11950	-2.85

Table 8.6: Modified variables for simulation.

Tension on fabrics	T	5000	N/m
Upstream wrap angle	α_1	1.2	*degree*
Downstream wrap angle	α_2	-0.2	*degree*
Blade width	w	50	mm

positive pressures all over the blade. However, if the doctoring effect is included, the two-dimensional model predicts the pressure at the top fabric is negative in a small region over the blade.

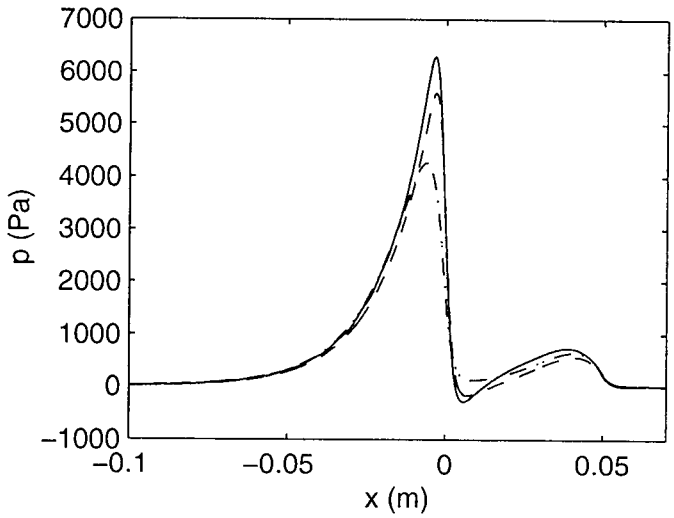

Figure 8.14: Pressure pulses at the top of the gap (– Blade # 4, -- Blade #3, and –.– 2D-model without doctoring effect).

8.5 Summary

The results of this chapter show that the effect of the doctoring pressure is highly localized. The model predicts that, in the doctoring process for typical operating conditions, the pressure in the water layer reaches its stagnation value some small distance away from the fabric-blade contact point, toward the blade support. The amplitude of the doctoring pressure felt by the lower fabric is less than the stagnation pressure, but is high enough to cause a large pressure gradient within the gap just upstream of the blade. The results also show that for commercial blade shapes the nose radius has no significant effect on the maximum doctoring pressure. However, increasing the nose radius of curvature increases the distance over which the doctoring pressure applies and increases the peak pressure pulse within the gap significantly. The doctoring pressure forces a portion of the water, which was expelled from the gap upstream of the blade, back between the fabrics through the bottom fabric. Under some operating conditions suction can be generated as the fabrics wrap the toe of a blade. This suction can draw water between the fabrics that had previously been expelled through the top fabric. This finding may explain an observation of Garner and Pye [27] in which a small amount of water reabsorbed over the blade close to leading edge. Some parts of the results on stagnation zone have been published in [58].

Chapter 9

Summary and Conclusions

This thesis has addressed key questions remaining from previous studies on the hydrodynamics of pressure pulses generated in blade gap forming. The major findings of this study can be classified in two following parts.

9.1 Extension of One-dimensional Analytical Model of a Thin Blade

A previously developed analytical model of the infinitely thin blade was extended to model finite width blades (with flat and curved surfaces) and to model a suction box. In these models the pulp suspension was assumed to be an inviscid fluid. These models provide a simpler approach to determine the pressure pulses than previously developed one-dimensional numerical models. The model of a finite width blade predicts that for a flat blade, for reasonable values of the fabric wrap around a wide ($w > 2\ cm$) blade, two pressure pulses are developed, one at the blade leading edge, and one at the blade trailing edge. The model also predicts that for a curved blade surface with a small crown ($c = 0.05\ mm$), most of the wrap is taken at the blade nose and tail, and therefore two distinct pressure pulses can be distinguished, as for a flat blade. As surface curvature increases to $c = 0.1\ mm$, the leading and trailing edge pulses merge to form a single pulse over the blade.

9.2 Two-Dimensional Viscous Models

Two-dimensional viscous models were developed for a single blade and suction box by solving the full Navier-Stokes equations for the flow in the gap and Darcy's Law or Forcheimers equation for the flow through the fibre mat and fabric. Major contributions of this thesis can be classified as follows:

Verification of the Previous Assumptions

By setting different values for the fluid viscosity and comparing obtained pressure pulses, it is found that the effect of viscosity on pressure pulses is small, Figure 3.6.

By solving Darcy's Law and Forcheimers equation for the flow through the fibre mat and fabric, it is determined that the influence of fluid inertia on drainage resistance of a typical sheet with basis weight $\approx 10 g/m^2$ (estimated value over the blades in gap formers) is negligible. Therefore, by independent means two major assumptions made in previous studies of blade gap forming have been validated. The pulp suspension may be treated as an inviscid fluid for calculating pressure pulses and Darcy's Law describes accurately the flow through the fabric and fibre mat.

Comparison with the One-dimensional Models

The viscous model predicts pressure pulses with lower amplitude than the one-dimensional models, but with a broader pulse peak. These findings are in agreement with the potential flow model of Zahrai and Bark [31] for a thin blade. The difference between the fluid and fabric velocities causes thin boundary layers to be formed on the fabrics. The variation of fluid velocity outside the boundary layer upstream of the blade is small, but downstream of the blade nose there are velocity variations in the gap, even outside the boundary layer.

Viscous Model of Suction Boxes

The suction model predicts that the pressure in the gap is a minimum shortly downstream of the first blade, and increases in the machine direction as the second blade is approached. For reasonable values of the fabric wrap around the second blade, the pressure between the fabrics becomes positive close to the second blade. Applying more suction decreases the suspension pressure close to the first blade and increases the peak-to-peak pressure. Increasing the blade separation produces a sharper pressure gradient close to the second blade.

Viscous Model of Stagnation Zone

To understand the doctoring effect a two-dimensional free surface model based on the Volume of Fluid (VOF) technique was developed and added to the two-dimensional model of flow in the gap. It was found that pressure in the water layer reaches its maximum value (stagnation pressure) some distance away from the contact point between the fabric and blade, Figures 8.7 and 8.8. As a result, the maximum pressure acting on the blade-side of the fabric is less than the stagnation pressure ($\approx$ 50% less under typical operating conditions), but is still much higher than that between the fabrics. Increasing the blade nose radius increases the distance over which the doctoring pressure acts, but barely affects the maximum doctoring pressure. The peak pressure pulse in the gap were significantly affected by the location of peak doctoring pressure, Figure 8.13. The doctoring pressure forces a portion of the expelled water back into the gap from the bottom fabric. Under some circumstances, the pressure at the top fabric becomes negative and causes a portion of the expelled water to be sucked back into the gap between the fabrics.

In conclusion, this work, coupled with earlier studies, enables us to predict the forming section pressure pulses in situations of practical interest. Analytical models that have been extended in this thesis can be employed simply by engineers and technicians in mills to estimate the pressure pulse distributions and the dewatering over the practical ranges used in this thesis. In addition, numerical models developed here, coupled with the roll former models of others, can also be used by researchers to improve the performance of paper machines. The model may also serve as a basis for linking paper properties such as formation to forming hydrodynamics. To create this link, it will be necessary to do experimental studies of paper formation over a wide range of papermachine operating parameters.

Chapter 10

Recommendations For Future Work

This thesis has shown how dewatering from a single blade and two adjacent blades with applied suction can be modelled in blade gap formers. Some studies which would extend our understanding of this process would be the following:

- Although the predictions of this thesis are based on rigorous analysis and are consistent with previous work, there is need for experimental verification of the predicted pressure pulses. Of the tests possible, perhaps the easiest is the effect of blade surface curvature, since this can be measured by static pressure taps on the blade surfaces.

- A remaining issue from this and earlier work is the determination of appropriate drainage resistance coefficients, both perpendicular and parallel to the fabrics, for use with the determined pressure pulses.

- Since most modern gap formers have roll forming followed by blade forming, an improved model of roll forming, including the early impingement zone, must be developed. With such a model, in combination with the models described in this thesis one would be able to simulate the forming section from the headbox slice through most of the forming section.

- When the pulp consistency is high, interfibre forces are correspondingly high. Some constitutive relationship for the pulp suspension must be developed to understand dewatering towards the couch end of the forming section

- Some modern gap former have opposed blades in the forming section. The models developed in this thesis can be extended to study the effect of this type of configuration on the flow field in the gap.

- As shown theoretically, the shape of the blade surface has an important effect on pressure pulse distributions. An experimental study is required to investigate and confirm the theoretical study.

Bibliography

[1] THORP, A. B. and KOCKUREK, M. J. "Pulp and Paper Manufacture.", Vol. 17, 1983.

[2] THORP, B., "Twin Wire Forming Rapid Commercialization Ahead.", TAPPI Twin Wire Seminar,1–13, 1985.

[3] HOHNS, W. J., and MAURANEN, P., "Mill Operating Experience With the Valmet Sym-Former R.", TAPPI Papermaker Conference, 139–144, 1984.

[4] MAURANEN, P., and HUJOLA, J. , "Valmet Former for Paper Machines Rebuilds and New Paper Machines.", CPPA Annual Meeting, 195–200, 1983.

[5] CARSON, J. E., "Top-Flyte: a Fourdrinier Top Wire Former for Increased Productivity and Twin Wire Sheet Characteristics.", TAPPI Papermakers Conference, 113–117, 1984.

[6] BRAUNS, R., "Wet End Developments.", CPPA Technical Section Annual Meeting, vol. A, 275–282, 1986.

[7] NORMAN, B., "Principles of Twin Wire Forming", *Svensk Papperstidning*, vol. 82(11), 330–336, 1979.

[8] SIMS, D. N., "Twin Wire Forming Developments.", TAPPI Twin Wire Seminar, 43–51, 1985.

[9] SINKEY, J., and WAHREN, D., "Quality Comparison of Twin Wire and Fourdrinier Papers.", TAPPI Twin Wire Seminar, 25–33, 1985.

[10] WAHLSTROM, B., "Escher Wyss Twin Wire Formers.", Twin-Wire Seminar, 61–69, 1985.

[11] GUSTSFSON, D. and DENNIS, L., "The Bel-Baie Twin Wire Former.", *TAPPI Journal*, vol. 53(3), 483–486, 1970.

[12] JUSTUS, E. J, and GUSTAFSON, D. E., "Bel-Baie Former Design Characteristics and Performance.", *TAPPI Journal*, vol. 54(9), 1455–1458, 1971.

[13] ANDERSON, I., "Periformer HR, Top Wire hybrid Former.", TAPPI Papermaker Conference, 131–138, 1984.

[14] MALASHENKO, A., DEPERIS, G., and LIDSTROM, R., "Dominion Dynaformer.", CPPA Annual Meeting, 139–147, 1982.

[15] HAUSER, L., "Duformer Performance of Commercial Installations and Comparison with Fourdriniers.", TAPPI Annual Meeting, 7–13, 1981.

[16] HEISSENBERGER, O. L., "Development in Paper Technology in a Global Perspective.", *Svensk Papperstidn*, vol.84(18), 32–39, 1981.

[17] HERGERT, R. E. and SANFORD, C. L., "Pressure Measurements in the Forming Zone of a Twin-wire Tissue Machine.", *Pulp and Paper Canada*, 134–137, 1984.

[18] SIEBERTH, R. G., "Duoformer F and H - Review.", TAPPI Twin Wire Seminar, 1–13, 1985.

[19] BOXER, T., DODSON, C. T. J, and SAMPSON, W. W., "Mathematical Modelling of Shotton's Roll Blade Former.", PITA Water Removal Conference, 39–44, 1997.

[20] BAINES, W. D., "The Papriformer Part II-Flow in the Forming Zone of a Two Wire Machine.", *Pulp and Paper Canada*, vol. 68(10), 497–505, 1967.

[21] ATKINSON, W. and MALASHENKO, A., "Commercial Development of the Papreformer.", *TAPPI Journal*, vol. 54(19), 1464–1467, 1971.

[22] WAHREN, D., STENBERG, G. and ZOTTERMAN, C., "Symmetrical Dewatering in Webster-type Formers", *Pulp and Paper Canada*, vol. 79(9), 276–279, 1978.

[23] MARTINEZ, D. M., "Characterizing the Dewatering Rate in Roll Gap Formers.", *Journal of Pulp and Paper Science.*, vol. 24(1), 7–13, 1998.

[24] BANDO, T., SAKAMOTO, K., MASUDA, H., and IWATA, H., "Development of the Mitsubishi New Former.", Pan-Pacific Pulp and Paper Tech. Conference, 213–220, 1992.

[25] IWATA, H., KUNO, H., and KURAGASAKI, M., "Pressure Measurements in the Forming Zone of a Twin Wire Former.", TAPPI annual Meeting, 1991.

[26] GOODING, R., ROMPE, A., "Probe Measurements of Blade Pulses.", Private Communication, 1999.

[27] GARNER, R. G., Pye, I. T., "High Speed Forming.", 86–89, 1985.

[28] ZHAO, R. H. and KEREKES, R. J., "Pressure Distribution Between Forming Fabrics in Blade Gap Formers: Thin Blades.", *Journal of Pulp and Paper Science*, vol. 21(3), 97–103, 1995.

[29] NORMAN, B., "Hydrodynamic Developments in Twin Wire Forming Overview.", *Paperi Ja Puu-Paper and Timber*, vol. 78(6), 376–381, 1996.

[30] ZHAO, R. H. and KEREKES, R. J., "The Effect of Consistency on Pressure Pulses in Blade Gap formers.", Paperi ja Puu., vol. 78, 36–38, 1996.

[31] ZAHRAI, S., and BARK, F. H., "On the Fluid Mechanics of Twin Wire Blade Forming in Paper Machines.", *Nordic Pulp and Paper Research Journal.*, vol. 4, 245–252, 1995.

[32] GREEN, S. I., "Analytical and Computational Modeling of Twin Wire Blade Forming.", *Journal of Pulp and Paper Science*, vol. 23(7), 353–357, 1997.

[33] GREEN, S. I., ZHAO, R. H., and KEREKES, R. J., "Pressure Distribution Between Forming Fabrics in Blade Gap Former: Blades of Finite Width and Fabrics Finite Stiffness.", *Journal of Plup and Paper Science*, vol. 24(2), 60–67, 1998.

[34] GREEN, S. I. and KEREKES, R. J., "Numerical Analysis of Pressure Pulses Induced by Blades in Gap Formers.", *TAPPI Journal*, vol. 81(4), 180–187, 1998.

[35] ZAHRAI, S., BARK, F. H., and NORMAN, B., "An Analysis of Blade Dewatering in a Twin Wire Paper Machine.", *Journal of Pulp and Paper Science*, vol. 23(9), 452–459, 1997.

[36] GREEN S. I., "Modelling Suction Boxes in Twin Wire Blade Forming: Theory.", *TAPPI Journal*, vol. 82(9), 136–142, 1999.

[37] GREEN S. I., "Modelling Suction Boxes in Twin Wire Blade Forming: Results.", PAPTAC Conference, vol. 1, 71–84, 1998.

[38] SHANDS J. A., "A Twin Wire Former Rebuild Option for Improved Formation and Drainage.", TAPPI Proceedings International Engineering Conference, vol. , 53–69, 1998.

[39] WILDFONG, V. J, GENCO, J. M., SHANDS, J. A., and BOUSFIELD, D. W., "Filtration Resistance Determination of Fibrous Suspensions Utilizing A Rapid drainage Tester.", TAPPI Proceedings International Engineering Conference, vol. 3, 927–939, 1998.

[40] HERZIG, R., and JOHNSON, D. B., "Investigation of Thin Mat Formed at High Velocity", TAPPI Engineering and Papermaker Conference, vol. 1, 109–120, 1997.

[41] JONG, J. H., BAINES, W. D., and CURRIE, I. G., "Experimental Characteristics of Forming Fabric and Fibre Mat", CPPA Proceedings International Engineering Conference, vol. 3, 927–939, 1998.

[42] PIRES, E. C., SPRINGER, A. M., and KUMAR, V., "A New Technique for Specific Filtration Resistance Measurement", *TAPPI Journal*, vol. 72(7), 149–154, 1989.

[43] SAYEGH, N. N, and GONZALEZ, T. O., "Compressibility of Fibre Mats During Drainage.", *Journal of Pulp and Paper Science*, vol. 21(7), 255–261, 1995.

[44] SAMPSON, W. W., and KROPHOLLER, H. W., "Batch Drainage Curves for Pulp Characterization. Part I: Experimental.", *TAPPI Journal*, vol. 78(12), 145–151, 1995.

[45] SAMPSON, W. W., and KROPHOLLER, H. W., "Batch Drainage Curves for Pulp Characterization. Part II: Modelling.", *TAPPI Journal*, vol. 79(1), 151–160, 1996.

[46] MANTAR, E., CO, A., and GENCO, J, M., "Drainage Characteristics of Pulp Slurries Under Dynamic Conditions.", *Journal of Pulp and Paper Science*, vol. 21(2), 44–50, 1995.

[47] GESS, J. M., "A New Drainage Analysis System.", *TAPPI Journal*, vol. 67(3), 70–73, 1984.

[48] INGMANSON, W. L., ANDREWS, B. D., "High Velocity Water Flow Through Fibre Mats.", *TAPPI Journal*, vol. 46(3), 150–155, 1963.

[49] FLUENT Manual, "User's Guide", vol.4:,1996.

[50] PATANKAR, S.V., "Numerical Heat Transfer and Fluid Flow.", Hemisphere Publishing Corp., Washington, DC, 1980.

[51] ROSHANZAMIR, A., GREEN, S. I., and KEREKES, R. J., "Two-Dimensional Simulation of Pressure Pulses in Blade Gap Formers.", *Journal of Pulp and Paper Science*, vol. 24(11), 364–368, 1998.

[52] FORCHEIMER, P. Z., Ver Deutsch Ing. 54, 1901.

[53] ROSHANZAMIR, A., GREEN S. I., and KEREKES, R. J., "The Effect of Non-darcy's Law Drainage on the Hydrodynamics of Blade Gap Former.", TAPPI Papermaker Conference., vol. 1, 701-708, 2000.

[54] ROSHANZAMIR, A., GREEN, S. I., and KEREKES, R. J., "Two-Dimensional Simulation of Suction Shoes in Blade Gap Formers.", *Journal of Pulp and Paper Science*, vol. 26(4), 158–162, 2000.

[55] APPEL, D. W., and YU, Y. S., "Free Streamline Analyses of Flow From Nozzles, Flow Through Side Inlets, and Flow Past Corners", The University of Kansas, vol. 17, 19–23, 1963.

[56] FLUENT Manual, "VOF Free Surface Model" User's Guide, 1996.

[57] Private communication, AstenJohnson Company.

[58] ROSHANZAMIR, A., KEREKES, R. J., GREEN, S. I., and OLLIVIER-GOOCH, C., "Hydrodynamic Pressure Generated by Doctoring in Blade Gap Formers.", TAPPI Engineering/Process and Product Quality Conference, vol. 3, 1181–1188, 1999.